

1989

Experimental and theoretical analysis of component behavior in top-and-seat-angle connections /

Robert B. Fleischman
Lehigh University

Follow this and additional works at: <https://preserve.lehigh.edu/etd>



Part of the [Civil Engineering Commons](#)

Recommended Citation

Fleischman, Robert B., "Experimental and theoretical analysis of component behavior in top-and-seat-angle connections /" (1989). *Theses and Dissertations*. 4955.
<https://preserve.lehigh.edu/etd/4955>

This Thesis is brought to you for free and open access by Lehigh Preserve. It has been accepted for inclusion in Theses and Dissertations by an authorized administrator of Lehigh Preserve. For more information, please contact preserve@lehigh.edu.

**Experimental and Theoretical Analysis
of Component Behavior
in Top-and-Seat-Angle Connections**

by

Robert B. Fleischman

A Thesis

Presented to the Graduate Committee

of Lehigh University

in Candidacy for the Degree of

Master of Science

in

Civil Engineering

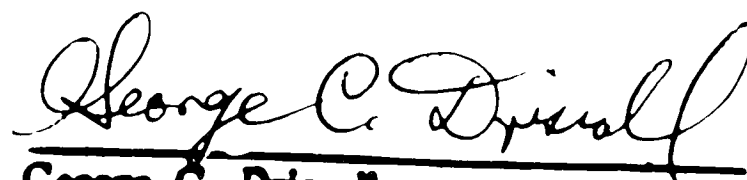
Lehigh University

December 1988

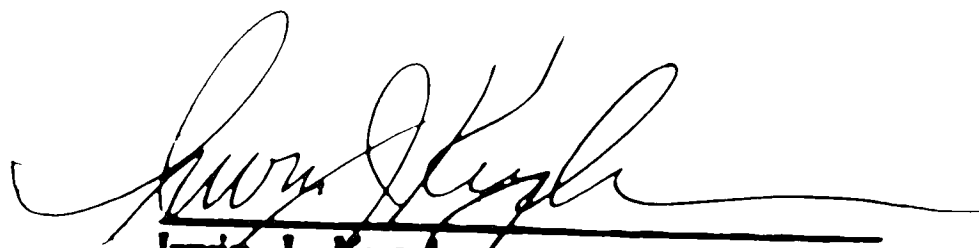
Certificate Of Approval

This thesis is accepted and approved in partial fulfillment of the requirements for the degree of Master of Science in Civil Engineering.

14 December 1988
Date



George C. Driscoll
Professor in Charge



Irwin J. Kugelman
Department Chairman

Acknowledgements

The studies reported here were conducted in the Engineering Research Center for Advanced Technology for Large Structural Systems (ATLSS) at Lehigh University. The ATLSS Center was created by a grant from the National Science Foundation. Dr. John W. Fisher is the Director of ATLSS which is headquartered at Lehigh University. Dr. Irwin J. Kugelman is chairman of the Department of Civil Engineering.

Special thanks are due to Dr. George C. Driscoll and Dr. Le-Wu Lu. Dr. Driscoll is the supervisor of the thesis and principal investigator for ATLSS Project A3.1. His patience and enthusiasm in regard to the teaching aspects of the project were greatly appreciated. It was his ideas that formed the basis for this paper. Dr. Lu provided constant supervision during the experiments. His persistence ensured that full utility of each specimen be reached.

Many thanks to Charles Hittinger, who located and ordered obscure detail material, while also conducting the fabrication process. Gene Matlock, Todd Anthony, and John Pinter each performed a large quantity of the specimen preparation. Russell Longenbach was responsible for the test specimen instrumentation. Pamela DeBellis created the shop drawings for the test frame. Robert Dales supervised the erection, and Richard Sopko did the photography.

Thanks to many who were not directly related to the project, but provided insight, assistance or their time: Dr. Roger Slutter, Jian Jin, Joseph Reed, and Philip Ritchie. Special thanks to my colleague, Cameron Chasten, who contributed to both the theoretical and experimental phases of this project.

Table of Contents

Abstract	1
1. INTRODUCTION	2
1.1 Semi-Rigid Connections	2
1.2 Top-and-Seat-Angle Connection	3
1.3 Current Design	3
1.3.1 Procedure	4
1.3.2 Backround Theory	4
1.3.3 Limitations	5
1.4 Previous Studies	6
1.5 Research Program	7
2. THEORETICAL STUDY	8
2.1 Modelling Philosophy	8
2.1.1 Common Practice	8
2.1.2 Component Modelling	9
2.2 STRUCTR Model	9
2.2.1 Topology	9
2.2.2 Procedure	10
2.2.3 Assumptions	10
2.3 Theoretical Work	11
2.4 Model Modification	13
2.4.1 Bolt Members	13
2.4.1.1 Model Bolt A	14
2.4.1.2 Model Bolt B	15
2.4.2 Critical Leg Adjustment	15
2.4.2.1 Model Leg A	15
2.4.2.2 Model Leg B	16
2.5 Theoretical Results	17
2.5.1 Hinge Occurence	17
2.5.1.1 Original Model	17
2.5.1.2 Models Bolt A, Bolt B	18
2.5.1.3 Model Leg A	18
2.5.1.4 Model Leg B	19
2.5.1.5 General Model Characteristics	19
2.5.2 Force Path	19
2.5.3 Moment Capacity	23
2.6 Model Comparison	23
3. TESTING PROGRAM	24
3.1 Experimentation Details	24
3.2 Varied Parameters	25
3.3 Material	25
3.4 Test Frame	26
3.4.1 Support Frame	26
3.5 Justification	27
3.6 Instrumentation	28

3.6.1 Force Path	28
3.6.2 Angles	29
3.6.3 Bolts	29
3.7 Equipment	29
4. EXPERIMENTAL RESULTS	31
4.1 Strength, Ductility, and Failure Mode	31
4.1.1 Test TP1A	31
4.1.2 Test TP2A	32
4.1.3 Test TP2B	32
4.1.4 Test TP2C	33
4.2 Connection Behavior	33
4.2.1 Test TP2A	34
4.2.2 Test TP2B	34
4.2.3 Tests TP3A, TP3B	35
4.3 Rotational Stiffness	35
4.4 Bolt Behavior	36
4.4.1 Bolt Behavior -- Two Rows	36
4.4.1.1 Full Pre-tension	36
4.4.1.2 Snug tight bolts	38
4.4.1.3 Ultimate Condition	40
4.4.2 Bolt Behavior -- One Bolt Row	40
4.4.2.1 Full Pre-tension vs. Snug-Tight	40
4.4.2.2 Failure Mode	41
4.4.3 Bolt Effect on Connection Behavior	42
4.4.3.1 One Bolt Row	42
4.4.3.2 Two Bolt Rows	42
4.5 Load Reversal	45
5. MODEL COMPARISON	47
5.1 Original Model	47
5.2 Revised Model Bolt A,B	47
5.3 Revised Model Leg A	48
5.4 Revised Model Leg B	48
5.5 Recommendation	48
6. CONCLUSIONS	49
6.1 Connection Behavior	49
6.1.1 Modal Behavior	49
6.1.1.1 Multiple Bolt Row	49
6.1.1.2 Single Bolt Row	50
6.2 Connection Qualities	51
6.2.1 Strength	51
6.2.2 Ductility	51
6.2.3 Rotational Stiffness	51
6.3 Insights	52
6.4 STRUCTR Modelling	53
7. FUTURE CONSIDERATIONS	54
7.1 Comments on Semi-Rigid Connection Design	54

7.2 Future Work	55
TABLES	58
FIGURES	61
Vita	94
REFERENCES	95

List of Tables

Table 1: Results of Theoretical Models.	57
Table 2: Testing Program: Top-and-Seat-Angle.	58
Table 3: Experimental Results.	58
Table 4: Bolt Pre-tension: Test TP2A.	59
Table 5: Bolt Pre-tension: Test TP2B.	59
Table 6: Bolt Pre-Tension: TP3A.	60
Table 7: Bolt Pre-Tension: Test TP3B.	60

List of Figures

Figure 1: Top-and-Seat-Angle Connection.	62
Figure 2: AISC Bearing Distribution on Seat-Angle (after Salmon and Johnston, 1980).	62
Figure 3: STRUCTR Model of Top-and-Seat Angle.	63
Figure 4: Plastic Mechanism for Simple Frame with Top-and-Seat-Angle Connections.	64
Figure 5: Mechanism of Critical Leg (after Chen, 1987).	65
Figure 6: Angle Rotation Relative to Bolt.	65
Figure 7: STRUCTR Models Bolt A, B.	66
Figure 8: Angle Geometry at Heel in Reference to Critical Leg.	67
Figure 9: Heel Member for STRUCTR Model Leg A.	67
Figure 10: STRUCTR Model Leg A.	68
Figure 11: Moment-Rotation and Load-Deflection Relationship: Original STRUCTR Model.	69
Figure 12: Moment-Rotation and Load-Deflection Relationship: STRUCTR Model with Bolts.	70
Figure 13: Moment-Rotation and Load-Deflection Relationship: STRUCTR Model Leg A.	71
Figure 14: Moment-Rotation and Load-Deflection Relationship: STRUCTR Model Leg B.	72
Figure 15: Initial Force Path from Original STRUCTR Model.	73
Figure 16: Ultimate Force Path from Original STRUCTR Model.	74
Figure 17: Relative Rotational Displacement of Outstanding Leg: Top-Angle vs Seat-Angle.	75
Figure 18: Cantilever Elements for Top-Angle and Seat-Angle Rotation.	76
Figure 19: Beam Moment Diagram: TP2A.	76
Figure 20: Comparison of STRUCTR Models.	77
Figure 21: Top-and-Seat-Angle Connection.	78
Figure 22: Propped Cantilever Test Frame for Beam-to-Column Connection.	79
Figure 23: Strain Gage Locations on Bolts.	79
Figure 24: Initial Yield Line.	80
Figure 25: Progressive Yield Line: Test TP2A (Full Pre-tension Bolts).	80
Figure 26: Yield Line: Single Bolt Row.	80
Figure 27: Moment-Rotation Relationships for Experiments.	81
Figure 28: TP2A : Bolt Load Increment.	82
Figure 29: TP2A, TP2B : Bolt Line Elongation.	82
Figure 30: TP2A : Bolt Bending.	83
Figure 31: TP2A : Bolt Prying.	83
Figure 32: TP2B : Bolt Load Increment.	84
Figure 33: TP2B : Bolt Bending.	84
Figure 34: TP2B : Bolt Prying.	85
Figure 35: TP3A, TP3B : Bolt Load Increment.	86
Figure 36: TP3A, TP3B : Bolt Line Elongation.	86

Figure 37:	TP3A,TP3B : Bolt Bending.	87
Figure 38:	TP3A,TP3B : Bolt Prying.	87
Figure 39:	A325 Bolt Load-Deformation Curve.	88
Figure 40:	Full Pre-tension Mode.	88
Figure 41:	Snug Tight Mode.	88
Figure 42:	Final Moment-Rotation Curve: TP2A vs.TP2B	89
Figure 43:	Moment-Rotation Hysteresis Curve: Test TP2A (Friction Tight Bolts).	90
Figure 44:	Moment-Rotation Hysteresis Curve: Test TP2B (Snug Bolts).	90
Figure 45:	Progressive Softening of Fully Tight Connection.	91
Figure 46:	Stable Stiffness of Snug Tight Connection.	91
Figure 47:	Comparison of Friction-Tight-Bolts STRUCTR Models with Experiment TP2A.	92
Figure 48:	Comparison of Snug-Tight-Bolts STRUCTR Models with Experiment TP2B.	93

Abstract

The Top-and-Seat-Angle Connection, a type of semi-rigid beam-to-column connection, is analyzed using an approach which examines the connection as a substructure comprised of individual components. Insight on how the overall connection behaves can be developed by observing force paths, component deflections and rotations, and locations of yielding.

A step-by-step, elastic-plastic computer procedure is used for theoretical study. It incorporates a line-type linear elastic structural analysis program supported by software which locates areas of yielding, updates the structure stiffness matrix, and increments the internal stresses and nodal deflections in a piecewise fashion. The connection is modelled within the structure as an assemblage of small beam type members. Several successful enhancements to the original model created a modified model which delivered a close approximation to actual behavior.

A testing program was conducted using a propped cantilever test frame. Two thicknesses of angle and two bolt configurations were used, as were two different degrees of bolt tightening. The connection was instrumented to observe force paths, component deflection, and locations of yielding.

The connection exhibited considerable strength and ductility. The bolts in the tension angle controlled the connection's behavior. Two pre-tension dependent modes of bolt behavior existed for multiple bolt row connections. Snug tight bolts performed better than full pre-tension bolts.

Chapter 1

INTRODUCTION

Beam-to-column connections in steel buildings play a major role in a structure's overall strength and stiffness. However, in many cases much of their rotational resistance is approximated or even ignored. Design occurs with the connection assumed to be purely simple (pinned) or purely rigid depending on the condition which is a closer approximation. In reality, there are no pure *rigid* or *simple* connections. The connections whose behavior falls well in between these pure conditions will be referred to as semi-rigid connections.

1.1 Semi-Rigid Connections

The reason that semi-rigid connections are approximated as rigid or simple is because of the complexities involved in using them. The moment-rotation relationship, which is the accepted *stiffness modulus* of a connection, is nonlinear making insertion into traditional structural analysis programs difficult. To further complicate matters, there are many types of semi-rigid connections, each markedly different from the last. Finally, the configurations within a certain type of connection are endless and more importantly, cannot be interrelated by mathematical functions. The types of connections that fall within the semi-rigid range are the tee stub, shear tab, end plates, web angles, header plate, and the top-and-seat angles.

1.2 Top-and-Seat-Angle Connection

This paper deals with the top-and-seat-angle beam-to-column connection, which consists of two angles framing the beam flanges (Fig. 1). The angles are fastened using bolts. Often the seat angle is fastened to the column in the shop (in some cases by welding) allowing a temporary ledge to support the beam during erection. The bolt pattern usually consists of one row of bolts on three of the four angle legs in the connection, while the seat angle's flush leg often is longer and takes as many as four rows.

There are quite a few related connections. A stiffened seat connection has a vertical stiffener welded to the seat angle to restrict outstanding leg rotation. Occasionally the top angle is replaced by a web clip near the upper flange. The top and seat angles may be combined with web angles to create a stiffer, stronger connection. In some cases, bolting is replaced with welding. This paper's concentration will be the pure top-and-seat-angle connection.

1.3 Current Design

Current design of connections is based on equilibrium, not compatibility. No moment resistance is accounted for in the tables provided. In the case of a top-and-seat-angle connection, the designer would be required to provide a shear which the connection would have to carry. Presumably, this value is found with a conventional structural analysis program with a rotational release at any beam end joined by this type of connection. The AISC Allowable Stress Design (ASD) (AISC, 1980) and Load Resistance Factor Design (LRFD) (AISC, 1986) manuals both contain tables to design the connection for a shear value.

1.3.1 Procedure

The AISC ASD and LRFD manuals both contain step-by-step, tabular design procedures, as follows:

1. Select a width of angle from column gage restrictions.
2. Using this value, along with the beam web thickness and yield strength, determine the seat angle's required thickness.
3. Using selected bolt size, type and fastening procedure, a bolt pattern is chosen from a group of six configurations depending on required capacity and column axis orientation.
4. Finally, the angle leg sizes are chosen from the bolt pattern and required thickness.

1.3.2 Background Theory

The angle thickness is based on the seat angle's moment capacity at the fillet of the outstanding leg. The critical moment is determined from assuming a bearing stress distribution across the outstanding leg. AISC has adopted an assumed stress distribution which acts at the center of the required bearing length (Fig. 2). The calculations are as follows:

$$N = \frac{P}{0.75F_y t_w} - k \geq k$$

where

$$\begin{aligned} t_w &= \text{thickness of the beam web} \\ k &= \text{outer fiber to fillet toe} \\ P &= \text{connection shear} \end{aligned}$$

determines the assumed bearing distance. The eccentricity at which an equivalent concentrated load acts is

$$e = \frac{N}{2} + ec - t_a - r_f$$

where

$$\begin{aligned} ec &= \text{erection clearance} \\ t_a &= \text{angle thickness} \\ r_f &= \text{radius of angle fillet} \approx 3/8 \text{ in.} \end{aligned}$$

Calculating bending at the critical section and using the allowable stress on solid rectangular sections bent about their weak axis, AISC-1.5.1.4.3, provides the formula for required seat angle thickness (Salmon and Johnson, 1980),

$$t^2 = \frac{8Pe}{f_y b}$$

1.3.3 Limitations

The following restrictions and intentional omissions in the AISC design should be noted:

- No moment resistance is accounted for in the design tables. In fact, since the connection is intended and designed only for shear transfer, moment resistance is undesirable and the angles are specified for flexibility.
- The design involves only one bolt row on the outstanding leg.
- There are no design guidelines for the bolts on the outstanding leg.
- Aside from specifying the need for the angle itself, no further design guidelines are given for the top angle.
- The tables only have provisions for 36 ksi angles

In this section on simple connections, the only mention of rotation stiffness are:

No ... moment resistance is considered in determining the tabulated values.

The inherent rigidity of the connection is a factor the designer should be aware of and consider where critical.

1.4 Previous Studies

Previous studies on the top-and-seat-angle connection are relatively rare, however more frequent than most other semi-rigid connections. Batho and Rathbun (Rathbun, 1936) and Johnston (Johnston and Mount, 1942) conducted experiments in the 1930's and 40's on riveted top-and-seat-angle connections. The work published in 1947 by Hechtman and Johnston (Hechtman and Johnston, 1947) was a thorough study of the parameters which affect the rotational flexibility. Radziminski and Azizinamini (Radziminski and Bradburn, 1984) published work on both static and cyclic testing of the top-and-seat-angle connection. This paper contains several important observations including the stiffening effect on the connection by the seat angle coming into bearing with the column on load reversal. Key parameters of the connection's response were identified as the bolt gage, angle thickness, and beam depth. Recently, a step-by-step, elastic-plastic computer model (Driscoll, 1987) was developed. This model will be discussed in detail in the next chapter. Chen and Kishi (Chen, 1985), in addition to some important work on semi-rigid effect on structures in general, and the development of a semi-rigid connection database (Kishi and Chen, 1986), recently produced work on the moment-rotation relationship of the top-and-seat angle connection (Chen and Kishi, 1987). The procedure analytically formulates an initial stiffness and ultimate capacity of the connection by assuming a mechanism developed in a previous study (Azizinamini, et al., 1982) and using a mechanics of materials approach on the connection. The procedure is attractive because it does not require empirical results, but it is iterative in nature.

1.5 Research Program

The current study was undertaken in three parts. Initially a literature survey was conducted on all existing works in the area. A theoretical analysis of the connection followed, which included the development of a mathematical model for the connection's response. Finally, full-scale testing was performed to expand the knowledge base on the connection and verify and calibrate the analytical model.

Chapter 2

THEORETICAL STUDY

2.1 Modelling Philosophy

Following a thorough literature survey on semi-rigid connection research (Chasten, 1987), it became apparent that development of an analytical mathematical computer model was the proper way to proceed. Because of the many configurations, empirical curve fitting involves a great deal of experimentation, while tables and charts become cumbersome. A rational computer model would not only overcome these obstacles, but would have the potential to be implemented directly into a structural analysis package.

2.1.1 Common Practice

Most analyses of connections involve treating the connection as a global unit linking a column to a beam. This method produces one number, a rotational stiffness. While compact in its information, it allows no inference on internal response of the somewhat complicated connection. The other tendency has been to study the connection using finite element methods. The exact opposite situation arises: the degree of detail of the connection is very high, but the volume of data makes it difficult to process into meaningful, concise conclusions. Furthermore, in this situation, finite element methods are too involved and expensive to be implemented by building designers, thus limiting this type of analysis to research.

2.1.2 Component Modelling

The rational model's underlying principle is to break the connection into a small number of structural components. A force path through the connection is obtained from the model, enabling the researcher to understand more fully the support provided by the connection, while giving the designer guidelines for fastener requirements. The individual rotations and deflections of the components allow the researcher to visualize the behavioral mechanics of the connection. Breaking the connection into a handful of components allows the engineer to comprehend the behavior of the connection with a manageable amount of data.

2.2 STRUCTR Model

Using this idea of modelling connection components, Driscoll¹ developed an elastic-plastic analytical procedure using a line type structural analysis computer program, STRUCTR.

2.2.1 Topology

The analysis involves modelling the top and-seat-angle connection as a subassemblage of two-dimensional beam-type members representing the legs of the angles (Fig. 3). For compatibility, dummy rigid members running from main member centerline to the angle were inserted to represent spatially the half-depth of the main members (beam or column). Thus the action of the angles would occur at the extreme fibers of the main members. Main member refers to either the beam or column connected by the top and seat angle, whether in the computer model or in the actual test frame. The angle members run from the heel to the center of the inner bolt line and have the cross-sectional

¹Professor of Civil Engineering, Lehigh University, Bethlehem, PA 18015

properties of the actual angle. The entire assemblage of beams, columns, and angles is analyzed as a rigid frame. (Driscoll, 1987)

2.2.2 Procedure

The procedure is step by step in fashion, wherein the original rigid frame is loaded, and upon reaching a location of yielding, the stiffness at that location is modified. Then the process continues from that point; in other words, the internal forces and deflection incurred by the first loading on the original structure remain while the program loads the new (once yielded) structure until the second occurrence. This procedure repeats until a mechanism is formed in the structure.

2.2.3 Assumptions

The original model was created with the intent of serving as a guide and easy educational tool for engineers to help them in understanding the connection's behavior. Therefore, there are several assumptions made by the model, many of which would not be found in a finite element analysis. They are as follows:

- Plane sections remain plane. This allows dummy rigid members to define extreme fibers of main members.
- No bending occurs in the angle from the inner bolt line to the outer edge of the angle. This allows angle member to run from the heel to the first bolt line.
- A rigid connection exists at the bolt. This allows rigid interface between the angle and main members.
- No local bending of the column flanges.
- Perfectly plastic behavior. This allows yielding to be simulated by placing an internal hinge at the location of yielding.
- No prying action occurs at the end of the angle legs.

2.3 Theoretical Work

A virtual work analysis based on the mechanism obtained from results of early STRUCTR runs was used to perform a parametric study to assess the strength capacity and end moment developed at ultimate by the top-and-seat-angle connection (Fig. 4). If we define

$$L_1 = g_t - t_t$$

$$L_2 = d_b + \frac{t_t}{2} + \frac{t_s}{2}$$

where

$$g_t = \text{gage to first bolt row, top angle}$$

$$t_t = \text{thickness of top angle}$$

$$t_s = \text{thickness of seat angle}$$

$$d_b = \text{depth of beam .}$$

It can be seen from Figure 4 that the relationship between the virtual displacements is

$$\Theta_1 = \Theta \frac{L_2}{L_1} .$$

Equating internal work with external work,

$$W_i = W_e$$

$$2M_{pt}(\Theta + 2\Theta_1) + 2M_{ps}\Theta + M_p(2\Theta) = \Theta \frac{L_c}{2} P_u$$

where

$$M_{pt} = \text{plastic moment of top angle} = \frac{1}{4} b_t t_t^2 \sigma_y$$

$$M_{ps} = \text{plastic moment of seat angle} = \frac{1}{4} b_s t_s^2 \sigma_y$$

$$M_p = \text{plastic moment of beam} = \sigma_y Z_x$$

$$b_t = \text{width of top angle}$$

$$b_s = \text{width of seat angle}$$

$$\sigma_y = \text{yield stress of member}$$

$$Z_x = \text{strong axis plastic modulus of beam}$$

$$L_c = \text{clear span of the beam.}$$

Substituting the virtual displacement relationship, cancelling and grouping terms, yields

$$P_u = (4 + 8\frac{L_2}{L_1})\frac{M_{pt}}{L_c} + 4\frac{M_{ps}}{L_c} + 4\frac{M_p}{L_c}$$

Recognizing P_o , the load that would form a plastic hinge in a simple span beam as

$$P_o = 4\frac{M_p}{L_c}$$

then a non-dimensionalized expression for the added capacity delivered to the beam by a given top-and-seat-angle is

$$\frac{P_u}{P_o} = (1 + 2\frac{L_2}{L_1})\frac{M_{pt}}{M_p} + \frac{M_{ps}}{M_p} + 1 .$$

It was the results of a parametric study using this analysis that were used later to design the test specimens and frame. Though only a pilot for the later work, the study's findings are very accurate when compared to later test results.

A comparison of our model with previous experiments (Hechtman and Johnston, 1947, Yusof, 1986), showed a slight overestimation of the initial stiffness and a large underestimation of the ultimate strength. It was surmised that the inaccuracies stemmed from the flexibility (both rotational and translational) of the angle-column interface at the bolt line, which was not accounted for in the initial model (See Sec. 2.2.3). This flexibility would soften the initial slope of the load-deflection curve and also would tend to relieve the bending stresses in the angle's critical leg, allowing the connection to achieve a greater ultimate strength. The *critical leg* is defined as the region in the tension angle from the inner bolt line to the heel (Fig. 5). Likewise, the inner bolt line on the column face of the tension angle is referred to as the *critical bolt line*. The outer bolt line on this face, if any, is referred to as the *secondary bolt line*.

Azizinamini (Azizinamini, et al., 1982) noted this as the region involved in the collapse mechanism of the top-and-seat angle connection. Exactly where this leg extends and how it changes through the life of a connection are discussed in Sections 2.4.2 and 4.2.

2.4 Model Modification

Coincident with the conclusion of the second experiment was an attempt to incorporate this bolt line flexibility into the model. Modelling this effect is not trivial, especially if the simplicity of the original model is to be preserved. Several options have been explored.

2.4.1 Bolt Members

The first group of options involves including the bolt within the model. Accurate axial stiffness can be incorporated easily enough using data from bolt tensile tests. However, the key is to choose proper length and rotational properties of the bolt. While the bolt itself has a specific length, much of that length is not involved in the structural interface. If it is assumed that the portion of the bolt at the nut connects rigidly with the member, then the determination is how much of the bolt is active in controlling the deflection of the angle. There exists a one-sixteenth to one-eighth oversize in diameter of the bolt holes, so one cannot assume that the bolt remains perpendicular to the member with which it is connected except at the aforementioned nut-member contact point (Fig. 6). Ideally, the bolt, if pretensioned, will not initially elongate until the clamping force on the plates is overcome (Douty and McGuire, 1965). Theoretically, there is no bolt bending prior to the bolt pre-tension being overcome since the plates that define the bolt's shape are clamped parallel to each other (Fisher and Struik, 1974). Furthermore, the bolt head does not behave rigidly with the shank, allowing rotations of the plate greater than that

of the bolt shank. It has been observed in the experiments that at excessive deformation the inner half of the bolt head yields and rotates while the other half remains relatively horizontal. This is important to note, since it is the bolt head which controls the rotational orientation of the angle. The final consideration is indirectly noted earlier in the section. The model must somehow simulate the dormancy of the bolt's axial response until the tensile force on the bolt exceeds the pretension.

2.4.1.1 Model Bolt A

This model included bolts in the tension angle only (Fig. 7). The bolt member ran from centerline of the flange to centerline of the angle. The bolt's modulus of elasticity was taken from tensile tests as 1.13 times larger than the value for the structural steel. The cross-sectional properties were those of the two bolts making up the bolt row:

$$A = 2 \times (\text{area of bolt}) = \frac{\pi d^2}{2}$$

$$I_x = 2 \times (\text{inertia of bolt}) = \frac{\pi d^4}{32}$$

The axial degree of freedom was restrained until the pretension was overcome. This was handled similarly to the resetting of boundary conditions after the occurrence of an internal plastic hinge (See Sec. 2.2.2). When a critical value is achieved in a bolt member, instead of inserting a hinge which is the case when a plastic moment occurs in an angle member, the axial material property identification is changed from rigid material to bolt material. The bolt's rotational flexibility was allowed from the onset. The value to overcome pretension for the the experiment with full pre-tension, for example, was $2 \times 0.7F_u$ or, 100 kips. Even though there were 4 bolts on a face for most of the experiments, it was assumed that the critical bolt row would carry all the load until this pre-tension was overcome (See Sec. 4.4.3).

2.4.1.2 Model Bolt B

The second model also contained bolt members on both interfaces of the tension angle, but additional bolt members were added on the beam interface of the compression angle (Fig. 7). This was done because there is some relative rotation between the beam flange and the compression angle outstanding leg. Since the bolt between the seat angle and the beam is in compression, only the bolt's rotational flexibility is brought into play. The compression angle flush leg bears against the column flange outstanding leg and does not require bolt flexibility.

2.4.2 Critical Leg Adjustment

The second way to account for the bolt line flexibility is to adjust the critical leg distance to the location of contact between the angle and the member. If the bolt line is pulling out and rotating, there still exists a location, farther up the angle where contact with the main member begins. It has been shown in experimental work that this surface migrates as the tension increases in the outstanding angle (See Sec. 4.2.1). Using the location of yield lines observed in this experiment, this leg has been taken empirically as one diameter from the center of the bolt line in one of the revised STRUCTR models (See Section 2.4.2.2).

2.4.2.1 Model Leg A

This model incorporated the bolt members of Bolt Model B; however there were two adjustments to the angle's configuration, a heel member and an additional angle member located between the critical and secondary bolt line.

As can be observed by examining a cut through a standard angle shape (Fig. 8), the region at and near the fillet has a variable thickness which is, at

every point through this region, larger than the nominal angle thickness. Since this is a small region, it was originally ignored and all previous models had angle members of constant cross-section. However, when considering that this enlarged section makes up about 30% of the critical bending leg, it seemed prudent to include it in the model. Using the observations from experiments and previous structural models, an additional *heel member* was inserted in each angle (Fig. 9). The heel member was oriented on the leg where the fillet hinge had occurred in previous analyses, correctly adjusting the critical leg length. In the other direction, the fillet was given infinite bending capacity because a hinge will only form on only one of the fillet's boundaries. The heel itself was also given infinite bending capacity.

The second adjustment was to add an additional angle section from the critical to secondary bolt line on the critical leg only (Fig. 10). This corrected the unrealistic rotation allowed when the critical bolt line's pretension was overcome. This extra section would remain infinitely flexible until the first row's pretension was overcome. In other words, a perfect contact surface was assumed between this second angle section and the column flange initially, and therefore, it would have no stiffness contribution to the structure until the critical bolt line separated from the column.

2.4.2.2 Model Leg B

This model was spawned from test observation. In all, two bolt row experiments, with either fully pre-tensioned and snug tight bolts, the yield line at the critical bolt line formed beyond the critical bolt line. This is a result of a combination of the bolt rotation and slight bolt elongation. With this in mind, Model Leg B was created. It resembles Model Leg A except that the angle segment beyond the critical bolt line extends only a short distance (to the point

of contact with the column flange). There is no bolt member at this connection, of course, and the angle is given infinite capacity at the bolt line to allow the yield line to form at the node beyond the bolt line.

2.5 Theoretical Results

The original and modified STRUCTR model analyses were performed for the top-and-seat-angle connection using 1-1/8 inch and 7/8 inch thick angles containing two bolt rows. The analyses were performed using a surrounding frame in both a propped cantilever and cantilever situation. These structural analyses were patterned after the testing program.

2.5.1 Hinge Occurrence

The results of the structural analyses are returned to the user in the form of a tabular sequence of forces and deflections, one for each location of a stiffness change. The calculations are assumed to be linear between points. Using these results, a step-by-step history of the *structure's* response can be created using the load-deflection relationship. Likewise, a similar history of the *connection's* response is provided by the moment-rotation relationship. The following sections describe the results of the analysis for each type of model. The joint being modelled in each case is the top-and-seat-angle connection from test TP2A (See Sec. 3.2): Two bolt rows per leg; fully pre-tensioned, 1" A325 bolts; 7/8" thick, 50 ksi angles; propped-cantilever test frame.

2.5.1.1 Original Model

Figure 11 shows the hinge sequences, load-deflection, and moment rotation relationships obtained from the original model (This is the unmodified model which is described in section 2.2. The first hinge, which occurs moderately early is at the bolt line of the critical leg (Point A). This is followed some time later with a hinge at the tension angle heel (Point B). After a large

additional loading accompanied by a disproportionately small additional moment, a hinge at the outstanding leg bolt line (Point C) occurs, followed closely by a hinge on the seat fillet (Point D). Finally, a plastic hinge under the load forms (Point E).

2.5.1.2 Models Bolt A, Bolt B

Figure 12 shows the hinge sequence, load-deflection, and moment-rotation relationships for models Bolt A and Bolt B. The order and time of occurrence are basically identical for these models. The first hinge forms at the tension angle heel (Point A) as opposed to the formation at the critical bolt line in the original model. A large load and moment increase occurs until the pretension is overcome on the critical leg bolt row. In both cases, the angle yielded at this location almost immediately after pretension was overcome (Point C). Then, after a large load increase with relatively no moment increase, the seat angle yielded at the heel (Point D). The final hinge was the plasticity under the load (Point E). The difference in hinge formation can be attributed to the rotational flexibility in the bolts which keeps the connection from yielding at the bolt lines. Instead, the large moments are redistributed to the angle heel which cannot accomplish the deflection of the flexible angle ends without yielding. This bolt line flexibility retarded the formation of a hinge in the column bolt line and completely eliminated the hinge at the beam bolt line.

2.5.1.3 Model Leg A

Figure 13 shows the hinge sequence, load-deflection, and moment-rotation relationships for Model Leg A. Because of the increased section at the heel, the first limit reached is the critical leg's pretension (Point A). Where in previous models, this would allow the angle at this bolt line to move quite flexibly, the added angle member provides the actual stiffness that the critical bending leg would feel from the rest of the angle. This causes the hinge to occur at the

released bolt line (Point B). Shortly afterward, the region near the heel yields (Point C). As in the other models, this is where the connection loses a good part of its rotational resistance. The joint rapidly allows rotation while a very slight moment increase occurs; the tension angle-beam interface bolt line reaches the pretension force (Point D) and then after a very large increase in load, the beam forms a hinge under the load (Point E).

2.5.1.4 Model Leg B

Figure 14 shows the hinge sequence, load-deflection and moment-rotation relationships for Model Leg B. The model is not very accurate for stiffness, however it is extremely accurate for ultimate strength. The stiffness error is believed to be a result of the difficulty of modelling a contact surface in the simple line-type structural analysis computer program. The strength accuracy stems from the empirical critical leg length, which provides the proper moment arm.

2.5.1.5 General Model Characteristics

There are quite a few behavioral traits shared by all the models. Note that there is very little stiffness change in the connection until after the first few hinges have occurred. After the critical leg has hinged at both ends, the connection loses most of its rotational capacity.

2.5.2 Force Path

The initial (elastic) force path for the original model is shown in Figure 15. The force path gives one an idea of the completely different function of the two angles. The angle on the compression side of the beam is pushed into the column flange with the outstanding leg providing the rotational stiffness. The tension angle, on the other hand, uses both legs to partially resist rotation. According to the structural model, the tension angle carries more of the shear

reaction than the seat angle, which is opposite of what is implied by current design (See Sec. 1.3). An explanation as to why this occurs is offered (Hooper, 1987). The seat angle's outstanding leg rotates an amount equal to the beam's end rotation, θ_{end} . The top angle does the same, however, since the tension angle heel is being pulled out, it rotates upward about the first bolt line by an angle ϕ_{flush} (Fig. 17). Therefore, to follow the beam's end rotation, the top angle's outstanding leg must rotate an angle whose value is the summation of the beam's end rotation and the flush angle leg, $\alpha = \theta_{end} + \phi_{flush}$, thus attracting a larger force (See the example on the following page). At ultimate (Fig. 16), the vertical shear increments are now evenly distributed between the top angle and the seat angle. The force symmetry is an effect of the hinge formation which eliminates the unequal rotation restraint.

By using small displacement assumption, ignoring the smaller moment in the angle at the outstanding bolt line (for both the top and the seat), and using assumptions from in section 2.2.3, the forces can be approximated as shown acting in Fig. 18. Examining Fig. 18b, it is seen that the seat angle rotates an amount equal to the beam's end rotation, θ_{end} , due to the proportion of connection shear, V_s , which is carried through the seat. As can be seen in Fig. 18a, the flange force and a moment from the eccentrically applied top angle shear cause a rotation at the end of the flush leg. The outstanding leg is acted upon by the proportion of the connection shear, V_t . If we recognize that α is the relative rotation of the outstanding angle leg to the flush angle leg, the equation for α can be rewritten:

$$\theta_{outsflush} - \phi_{flush} = \theta_{end}$$

In order to establish to what proportion these shears are distributed, the following example will be provided, using geometries and force values from one of the experiments (TP2A):

The angle legs are modelled as cantilever elements. From virtual work, the end rotation is

$$1 \cdot \theta = \int_0^l \frac{Mm}{EI} dx$$

For the case of the seat angle (Fig. 18b),

$$\theta_{end} = \int_0^g \frac{g(V_s x)(1)}{EI} dx = \frac{V_s g^2}{2EI}$$

$$\rightarrow V_s = \frac{2EI}{g^2} \theta_{end}$$

The rotation of the top angle is composed of two terms (Fig. 18a),

$$\phi_{flush} = \int_0^g \frac{g(Fx)(1)}{EI} dx + \int_0^g \frac{g(V_t g)(1)}{EI} dx = \frac{(F - 2V_t)g^2}{2EI}$$

$$\theta_{outs} = \int_0^g \frac{g(V_t x)(1)}{EI} dx = \frac{V_t g^2}{2EI}$$

Using the relative angle relationship,

$$\theta_{end} = \frac{V_t g^2}{2EI} - \frac{(F - 2V_t)g^2}{2EI} = \frac{(3V_t - F)g^2}{2EI}$$

$$\rightarrow V_t = \frac{2EI}{3g^2} \theta_{end} + \frac{1}{3}F$$

Now, if a relationship for F , the flange force, can be derived, it will be possible to approximately compare V_t and V_s . At this point, experimental data is required. The %rigidity of the connection in experiment TP2A was approximately 40%. On the following page, this empirical value will be used to evaluate V_t .

In symbolic terms, this percentage is

$$\frac{M_{end}}{M_{mid}} \times 100 = 40$$

Examining Fig. 19, it is seen that

$$M_{end} = Fd$$

$$M_{mid} = \frac{PL}{4} - Fd$$

Inserting these relationships into the symbolic equation,

$$\frac{Fd}{\frac{PL}{4} - Fd} = 0.4$$

$$F = \frac{PL}{6d}$$

From the test frame geometry (Fig. 19),

$$P \approx \frac{1}{2}(V_t + V_s)$$

and

$$\frac{L}{d} \approx 10$$

These two relationships, combined with the previous equation, yield

$$F \approx 1.67(V_t + V_s)$$

Substituting this value for F in the equation for V_t gives

$$V_t = \frac{2EI}{3g^2} \theta_{end} + \frac{1.67(V_t + V_s)}{3}$$

Inserting the relationship for V_s and regrouping,

$$V_t - 0.5567V_t = 0.333V_s + 0.5567V_s$$

$$0.4433V_t = 0.8899V_s$$

$$\rightarrow V_t \approx 2V_s$$

2.5.3 Moment Capacity

The results showed the angle develops 17.8% of the beam simple plastic moment at ultimate in the original analysis. Models Bolt A and Bolt B developed a slightly higher value of 22.9% in the modified analysis. This can be attributed to the relieving of the bending stresses in the angle's critical section. Model Leg A developed 28.6% of the beam's simple plastic moment while Model Leg B achieved 42.9%. A complete summary of the STRUCTR results is presented in Table 1.

2.6 Model Comparison

Figure 20 shows a plot of the moment-rotation relationship for the five models. The first segment of each curve represents the pure cantilever initial portion of loading (See Sec.3.4.1). The original model, as expected without bolt flexibility, has the highest initial stiffness. The two bolt models are initially more flexible due to the bolt's small rotational freedom (Region A). The bolt model's stiffness lowers by a large amount in the next portion while the leg model's reduction is slighter (Region B). This is due to the additional member in leg model A. When the pretension is overcome at the critical bolt line, this model is able to provide the actual stiffness this area receives from the remainder of the angle beyond the critical bolt line. In the bolt models, the bolt line rotates and elongates with an unrealistic complete freedom. The bolt models achieve a greater ultimate moment than the original model because the critical leg mechanism occurs later due to the bolt's flexibility relieving the end conditions (Region C). Model Leg A achieves an even greater ultimate moment because the increased cross section at the fillet is recognized. Model Leg B is the most accurate for strength prediction because the critical moment arm is taken from empirical observation. However, the inability to correctly model the contact surface creates unrealistic stiffness.

Chapter 3

TESTING PROGRAM

3.1 Experimentation Details

The testing program for the top-and-seat-angle connection consisted of six separate full-scale tests experiments. The connection was on the strong axis of the column; in other words, connected to the column flange. All bolts had one washer and there were no shims between the angle and main members. All angles were cut to a width to match the beam flanges, ten inches. The beam's erection clearance was one-half inch.

The angle configurations were the same for the first four tests (Fig. 21a): each angle leg contained two rows of two bolts; the bolts were spaced five inches apart, the rows spaced at three inches; the distance from the heel to centerline of the first bolt line was also three inches. The tests were designed, with the help of the parametric study (See Sec 2.3), so that the bolts would retain their load carrying capacity throughout the usefulness of the test. They were all cyclically loaded, though more to determine shakedown effects (Sourochnikoff, 1950) than to observe seismic response.

The final two experiments used connections which had only one row of bolts on the critical leg (Fig. 21b). To carry the additional force per bolt, the diameter was increased from 1 inch to 1-1/8 inches. In this case, it was not possible within the design constraints to eliminate bolt fracture as a failure mode. These tests were monotonically loaded.

3.2 Varied Parameters

The parameters which were varied through the testing program were the thickness of the angles, the number of bolt rows on the critical leg, and whether the bolts were *friction tight* or *snug tight*. Table 2 contains a complete description of the testing program. In the first experiment, test TP1A, the angle thickness was 1 1/8 inches. The reason for the extreme thickness of the first angle was that it was not certain how the angles would perform in a frame of the size used (See Sec. 3.4.1). As it turned out, the angles were too strong. The next two tests, TP2A and TP2B used 7/8 inch angles. Tests TP1A and TP2A contained friction tight bolts, while TP2B and TP2C had bolts which were tightened to the snug condition. The bolts were 1 inch, A325. Friction tight refers to bolts tightened to the required prestress for a tensile connection, $0.7F_u$, where F_u is the ultimate tensile strength of the bolt. This is also referred to as *fully pre-tensioned*. Snug tight is loosely defined as "enough to pull the two plates together", ideally performed by one worker with a spud wrench. In our case, $0.7F_u$ is 50 kips. It was determined that the snug tight bolts carried a pretension of about 20-25 kips or about $0.3F_u$. The final tests, TP3A and TP3B, were identical to the TP2 series, except that only one bolt row was used on the critical leg. These bolts were A325, 1-1/8 inch in diameter.

3.3 Material

All the steel used in the frame with the exception of the base beam was A588, 50 ksi steel. This includes the connection detail material itself. The bolts in all tests were A325, 1 inch or 1-1/8 inch diameter, high-strength bolts.

3.4 Test Frame

Most past connection tests have been performed in a "T" shaped frame where the beams act in a cantilever mode. This cantilever action causes high moments with unrealistic shear for a building frame situation (Chasten, 1987). Bolt strength, which is affected by shear-tension interaction (AISC, 1980), will be different for connections in cantilever frames than for building frames.

3.4.1 Support Frame

For the reasons of the previous paragraph, a propped cantilever test frame was designed and built (Fig. 22). The pin action was developed by allowing the free end of the beam to bear against a horizontal roller housed in a channel tower. Arriving at a frame which developed a large enough moment at the end before the beam reached its plastic moment in the middle, and which was able to withstand a large upward moment and axial force at the column base was quite a task. A suitable design located the load almost at center span, the span being 19 feet from column to the prop. Attached to the column were two braces, one below the beam to aid in resisting upward axial force, the second above the beam to provide extra rotational stiffness in the column for beam end moment increase. The pins were moved 3/4" from the initial resting position of the beam to allow a small initial cantilever action to occur. This, in turn, developed a large initial moment at the connection.

Not all of the tests were performed with the prop in place. For comparative data, test TP2C was conducted in a pure cantilever frame. Otherwise, it was identical to test TP2B. The TP3 series was also conducted as a pure cantilever and the loads were applied monotonically.

The main members were quite massive. The column was a W14x193 and the beam was a W27x94. This is believed to be the deepest beam ever used in a top-and-seat-angle test.

The loads were applied cyclically using a 5 million pound testing machine² from above and a 400 kip railroad jack from below. The beam was prevented from out-of-plane torsional buckling with a lateral bracing system.

3.5 Justification

There are a few characteristics of this testing program which differ from current practice in industry:

- The top-and-seat-angle connection is not normally used on sections as large as in the experimentation.
- 50 ksi steel is almost never used for detail material.
- 1 1/8 " thick angles are not used for this connection.
- 8" x 8" angle legs are not used for this connection.
- Two rows of bolts are not used on the outstanding leg.
- Symmetry about the top and seat is not common practice.

In defense of all these deviations from common practice, it is to be noted that this study is not an industrial test to add information on the current design situation. Rather, it is an experimental effort to view this connection in a completely different light, that is, as a moment-carrying structural member. Along these lines, the decisions to use details contrary to usual procedure were made in the best interest of expounding the untapped resources of this connection.

²Tinius-Olsen machine located at Fritz Laboratory, Lehigh University

3.6 Instrumentation

The configuration of the instrumentation was based on the component model discussed in Section 2.1.2. The connection was gaged to acquire data on planar component deflection. Strain gages were mounted to the main members to determine force path data. For the component behavior, a combination of linear measuring devices was used to supply geometric data to quantify the kinematics. These devices measured deflection at the bolt line normal to the column face to determine flexibility at the bolt line, both at and in between the bolts; the angle's deflection at certain points (enabling the calculation of angular rotation of the angle legs); separation of the angle from main members at key locations; and slip of the angle along the members. The beam at the connection was monitored at two locations to find the center of rotation.

For the overall frame response and global representation, the deflection under the load and the rotation at the connection were measured. Strain gages were applied to the channel prop section and the column braces to determine the redundant forces.

3.6.1 Force Path

Strain gages were mounted on three cross-sections of the beam to find the moment diagram. Only data from two cross-sections is required to determine the moment diagram, however, due to previous load cell calibration uncertainties, a redundant reading was desirable. The column was gaged above, below, and in between the angles. This was done not only to develop axial and bending moment diagrams, but also to examine the vertical shear distribution between the angles.

3.6.2 Angles

Strain gages were mounted on the angles, however it was only possible to mount the gages on one outer face per cross-section because the other side was flush with a main member flange. This obviously did not allow a strain diagram through the section to be obtained, but it gave an idea of relative strains between sections of angle separated by bolt lines. In a forthcoming experiment, the angle is to be gaged on both sides of the cross-section (in a milled recess) to determine the actual forces travelling through sections of the angle. Unfortunately, results of this experiment will not be available before the completion of this paper.

3.6.3 Bolts

The bolts were instrumented by machining flat surfaces opposite each other in the shank. The wires were run from the gage through the head of the bolt to avoid being crushed in bearing (Fig. 23). The bolts were positioned in two ways. Most were placed with the gages in the direction of the force, enabling the bending strain gradient to be read. A handful were oriented with the gages perpendicular to the bending. These, though only giving information on the average axial strain, were used to check the first orientation's susceptibility to the gage being crushed by the plate.

3.7 Equipment

The equipment used was standard. For deflection, Linear Voltage Deflection Transducers, and one-thousandth and ten-thousandth inch dial gages were used. The rotation readings were obtained from Sperry Tiltmeters. Ordinary half-bridge strain gages were used on the beam, columns, angles and bolts. The load was measured with a Strainsert load cell.

The data were gathered and initially processed with a MEGADAC 2300C data acquisition system.⁸ Using an Ethernet network, the data were quickly transferred to a Microvax system where support software and plotting packages were used to process the data.

⁸256 channel/20,000 Hz data acquisition system developed by Optim Software, Inc.

Chapter 4

EXPERIMENTAL RESULTS

4.1 Strength, Ductility, and Failure Mode

The top-and-seat-angle connection exhibited remarkable strength and considerable ductility in the tests. It should be noted, that for reasons discussed in Section 4.5, all results reported refer to the upward loading unless otherwise indicated. The experimental program included: test TP1A -- 1 1/8" angle thickness and friction tight bolts; test TP2A -- 7/8" angle thickness and friction tight bolts; test TP2B -- 7/8" angle thickness and snug bolts; test TP2C -- pure cantilever test of specimen identical to TP2B; test TP3A -- identical to TP2B except containing only one row of larger bolts and monotonical pure cantilever loading; test TP3B -- identical to TP3A except bolts were fully pre-tensioned. Hysteresis curves are presented in Section 4.5, while moment-rotation curves are presented in Section 4.3.

4.1.1 Test TP1A

The first test was halted due to test frame limitations at a load of 400 kips with the top-and-seat-angles connection still intact. The beam had reached a partial plastic hinge underneath the point load. Despite the frame related stoppage, the connection did achieve approximately $3\Phi_Y$ while remaining intact, where Φ_Y is the rotation at initial yielding of the connection. A thinner angle was proposed for the next tests because of the unexpected strength of the connection.

4.1.2 Test TP2A

When the 7/8 inch angle was used in test TP2A, the test achieved a load of 404 kips, while the moment under the jack was approximately 22,000 k-in, or about 1.2 times the beam's simple plastic moment. The bolts in the critical leg broke at 400 kips, introducing a dynamic impact which snapped a lateral brace. Even so, the connection performed for two more load increments and during the unloading. The bolts were then replaced and the connection was loaded in the opposite direction until failure. The test was stopped because of local yielding in the beam flange under the load, despite the stiffeners located at that point. At that point a rotation of approximately $3\Phi_Y$ was achieved. The stiffness curve of the connection had reached a plateau as shown in Fig. 27.

4.1.3 Test TP2B

Test TP2B achieved a load of 409 kips and a maximum moment under the jack of 26,000 k-in or 1.4 times the beam's simple plastic moment. As in test TP2A, the connection was ductile enough to allow a plastic hinge to form under the load, and the test was concluded due to the local yielding under the load. The rotation achieved at the test's conclusion was approximately $2.5\Phi_Y$. It should be noted that if the connection were actually pinned, the load to cause a plastic hinge in the test frame would be 295 kips. In other words, the partial restraint of the top-and-seat-angle connection permitted a 40% increase in the load carrying capacity of the beam.

4.1.4 Test TP2C

Test TP2C was identical to TP2B in every respect except the beam was supported in a pure cantilever mode to try to fail the connection. In both directions the load-deflection curve reached a long, flat plateau. The connection did not fail and the test concluded because the jack stroke reached its limit.

4.2 Connection Behavior

The connection stayed linear well into its loading: 378 kips in test TP1A, 325 kips in test TP2A, and 354 kips in test TP2B. While this occurred, the seat angle, in compression against the column, slid slightly down the column; the tension angle separated from the column by a hairline in the region between the critical bolt line and the heel. The second region of behavior involved a slightly softer load-deflection slope; the head of the critical bolts rotated very slightly in the direction of the tension angle's movement away from the column face and some minor flaking of the mill scale occurred in the tension angle. In the final region of response, the bolts in the critical row elongated noticeably. The angle heel was now about 1/8 to 1/4 inch off the column and the separation traveled almost halfway between the two bolt lines. The bolts were now visible and curved in the space behind the angle. The flaking in the tension angle had turned into full-fledged bands of yielding about 1/2" thick across the angle (Fig. 24). Location and order of occurrence of these yield lines are dependent on factors which are discussed in Section 4.4.3. Comparison of order of occurrence to the computer analysis can be made by reviewing section 2.5.1. Yielding also initiated in the seat angle. It was in this region that the stiffness curves flattened dramatically. There was considerable bolt slip throughout the test. It occurred in two cases. First, at high loads, when virgin territory was reached and second, at low loads during reversal in later cycles.

4.2.1 Test TP2A

In the case of pre-tensioned bolts, at a load of about 175 kips, slight flaking occurred at the critical bolt row. At approximately 310 kips, the bolt pre-tension was exceeded and the bolts in the critical line elongated and rotated slightly, causing the critical leg length to increase. The corresponding larger moment arm caused the first yield line to occur just beyond the bolt line. This plasticity caused a redistribution of higher forces to the outstanding leg fillet. As this yield line allows the flush leg to rotate, a yield line in the heel of the tension angle must form to follow the beam's end rotation. This freedom in the tension angle allowed the beam to rotate more and redistribute some of the force to the seat angle. It was there that the final hinge occurred (at the seat angle's outer fillet) due to the seat angle's outstanding leg rotation. What was interesting to notice during the experiment was the progressive yield lines caused by the elongating bolt row. Initial flaking occurred at the bolt row; the first yield line appeared directly beyond the critical bolt row; the final yield area occurred just in front of *secondary* bolt row (Fig. 25).

4.2.2 Test TP2B

In the case of snug tight bolts, light flaking near the bolt line occurred at about 175 kips. At 290 kips, flaking was taking place in front of the second bolt line. A full yield line did not appear until 380 kips, and it was located a full diameter beyond the center of the critical boltline (See Fig. 24). The yield line at the tension angle's outstanding leg fillet occurred later than in the full pre-tension tests (390 kips).

4.2.3 Tests TP3A, TP3B

Both single row tests basically behaved the same, and their behavior will be presented jointly in this section. The yield line formed on the critical bolt line (Fig. 26), as opposed to all the multiple bolt row tests whose yield line(s) formed beyond the critical bolt line. The flaking of the yield line began later in the snug tight test TP3A, $M_{end} = 2432 \text{ k-in.}$, than in the fully-pretensioned test TP3B, $M_{end} = 1688 \text{ k-in.}$ However, both formed full-fledged yield bands at the same load, $M_{end} = 3193 \text{ k-in.}$ In both cases, at the ultimate load, $M_{end} = 4350 \text{ k-in.}$, the bolt heads broke off on the critical bolt line bolts. From the strain gage readings and the sounds at bolt fracture, it seems that one bolt broke and the second bolt followed almost immediately. The bolt fracture in both experiments was ductile.

4.3 Rotational Stiffness

The rotational stiffnesses of the connections were substantial and the beam end moment did reach a high percentage of the beams plastic moment, M_p . The initial stiffness of the tests were in this order: TP1A was most stiff, followed by TP2A, TP2B, TP3B, and finally, TP3A which had the most flexible initial response. In test TP1A, the end moment reached about $48\%M_p$; test TP2A reached $38\%M_p$; test TP2B reached $49\%M_p$; test TP2C reached $40\%M_p$; and tests TP3A and TP3B reached approximately $27\%M_p$. Note that test TP2B, identical to TP2A in every way except the degree of bolt tightening actually is a *stiffer* connection than its fully pre-tensioned counterpart. An attempt at an explanation is found in Section 4.4.3. It is also important to note that connection TP1A was not loaded to its ultimate strength and test TP2C was still able to carry additional moment when other constraints caused a stoppage of the experiment. It seems reasonable to assume that the 1-1/8" angles could

have developed over 60% of the beam's plastic moment, while TP2C was heading for $50\%M_p$ like TP2B. A plot of each tests maximum-cycle moment-rotation curve is shown in Fig. 27. For a complete description of connection behavior see Table 3.

4.4 Bolt Behavior

The bolt groups under full pre-tension acted quite differently than the snug bolts. Table 4 contains the pre-tension values for test TP2A. The bolts that did not have strain gages were tightened using the turn-of-the-nut method. Table 5 contains the pre-tension values for test TP2B. The bolts were tightened using a two-pass, inner-to-outer pattern. Table 6 contains the pre-tension values for test TP3A. Table 7 contains pre-tension values for test TP3B.

4.4.1 Bolt Behavior -- Two Rows

This section will examine the behavior of bolts in the critical and secondary bolt line of the top-and-seat-angle connection with two bolt rows. Load increment refers to the bolt axial load above the pre-tension. The cycling of loads created hysteresis curves for the bolt load increment plots. Instead of plotting bolt response versus load or end moment, this section will usually present bolt data versus flange force, where flange force is taken as the end moment divided by the nominal beam depth, ($\frac{M}{d}$).

4.4.1.1 Full Pre-tension

The bolts on the friction tight tests were pre-tensioned to $0.7F_u$ or 51 kips. The average yield load of these bolts was approximately 63 kips.

Bolt Load Increment -- Figure 28 shows the load increment of bolts from the critical and secondary bolt line. The critical bolts carry a disproportionate amount of the load. In fact, during the early cycles, the secondary bolt line carries none of the tensile force. The critical bolt's response is similar to an ordinary tensile coupon test with periods of unloading. The unloading in the actual experiment occurs when the load is reversed. The unloading curves have two slopes: The upper slope describes the bolts response as the angle travels back to its initial position against the column; The nearly vertical lower slopes pertains to the situation when on full load reversal, the original critical (tension) leg that we are examining becomes the compression angle. In this case, the bolt is only loaded in shear as there is no physical connection between the bolt head and the angle.

Bolt Elongation -- The clearest way to examine the bolt elongation is to plot it versus load step. Figure 29 shows the elongation of the critical bolt line for this series of experiments. Examining, for now, only the friction tight situation, the bolt pre-tension is overcome between load step 30 and 50. The bolt line begins to elongate noticeably at load step 105. At this load step, the end moment was calculated as 3300 k-in, which corresponds to a flange force of near 120 kips or two times the bolt pre-tension *even though there are four bolts total*. This supports the finding in the previous paragraph that the secondary bolt line of friction tight bolts does not participate. As the experiment continues, notice the inelastic elongation of the bolt line i.e., it never returns to its original position despite load reversal.

Bolt Bending -- From tensile and torque-tension tests it was determined that the yield strain of the bolts was approximately 2600 microstrains. Examining the strain gages on the tension side of the bending separately, it was

found that the critical line bolts began to yield at a flange force of 105 kips or 88% of the axial load that would yield the bolt line. This 12% reduction shows the significant effects of bending forces in bolts. A plot of bending versus flange force for the critical and secondary bolt rows (Fig. 30) shows, again, how the critical bolt row is taking the brunt of the applied stresses.

Prying -- Figure 31 shows a plot of bolt force versus flange force for the friction tight case. The vertical difference between the plot and the solid line $y = x$ represents the prying force, which is considerable. This prying force takes place at the contact surface *between* the bolt lines as will be explained in the section on connection behavior.

4.4.1.2 Snug tight bolts

The snug tight bolts were tightened with an ordinary wrench to 25 kips or $0.35F_u$.

Bolt Load Increment -- Figure 32 shows a plot of critical and secondary line bolt load versus flange force. Notice how both bolt rows share the tensile flange force, which is markedly different than the friction tight case. Also dissimilar to the friction tight test is the fact that, even though both experiments were identically loaded, the bolts show no permanent elongation until the final cycle. The critical bolt has a lower bound of its pre-tension while the secondary bolt loses almost all of its initial tightening. This is a result of different initial contact surfaces. When the critical bolt line was tightened, the faying surfaces were clamped tightly. However, when the secondary bolt row was tightened, there was an imperfect fit. On load reversal, when the angle goes into compression, it flattens against the column. Since the bolts are well within their elastic range, they will follow the angle and lose a portion of their pretension.

Bolt Elongation -- Referring back to Fig. 29, it is observed that the critical bolt line elongation for the snug-tight case does not show any excessive deformations until near the experiment's conclusion. Prior to this, the bolt line has minor deformations and returns to near its original position. However, notice that the deformations begin immediately due to the low pre-tension. Near the conclusion of the experiment, at load step 170 and a corresponding moment of 6500 k-in, the first appreciable elongations occur. This corresponds to a flange force of about 240 kips which is four times the bolt yield force. This correlates the finding in the previous paragraph that all four bolts on the critical face partake in the load carrying. Since all the bolts yield at once the elongation propagates to the ultimate condition.

Bending -- It should be expected that both bolt rows will bend more evenly and less severely than the corresponding fully pre-tensioned connection, and Fig. 33 corroborates this point. Notice, however, at low loads the curvature of the bolt rows is opposite. This is caused by the combination of low pre-stress and elastic behavior. The bolts allow the angle freedom, but do not elongate considerably. This causes a dishing effect of the angle which locates a contact surface in between the bolt lines and places the bolts in opposite curvature. (See Sec. 4.4.2)

Prying -- Figure 34 is a plot of bolt force versus flange force for the entire bolt pattern on the critical face. Again, the vertical distance from the plot and the line $y = x$ represents the prying force. This force is considerably smaller than the prying on the fully pre-tensioned connection and is also distributed to four bolts. The initial high prying force is believed to be a result of the dishing effect described in the previous paragraph. The lower prying forces in this experiment are a result of the different mode of behavior that a multiple bolt row tension

connection experiences for snug tight bolts. The two modes are described in Section 4.4.3.

4.4.1.3 Ultimate Condition

The bolt tests with two bolt rows were designed so that the four bolts would not fail throughout the entire experiment. This was the case in the snug test, in fact, the critical bolts plastically elongated to the extent that they could be spun by hand while remaining in the unloaded frame. In the friction tight test, however, the critical bolts both fractured at the ultimate condition.

4.4.2 Bolt Behavior -- One Bolt Row

This section examines the behavior of the single bolt row in the critical leg for the monotonically loaded experiments. The characteristics of these plots will be different than in the previous section because of the absence of load reversal. Since the behavior of the snug tight and full pre-tension experiments were forced to be similar for the one bolt row experiments, they will be presented together in the following section.

4.4.2.1 Full Pre-tension vs. Snug-Tight

The bolts in this experiment are 1 1/8", A325. The tightening condition was 61 kips ($0.7F_u$) for the fully tightened and 27 kips ($0.3F_u$) for the snug-tight condition.

Bolt Load Increment -- Figure 35 shows a plot of bolt load versus flange force for both tightening conditions. The curves are practically the same at the higher loads. At the low loadings, the snug tight experiment responds earlier due to its lesser pre-tension. Note that there exists a region between 60 and 75 kips of bolt load where both cases respond but at different levels. This is due to prying action and will be discussed shortly.

Bolt Elongation -- Figure 36 shows the elongation at the bolt line for the fully pre-tensioned experiment. The three curves are elongation at the two bolts and elongation of the angle at a point on the bolt line halfway between the bolts. The angle deflection between the bolts is much higher than at the bolts. This situation also occurs in the snug case for one bolt row. However, in the multiple bolt row tests the bolt line deflection was nearly rigid body motion. The bolt elongation travels inward at low loads, a phenomenon which did not occur in the multiple bolt row tests either.

Bolt Bending -- Figure 37 shows a plot of bolt moment for the two tightening cases. The bolt moment relationships of the two tightening cases are similar, however in the snug case, bending is initiated at a lower flange force. Once the pre-tension is overcome in the full case, the curves are almost identical.

Prying -- Figure 38 visually details the prying action in the two tests. The snug test exhibits low level prying almost immediately. When pre-tension is overcome for the full case, the two curves join together as was the case with the bolt bending plot.

4.4.2.2 Failure Mode

In both the fully pre-tensioned and snug-tightened cases the failure was the same. At approximately the same load the bolt heads broke off the critical line bolts. From the strain gage readings and the sounds at bolt fracture, it seems that one bolt broke and the second bolt followed almost immediately. The fracture surface in both cases was ductile.

4.4.3 Bolt Effect on Connection Behavior

4.4.3.1 One Bolt Row

The connections with one bolt row acted independently of degree of pre-tension. There were only subtle differences in response and the connections both developed the same ultimate moment and rotation. The snug test was slightly more susceptible to bending and prying at early loads.

4.4.3.2 Two Bolt Rows

The bolt groups under full pre-tension acted quite differently than those under snug-tightening. In fact, two modes of bolt-induced connection behavior exist. In the case of fully pre-tensioned bolts, the first bolt row becomes inelastic quite early. A progressive softening of the connection occurs on reversal. In snug bolts, the bolts remain linear until near the maximum capacity.

Full Pre-tension Mode -- In the case of fully pre-tensioned bolts, ideally there exists an initial perfect contact surface between the secondary and critical bolt rows. Referring to Fig. 39, which shows the force-deflection relationship for an A325 high strength bolt, a force

$$P_f = N \times F_{pr}$$

where

N = number of bolts per bolt row

P_f = flange force

F_{pr} = pre-tension force

will cause the first row of bolts to start travelling on their force-elongation curve, beginning at point A. Concurrently, the contact surface travels toward the secondary bolt line. Because the proportional limit (Point B) of the bolt is near its pre-tension value (Point A), the first row of bolts yield before the contact surface reaches the second row, i.e., before the second row of bolts begin to assist

in carrying the tensile force. Thus, the "Full Pre-Tension Mode" of multiple bolt row connections is one in which the inner bolt row deforms excessively due to an eccentric tensile force, while the remaining bolt rows do not participate (See Fig. 40). This results in a much more flexible connection and the tendency of an early yield line between the bolts.

Snug Tight Mode -- In the case of snug-tight bolts, under low loads the pre-tension is overcome, but as the contact surface is travelling toward the second bolt row, the critical bolts are deflecting along the path beginning at C. This allows the first bolt line to act elastically while the small amount of pre-tension is overcome in the secondary row. The second bolt line becomes useful and with four unyielded bolts a force of

$$P_f = 2 \times N \times F_y$$

is required to put any bolt into yield, where

$$F_y \approx F_{pr} = \text{yield load for the bolt.}$$

The deflected shape of the angle under moderate loads is close to the depiction in Fig. 41. The prying force actually occurs between the bolt lines and affects both rows. This is the dishing effect which caused the reverse curvature in section 4.2.2.

It is not surprising that the snug connection achieved greater strength and stiffness, given the two modes of behavior. Even though the critical bolt arm is only about 3 inches, it holds tremendous leverage over the beam's end rotation (Refer back to Fig. 17). The occurrence of yielding at the first bolt row in the full pre-tension case allows a considerable increase in connection flexibility.

Verification -- To verify the modal behavior, a check of proportional limit for the connection is performed. In the full pre-tension test case, a flange force of

$$P_f = 2 \times 60 = 120 \text{ kips} ,$$

which represents an end moment of

$$M = P \times d = 120 \times 27 = 3240 \text{ k-in.}$$

will cause a *full pre-tension mode* of yielding to occur. This occurs by load step 105. Note in Fig. 29, load step 105 is the location of the first excessive deflection of the bolt line. For the snug bolts, the load required for a *snug tight mode* of yield is

$$P_f = 2 \times N \times F_y = 2 \times 2 \times 60 = 240 \text{ kips}$$

which represents an end moment of 6480 k-in. This does not occur in test TP2B until loadstep 170. Refer back to Fig. 29 for verification. Note that when yielding finally does occur, all the bolts will yield at about the same time as witnessed by the rigid-plastic nature of the snug-tight curve.

Modal Effect on the Connection -- The connection with snug bolts was stiffer than the connection with fully pre-tensioned bolts. At ultimate, the 7/8 inch angle connection developed about 35-40% of the beam's M_p for fully pre-tensioned bolts, while the snug bolts reached 45-50% M_p (See Fig. 42). The lower value for the fully pre-tensioned case can be attributed to the yielding of the critical bolt line, coupled with the hinge in the angle as was shown in Fig. 40. Though only of small length, this arm holds tremendous leverage over the rotation, and hence the stiffness of the joint.

The friction tight test began with a slightly higher rotational stiffness, however, with each load reversal the connection softened considerably. This is not the case for the snug-tight bolt test. While beginning at only 75% stiffness

of its fully pre-tensioned counterpart, the snug test remained at that stiffness until the last cycle of loading. The snug test's rotational stiffness stayed linear further into the loading than the fully pre-tensioned: The fully pre-tensioned test showed nonlinearity at $0.8P_u$; the snug remained linear until $0.87P_u$.

4.5 Load Reversal

Loading in two directions had the effect of delaying inelastic behavior in the second (downward) cycle. After the loading became high enough to overcome the bolt pre-tension in the tension angle, the bolt almost immediately enters the inelastic range. When unloading occurs, the bolt contains a permanent set and the angle heel remains off the column surface. Then, when the load is reversed, a considerable portion of the opposite loading is consumed pushing the angle back into bearing against the column. This had a cumulative effect on the downward loading, which was always after the upward loading in each cycle. For this reason, connection and bolt yielding occurred much earlier during the upward direction (Fig. 43, Fig. 44).

When using friction tight bolts, the small permanent set has a propagative effect on the rotational stiffness as the connection undergoes load reversals (See Fig. 45). This is due in part to the complete change in function of the angle when the load direction is switched. This phenomenon did not occur in the snug tight connection (See Fig. 46). The cyclic fully pre-tensioned experiment experienced progressive yield lines caused by the elongating bolt row. Initial flaking occurred at the bolt row; the first yield line appeared directly beyond the bolt row; the final yield area occurred just in front of *second* bolt row (See Fig. 25). In the snug tight test, the full yield line was located a full diameter beyond the center of the critical boltline.

Upon load reversal, even before the load became very high, bolt slip occurred. There were two kinds of slip, *minor* and *major*. Minor slip caused a small *ping* and did not cause any jump in the instrumentation readings. Major slip was accompanied with a deep resounding sound and caused a jump in readings. In the tests with snug bolts, the slip occurred often and early, while in the tests with friction tight bolts this only occurred in the later cycles.

Chapter 5

MODEL COMPARISON

At this point, it would be advantageous to compare the original and modified models with the actual experiments. The following sections compare the moment-rotation relationship of each model with the actual moment-rotation relationships from both the friction tight bolts and snug bolts top-and-seat-angle connection tests.

5.1 Original Model

This was the original STRUCTR model (See Sec. 2.2) consisting of main members, rigid members to space the detail material properly, and beam-type members to represent the angle legs. By examining Fig. 47, one can see the overestimate of stiffness and large underestimate of strength for two bolt row connections. It, as is the case with the bolt models is fairly accurate with the single bolt row connections.

5.2 Revised Model Bolt A,B

The bolt model's flexibility at the bolt line caused a closer prediction of the moment rotation relationship to be attained when compared with the original model (Fig. 47). The initial stiffness is closer for model A which contains tension angle bolt flexibility and for model B which has an additional bolt member at the seat angle-beam interface. Since the tension angle controls the mechanism, they both reach the same ultimate moment which is also closer to actual than the original model. For the snug condition, the performance is encouraging, since it also indicates reserve strength over the fully pre-tensioned case (Fig. 48). The comparison to the single bolt row tests are more favorable, since the models only contain a leg to the first bolt row.

5.3 Revised Model Leg A

Model Leg A which incorporates the bolt members, has two features not found in the bolt models. It has a larger cross-section at the heel and has one additional angle member extending from the critical bolt line to the second bolt line. As can be seen in Fig. 47, the two desirable effects of these features are a stiffer intermediate path (point 1 to 2) from the additional angle member; and a higher ultimate moment from the heel members. See Section 2.6 for an explanation. It does not reflect the reserve strength in the snug tight case as was shown in the experimentation.

5.4 Revised Model Leg B

Model Leg B is fairly accurate for strength prediction, because the moment arm was determined from empirical observation. The stiffness prediction is unrealistic, due to a crude model for the contact surface.

5.5 Recommendation

Model Leg A, which really is a combination bolt member and leg-adjusted modification of the original model, is the most accurate for the multiple bolt row full pre-tension tests. Model Leg B is fairly accurate for strength prediction. Model Bolt A or Bolt B are accurate for the single row experiment, and show increase in strength for the snug tight case.

Chapter 6

CONCLUSIONS

6.1 Connection Behavior

In the experimental work performed for this paper, the top-and-seat-angle connection's behavior as a structural component is primarily dependent on the bolts of the critical line in the tension angle. For top-and-seat-angle connections in general, the most important parameter might be one which relates the bolt row pre-tension value to the angle's plastic modulus for a given bolt gage, and beam depth.

6.1.1 Modal Behavior

There existed three modes of behavior for the top-and-seat-angle connection: multiple bolt row, full pre-tension; multiple bolt row, snug tight; and single bolt row.

6.1.1.1 Multiple Bolt Row

Two modes of bolt-induced connection behavior exist. In the case of pre-tension bolts, the first bolt row becomes inelastic quite early. A progressive softening of the connection occurs on reversal (Fig. 45). In snug bolts, the bolts remain linear until near the maximum capacity (Fig. 46). It can be construed that in these tests, the yield lines in the tension angle are *responses* to the deformation that the bolts are *permitting* the beam to impose on the angle. The plastification of critical angle sections occurs later than previous models have shown (Driscoll, 1987, Chen, 1985) presumably from the rotation of the bolt heads and the large area occupied by the thicker fillet. Secondly, from the bolt rotating and pulling out slightly, the hinge forms *behind* the bolt line. Again, if the bolts don't elongate, the plastic hinge is meaningless in describing the

connection stiffness. Another point that should be noted is that a line of plastification does not necessarily mean a substantial change in connection behavior. For instance, when the plastic hinge forms on the outstanding leg fillet of the tension angle, the angle leg does not rotate freely, it rotates to wherever the beam end rotation takes it. In summary,

- The connection with the snug bolts achieved *more* strength, while actually behaving *stiffer* for the majority of the experiment. This can be attributed to their lower (elastic) pre-tension.
- The snug connection reacted less adversely to load (wind) reversal and remained linear longer.
- The snug connection developed 50% of the beam's plastic moment, while the fully pre-tensioned connection achieved 40%.
- In the fully pre-tensioned experiment, only the inner bolt row participated in carrying the tensile force, while all bolts participated in the snug tight test. This different mode of behavior caused higher bending and prying forces in the fully pre-tensioned case.
- The snug connection exhibited more ductile behavior than the fully pre-tensioned connection. The bolts in the snug connection survived the entire experiment, while the fully tightened bolts fractured at near the maximum load.

6.1.1.2 Single Bolt Row

The connections behaved almost identically, independent of pre-tensioning level. The yield line occurred in line with the critical bolt row, not beyond it as was the case in the multiple bolt row experiments. The bolts fractured at the bolt head.

6.2 Connection Qualities

6.2.1 Strength

The connections' strength was admirable to say the least as 3 of the 6 tests were performed in which an outside factor caused the stoppage of the test with the connection intact (See Sec. 4.1), and applied loads in excess of 400 kips. This points out an advantage of propped cantilever testing. The moment capacity of the connection was spent, however, the test frame allowed the examination of the connection's additional shear capacity.

6.2.2 Ductility

The snug tight, multiple bolt row connection's moment-rotation relationships contained a plateau of approximately $3\Phi_Y$ without any angle or bolt failure. The fully tightened multiple bolt row achieved the same plateau but bolt fracture occurred. This points out the usefulness of the top-and-seat-angle connection: a connection which can deliver a good percentage of the beam's M_p , yet remain ductile. Most connections which engage the beam flanges do not have such a forgiving nature. The single row connection achieved over $4\Phi_Y$ before the bolts fractured. The fracture surface was ductile.

6.2.3 Rotational Stiffness

The stiffness was high enough to justify taking advantage of it in design. The connection with snug bolts was stiffer than the connection with friction tight bolts. At ultimate, the 7/8 inch angle connection developed about 30-40% of the beam's M_p for friction tight bolts and 40-50% M_p for snug bolts. The single bolt row experiments developed approximately 25% M_p . This lower value is expected since the single bolt row experiments had a longer gage length to the bolt line (4.5 in. versus 3.0 in.).

6.3 Insights

Several insights on the top-and-seat-angle connection were discovered through the experimental program. They were as follows:

1. Shear Force Path -- The connection carries the vertical shear at least evenly between the top angle and the seat angle, if not more going to the top angle. This is contrary to what is implied in current AISC design.
2. Bolts -- The number of bolt rows and the degree to which they are tightened control the behavior of this connection.
3. High Strength Steel -- The 50 ksi steel angles provided tremendous strength to a connection generally viewed as weak. The ductility of the connection did not seem to suffer. Since the higher cost of high strength steel is felt in volume, it seems that it would be ideal for detail material, especially if used in conjunction with A36 main members.
4. Working Range Linearity -- All the connections exhibited linear behavior well into the tests. The earliest occurrence of nonlinearity was at a load of 300 kips in test TP2A. This corresponds to a value well above the working load in many building situations.
5. Reversal Effects -- While the previous item could allow simplification of the connection analysis and design, the reversal effects that were observed point back toward complexities. When using friction tight bolts, the small permanent set has a propagative effect on the rotational stiffness as the connection undergoes load reversals. This is due in part to the complete change in function of the angle when the load direction is switched.
6. Seat Angle Bearing Distribution -- The AISC adopts a vertical shear distribution on the seat angle's outstanding leg which extends from the inner edge of the beam a distance equal to the required bearing area. In test observation, the beam flange and the seat angle separated at the inner edge. This locates the center of bearing near the centroid of the bolt pattern. This point may be moot since the total value of the end reaction is used in the AISC calculation.
7. Snug vs. Tight -- Snug tight bolted connection performed equally for single bolt row experiments, and better for multiple bolt row experiments. The increased strength and stiffness is a result of the mode of behavior. The yielding of the critical leg allows much larger rotations because of the tremendous leverage it holds on the beam's end rotation.

6.4 STRUCTR Modelling

If nothing else, the STRUCTR model for the top-and-seat-angle connection provides a simple, unintimidating tool for an engineer to help in visualizing the mechanics of a connection. The model, especially with the modifications, is fairly accurate and safely conservative. The trade off for the increased accuracy is an increase in nodes at the joint: the original model contains 9 nodes; the most accurate modified model contains 17 nodes. Even though this represents an almost 100% increase, the number of nodes is still quite small when compared to a finite element model of the same connection. A trial finite elements mesh created by the author contained 126 nodes.

Chapter 7

FUTURE CONSIDERATIONS

7.1 Comments on Semi-Rigid Connection Design

While beam-to-column connections in a building are a key structural component and connection related expenses make up a large portion of fabrication and erection costs, the design, selection, and interaction between designers and fabricators remain in a primitive stage. Three main obstacles causing the lack of advancement are:

1. Complex connection behavior
 2. Too many connection types
 3. Involvement of two or three parties, each with separate interests and roles in the final product.
- Obstacle 1 requires rational, analytical computer models if it is to be overcome.
 - Obstacle 2 would not be a problem if a categorized database were available.
 - Obstacle 3 exists because there is no efficient interface between the parties.

This paper makes an attempt to initiate thought and expand the knowledge on the first category. Charts and tables are not the answer. A moment-rotation relationship is not an independent description of a connection's behavior. There are variables such as beam depth, or cantilever versus frame loading, that are not connection properties, yet have a significant effect on the connection's response. With recent computer technology advancing at an accelerated rate, it seems that semi-rigid connection behavioral complexities can be overcome and the beneficial rotational stiffness should be utilized in structural design.

Even an accurate yet simple connection model cannot stand on its own if it is to be practical. An interactive, qualitative and *quantitative* knowledge-based system for connections could incorporate these rational models to provide a complete tool for the designer.

7.2 Future Work

If the top-and-seat-angle connection is to become a dependable, fully utilized, partial moment developing structural component there is a considerable amount of future work to be done. The previous section touches on some of the support developments that are required. Within the area of connection behavior, studies must be undertaken on the effects of different bolt configurations, single bolt lines, and A490 bolts. A parametric study on bolt pretension vs angle thickness should be performed. Fatigue and fracture studies on high strength steel detail material would be of use. Wind reversal effects in sway frames could also be studied. Finally, it is imperative to build on the existing knowledge base on connections in general, and organize the information into an accessible and orderly set.

TABLES

STRUCTR Model Results			
Model	# nodes	K_o (k-in./rad)	Mom_u (k-in)
Original snug tight	10	-	-
		2380×10^3	2400
		2380×10^3	2400
Bolt A/B snug tight	13	-	-
		920×10^3	3450
		2820×10^3	3180
Leg A snug tight	18	-	-
		2120×10^3	5400
		1100×10^3	4000
Leg B snug tight	17	-	-
		3500×10^3	6200
		2200×10^3	7600

Table 1: Results of Theoretical Models.

Top-and-Seat-Angle Testing Program				
Test	t_a (in.)	# rows	Tight	Frame
TP1A	$\frac{1}{18}$	2 @3"	full	prop
TP2A	$\frac{7}{8}$	2 @3"	full	prop
TP2B	$\frac{7}{8}$	2 @3"	snug	prop
TP2C	$\frac{7}{8}$	2 @3"	snug	cant
TP3A	$\frac{7}{8}$	1 @4.5"	snug	cant
TP3B	$\frac{7}{8}$	1 @4.5"	full	cant

Table 2: Testing Program: Top-and-Seat-Angle.

Experimental Results				
Test	K_o^i	K_o^f	M_y (k")	M_u (k")
TP1A	2846	1692	*	*
TP2A	2164	954	4500	6000
TP2B	1411	1541	7255	9650
TP2C	686	172	4250	5800
TP3A	855	*	1000	4520
TP3B	860	*	1820	4780

Table 3: Experimental Results.

K_o^i = Initial stiffness, 1st cycle

K_o^f = Initial stiffness, Final cycle

Units = (k·in/rad) × 10³

Bolt Pre-tension			
Bolt	E (ksi)	F_u (ksi)	T_{pr} (k)
SABI	33530	151	51.4
SABO	34590	135	50.4
TABI	34530	149	50.9
TABO	34630	131	51.4
SACO	33200	133	51.2
TACI	32817	131	38.1
SACI	39006	126	52.5
TACO	33935	139	50.4

Table 4: Bolt Pre-tension: Test TP2A.

Bolt Pre-tension		
Bolt	F_u (ksi)	T_{pr} (k)
SACI	142	26.2
SACO	147	23.5
SACI	143	28.3
TACI	143	27.3
TACO	139	25.5
SABO	143	26.8
TABI	145	25.4
SABI	131	23.4
TABO	130	27.2

Table 5: Bolt Pre-tension: Test TP2B.

SA = Seat Angle; TA = Top Angle;
B = Beam; C = Column;
O = Outer; I = Inner.

Bolt Pre-tension			
Bolt	E (ksi)	F_u (ksi)	T_{pr} (k)
CRIT	35730	147	25.47
CRIT	32780	133	25.19
COMP	32220	137	25.01
COMP	35130	148	24.80

Table 6: Bolt Pre-Tension: TP3A.

Bolt Pre-tension		
Bolt	F_u (ksi)	T_{pr} (k)
CRIT	144	59.2
CRIT	139	62.7
COMP	147	56.7
COMP	141	61.2

Table 7: Bolt Pre-Tension: Test TP3B.

FIGURES

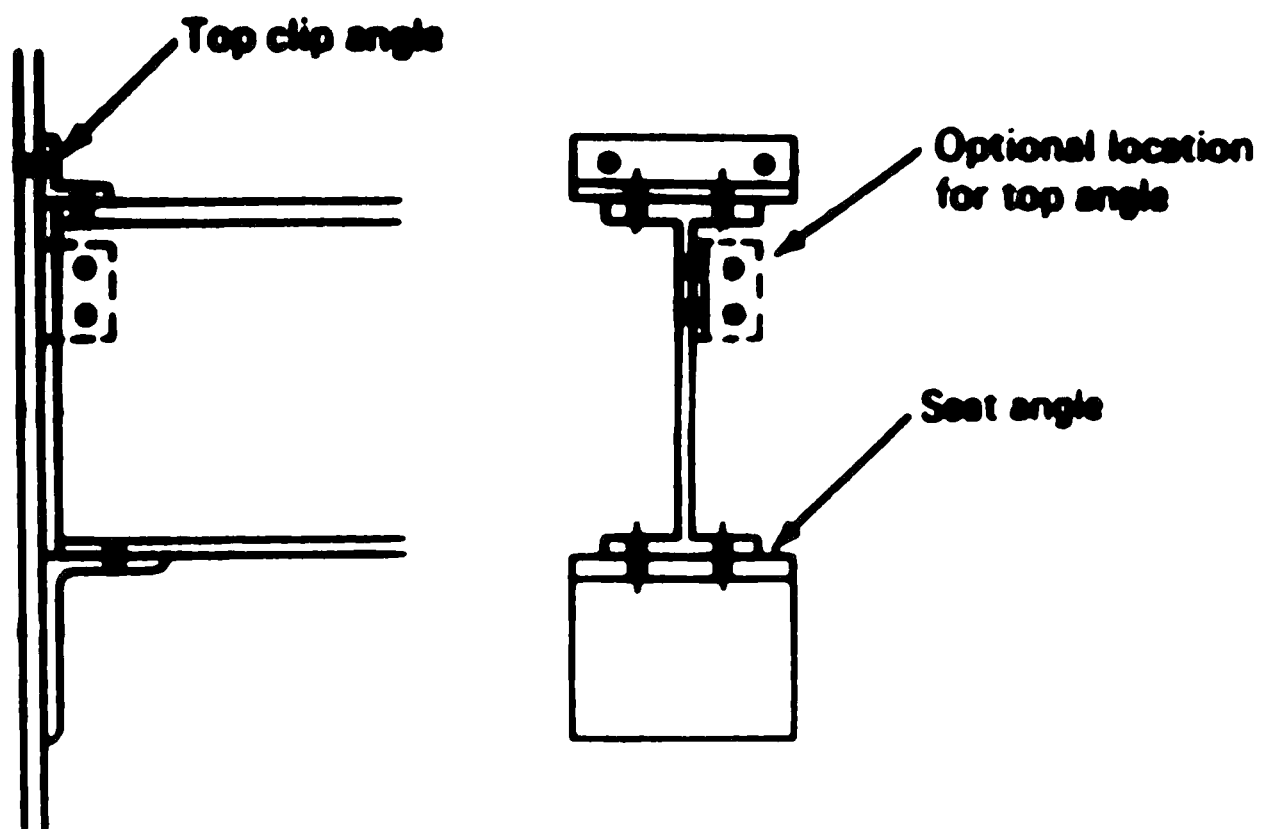


Figure 1: Top-and-Seat-Angle Connection.

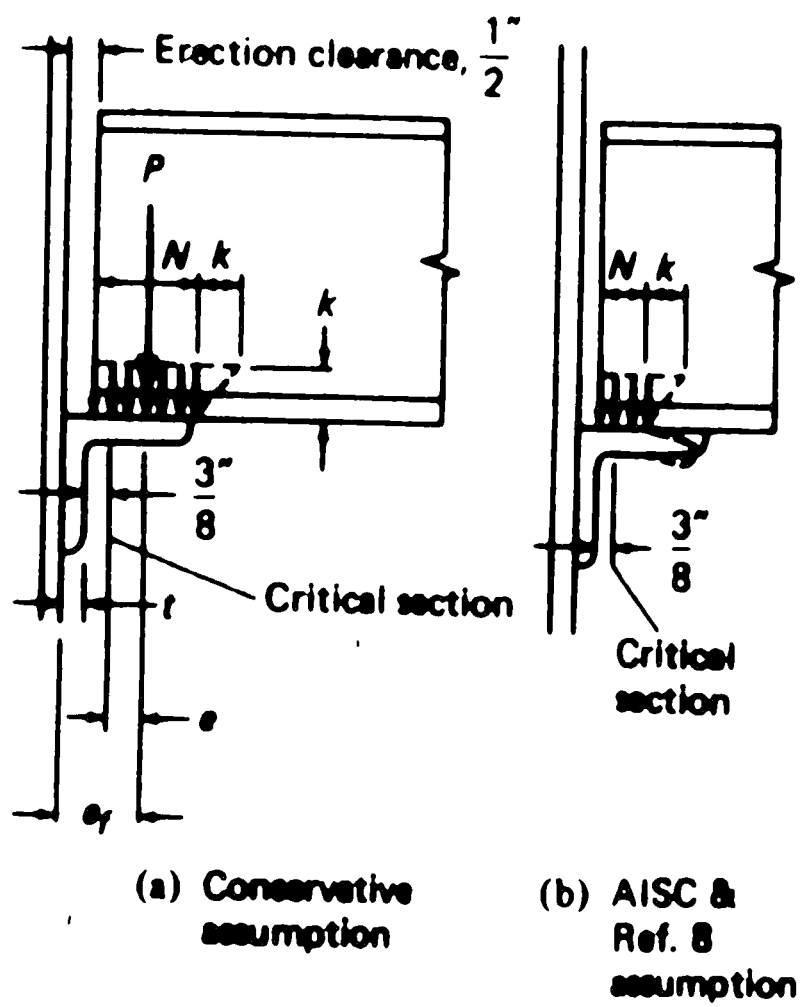


Figure 2: AISC Bearing Distribution on Seat-Angle (after Salmon and Johnston, 1980).

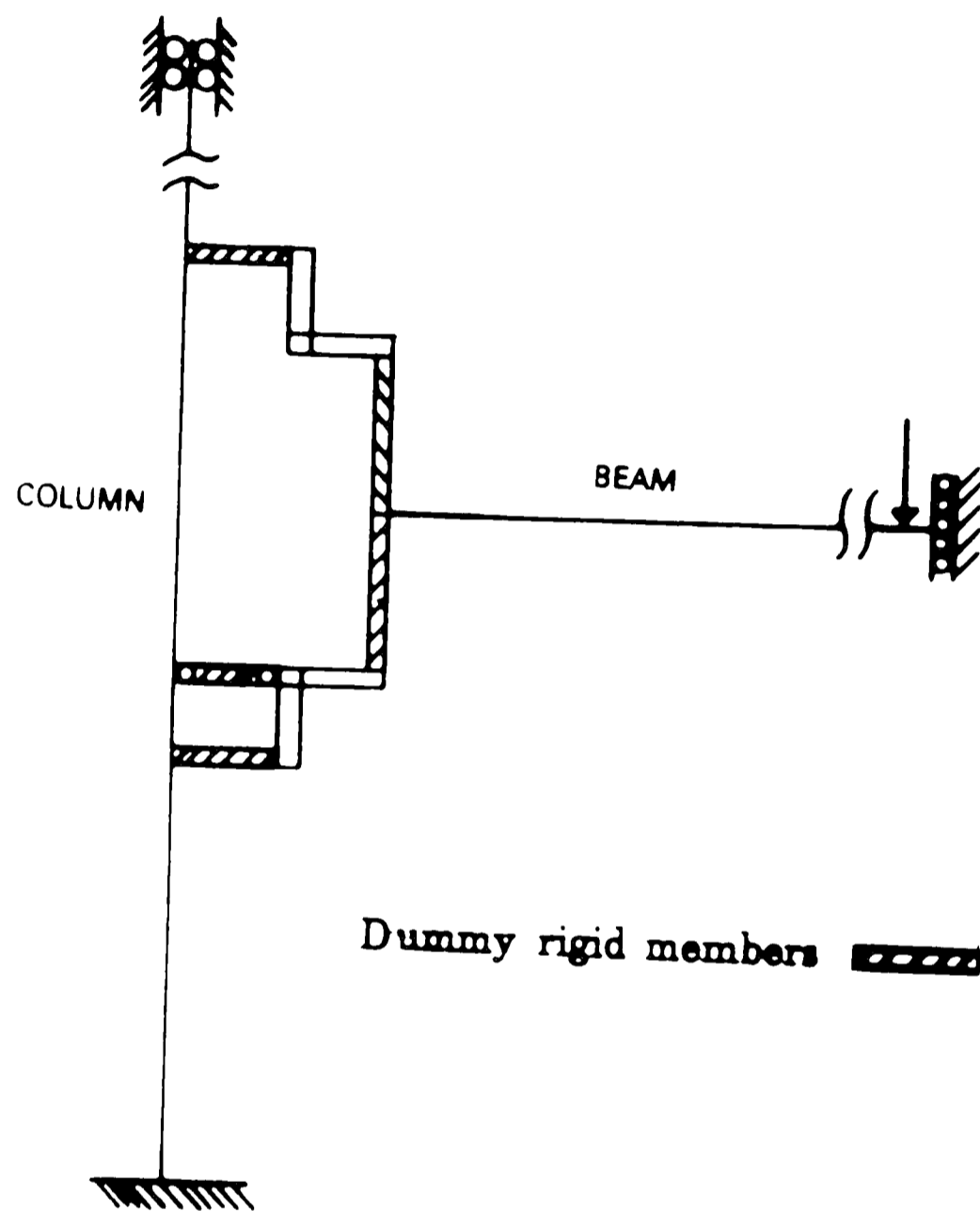


Figure 3: STRUCTR Model of Top-and-Seat Angle.

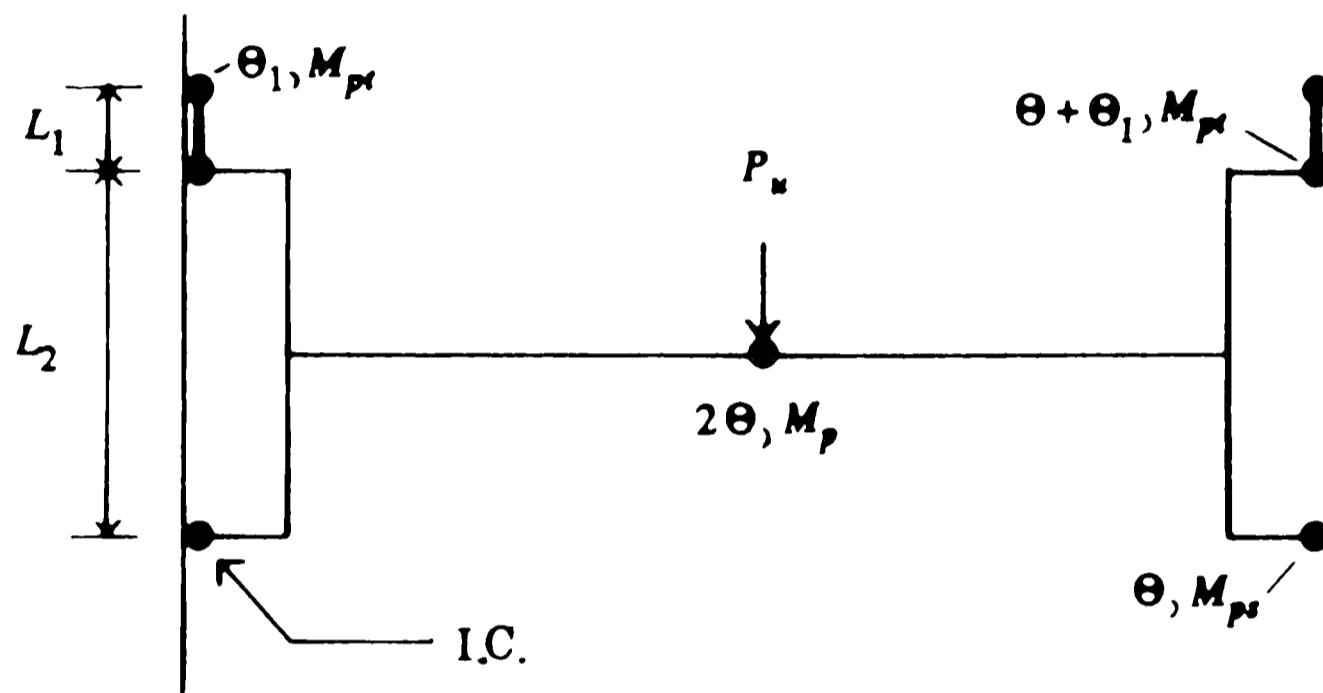


Figure 4: Plastic Mechanism for Simple Frame with Top-and-Seat-Angle Connections.

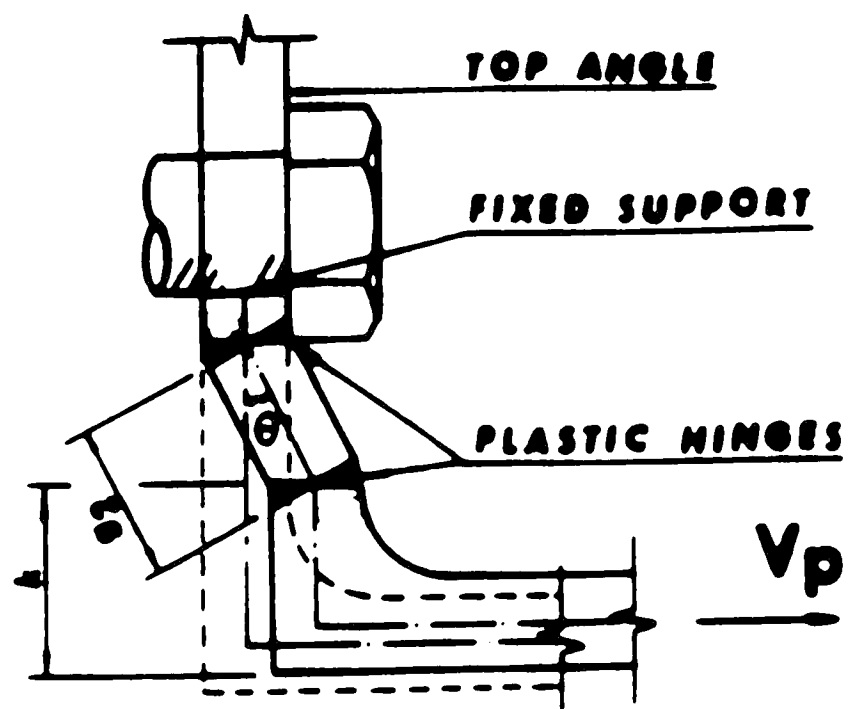


Figure 5: Mechanism of Critical Leg
(after Chen, 1987).

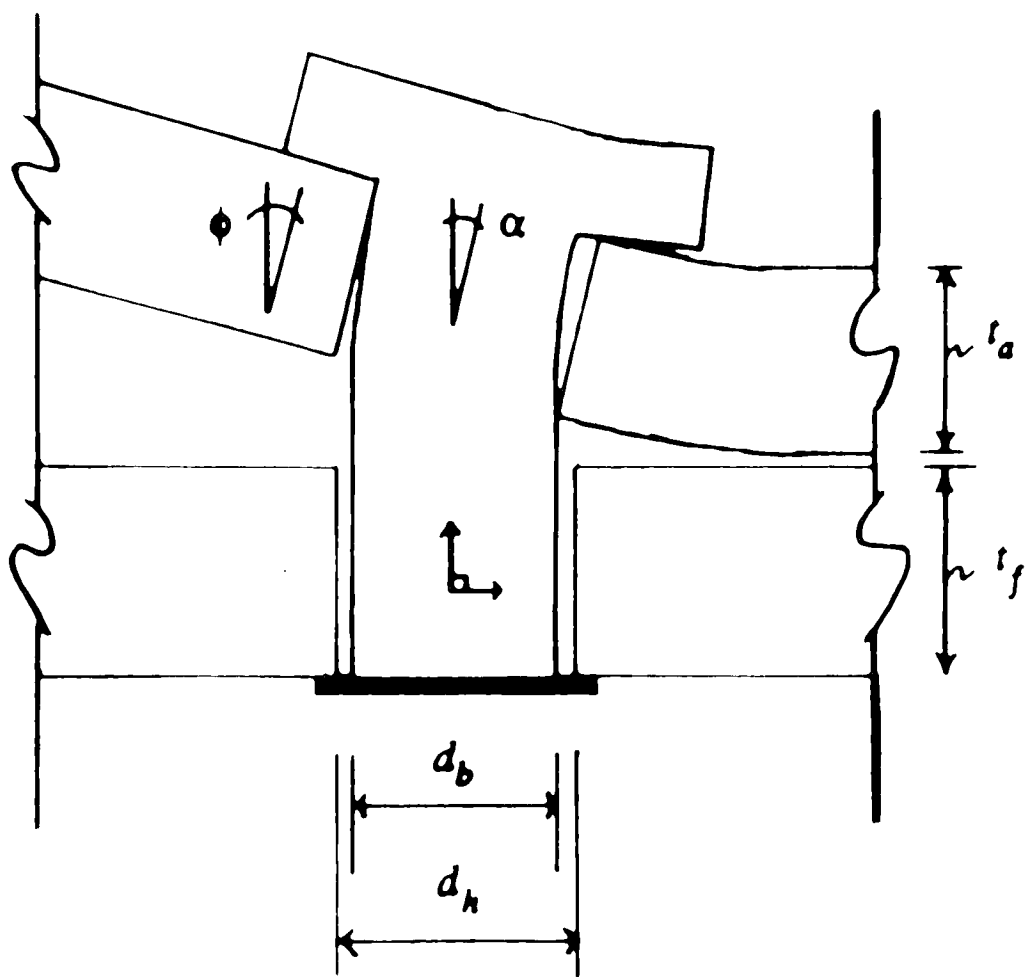


Figure 6: Angle Rotation Relative to Bolt.

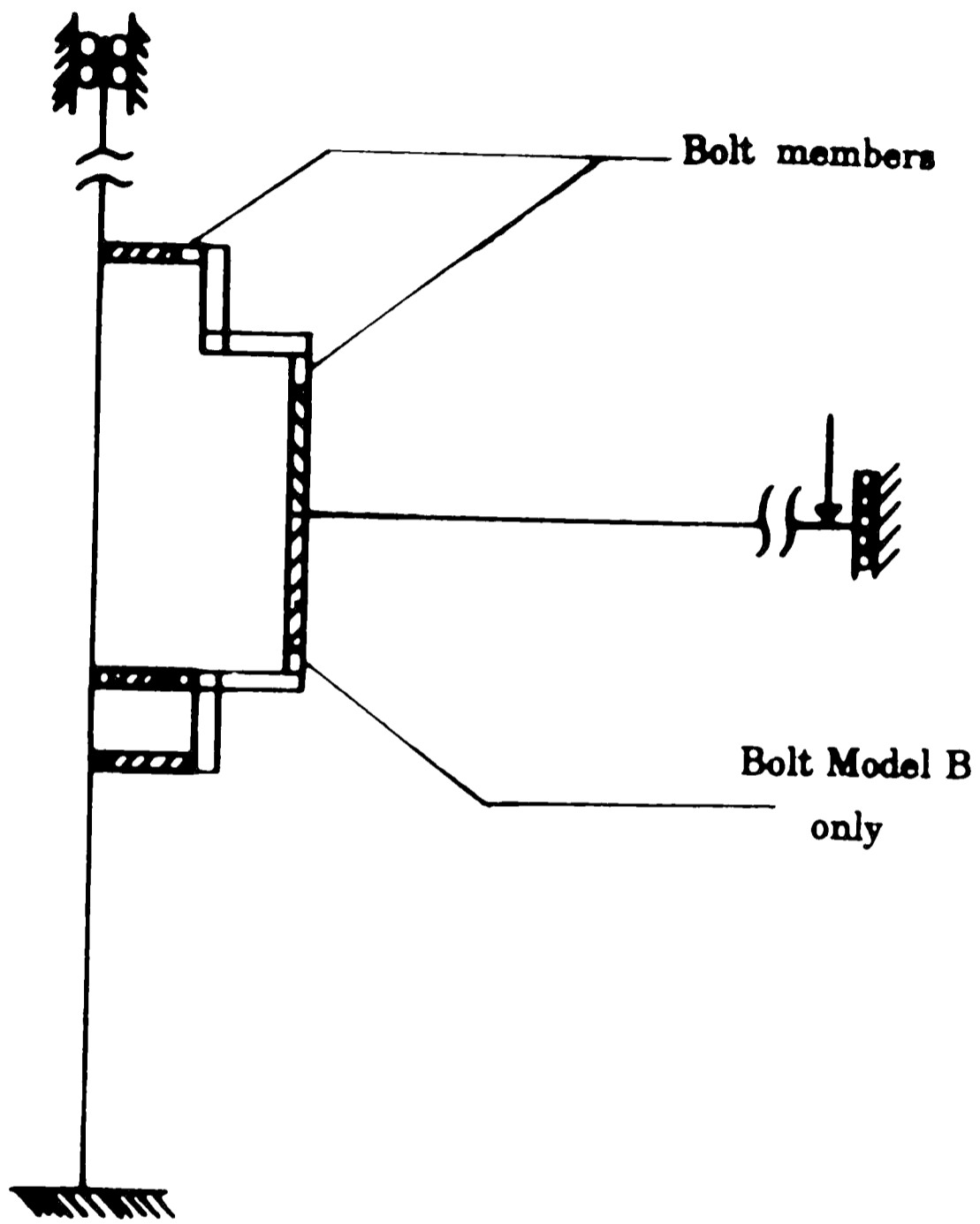


Figure 7: STRUCTR Models Bolt A, B.

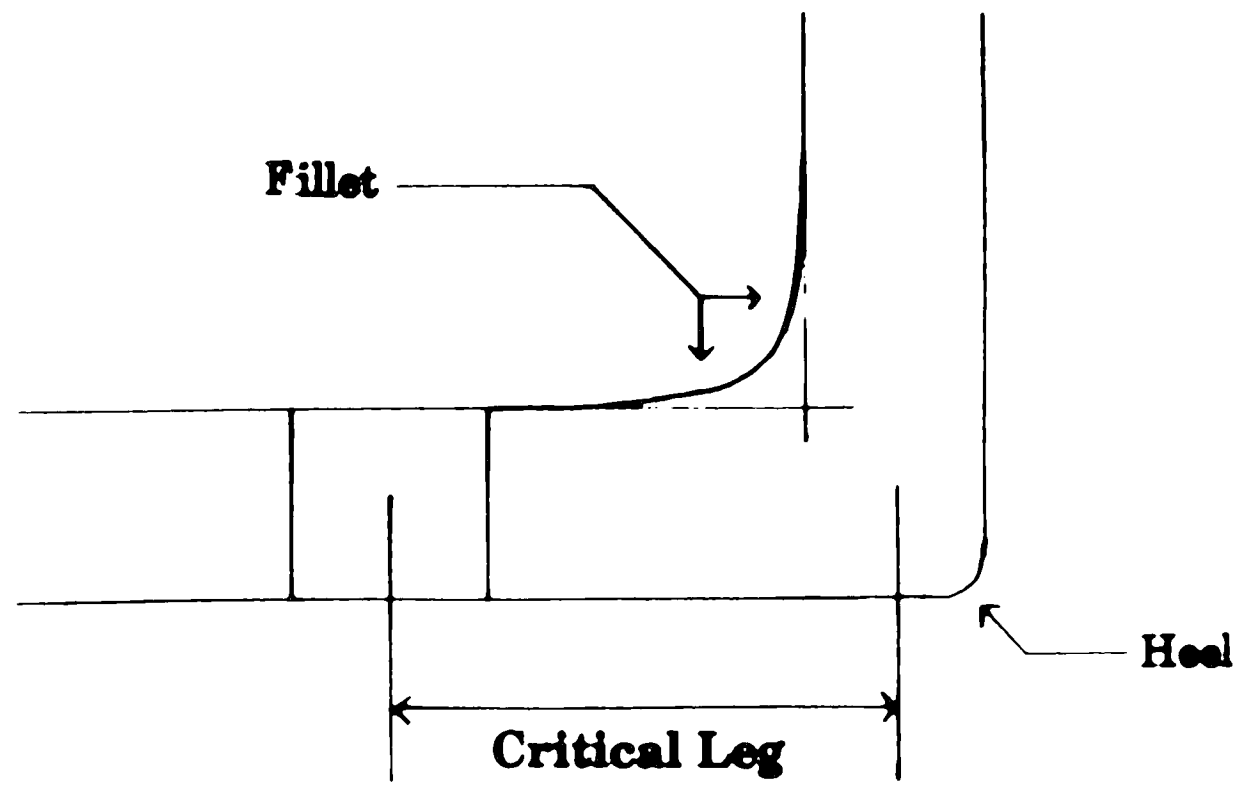


Figure 8: Angle Geometry at Heel in Reference to Critical Leg.

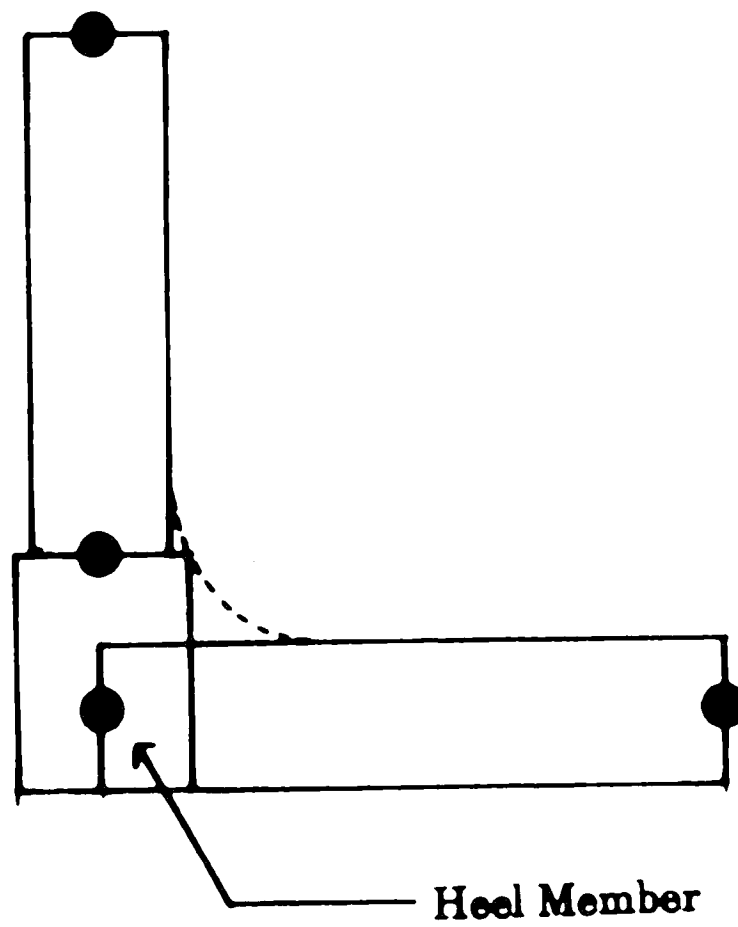


Figure 9: Heel Member for STRUCTR Model Leg A.

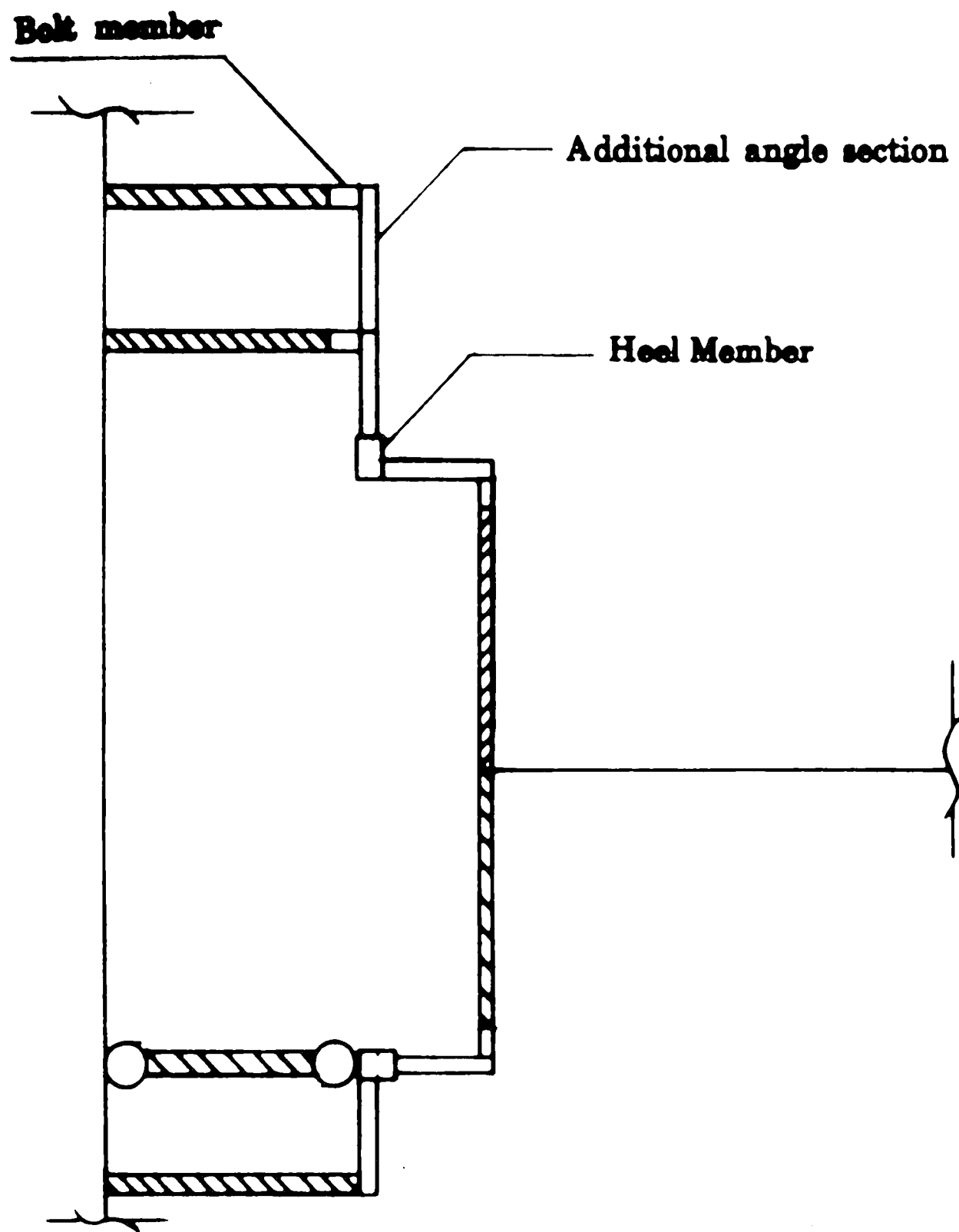


Figure 10: STRUCTR Model Leg A.

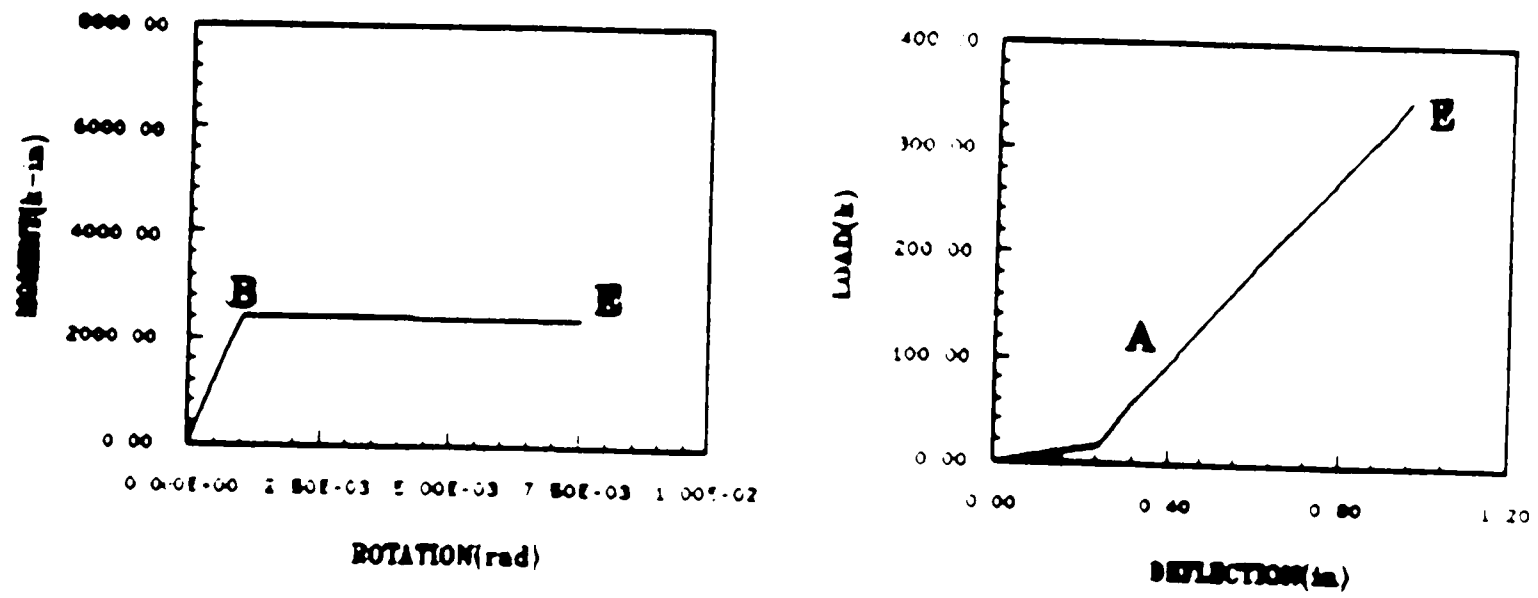


Figure 11: Moment-Rotation and Load-Deflection Relationship:
Original STRUCTR Model.

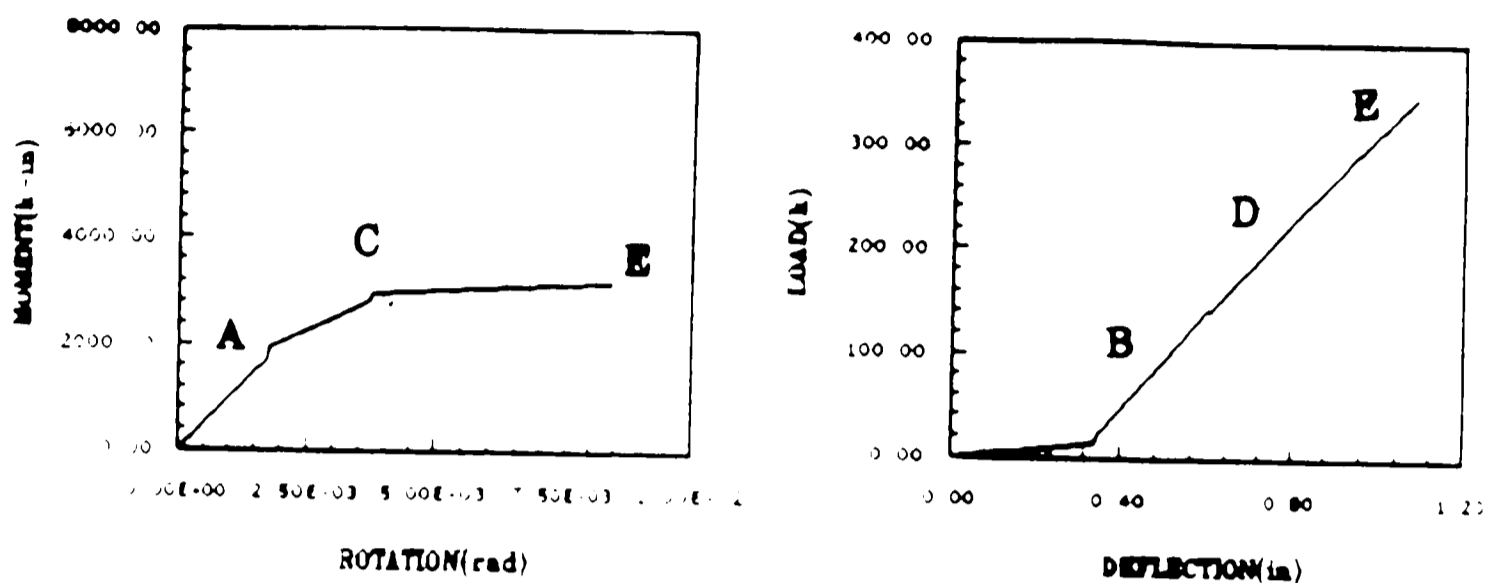
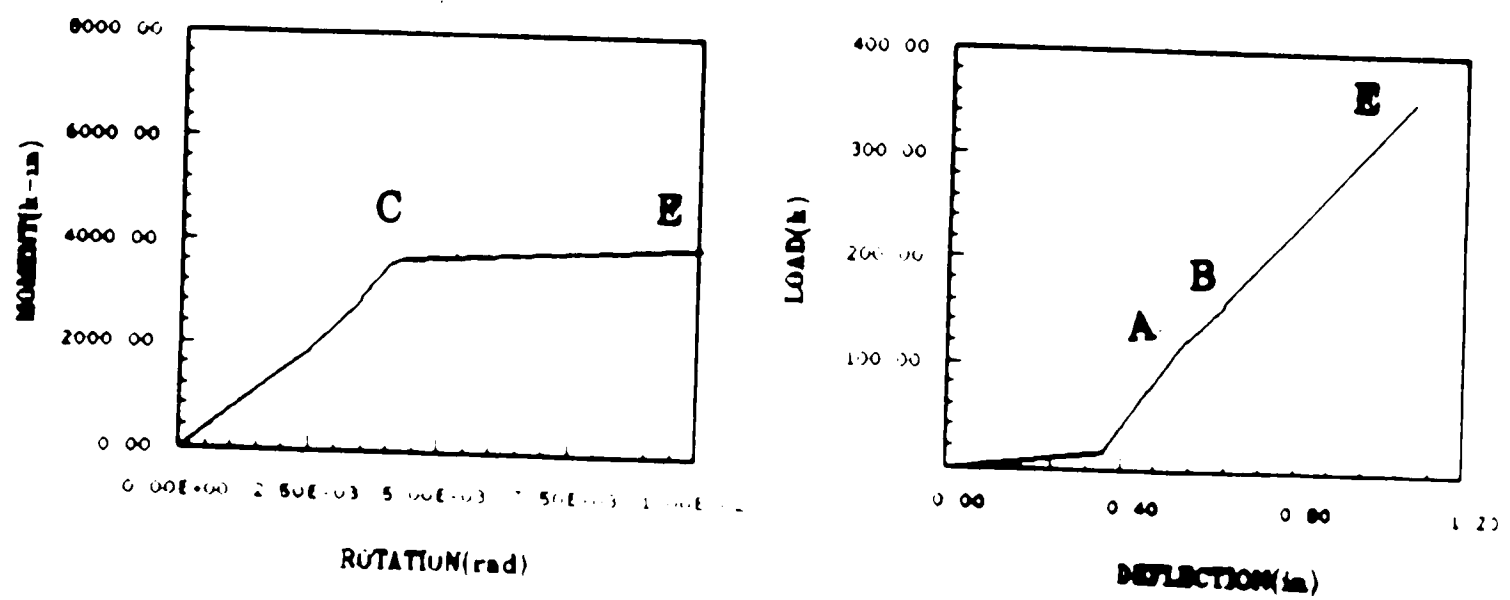
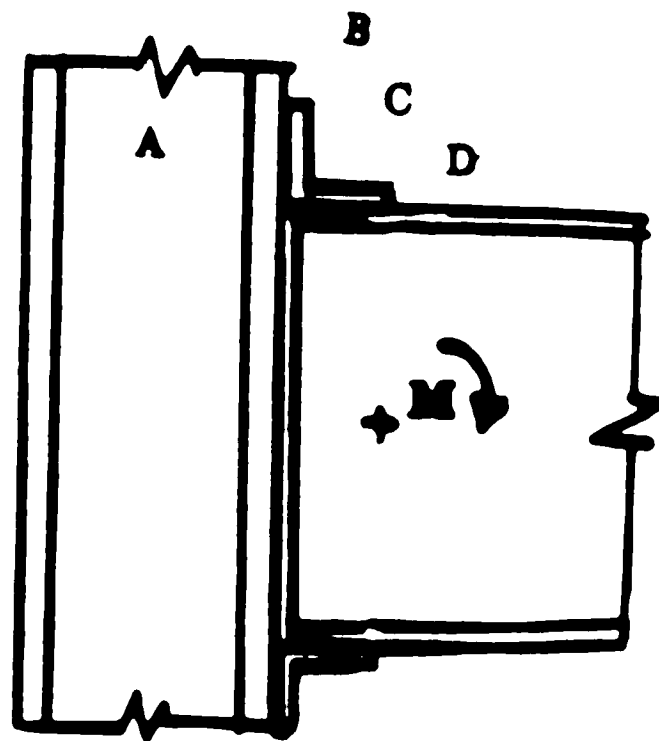
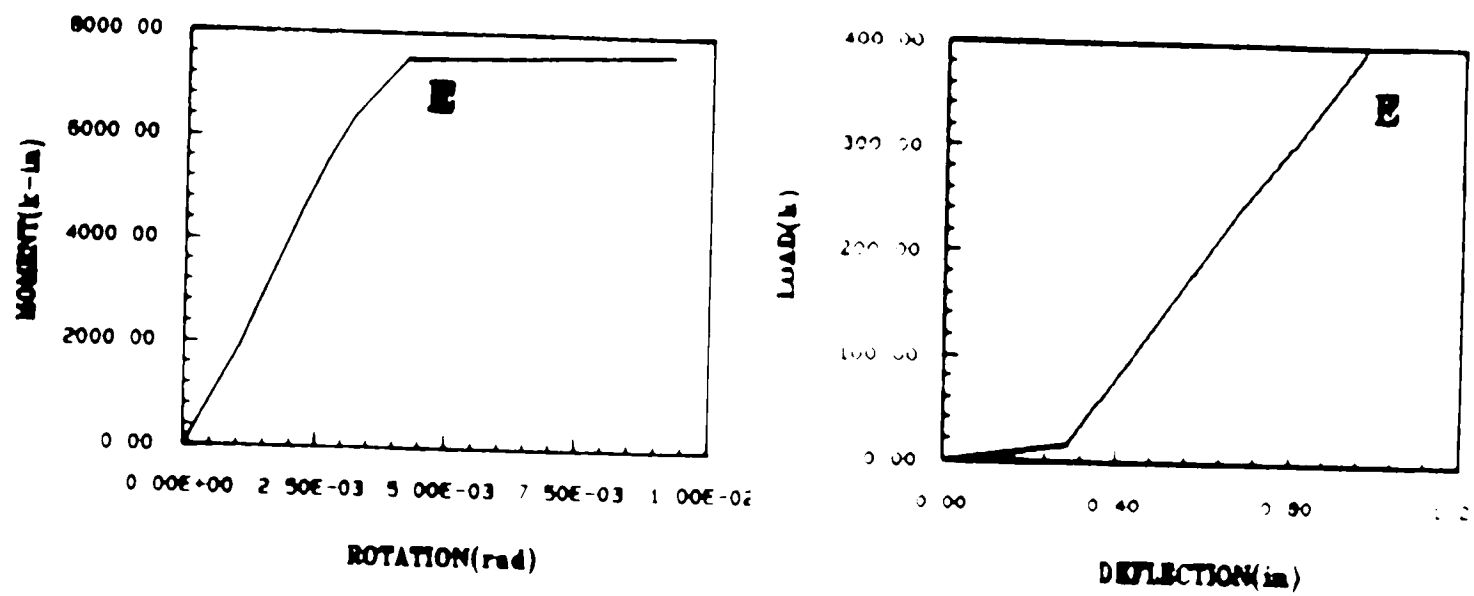


Figure 12: Moment-Rotation and Load-Deflection Relationship:
 STRUCTR Model with Bolts.



**Figure 13: Moment-Rotation and Load-Deflection Relationship:
STRUCTR Model Leg A.**



**Figure 14: Moment-Rotation and Load-Deflection Relationship:
STRUCTR Model Leg B.**

$L = \text{distance from centerline column to midspan beam}$

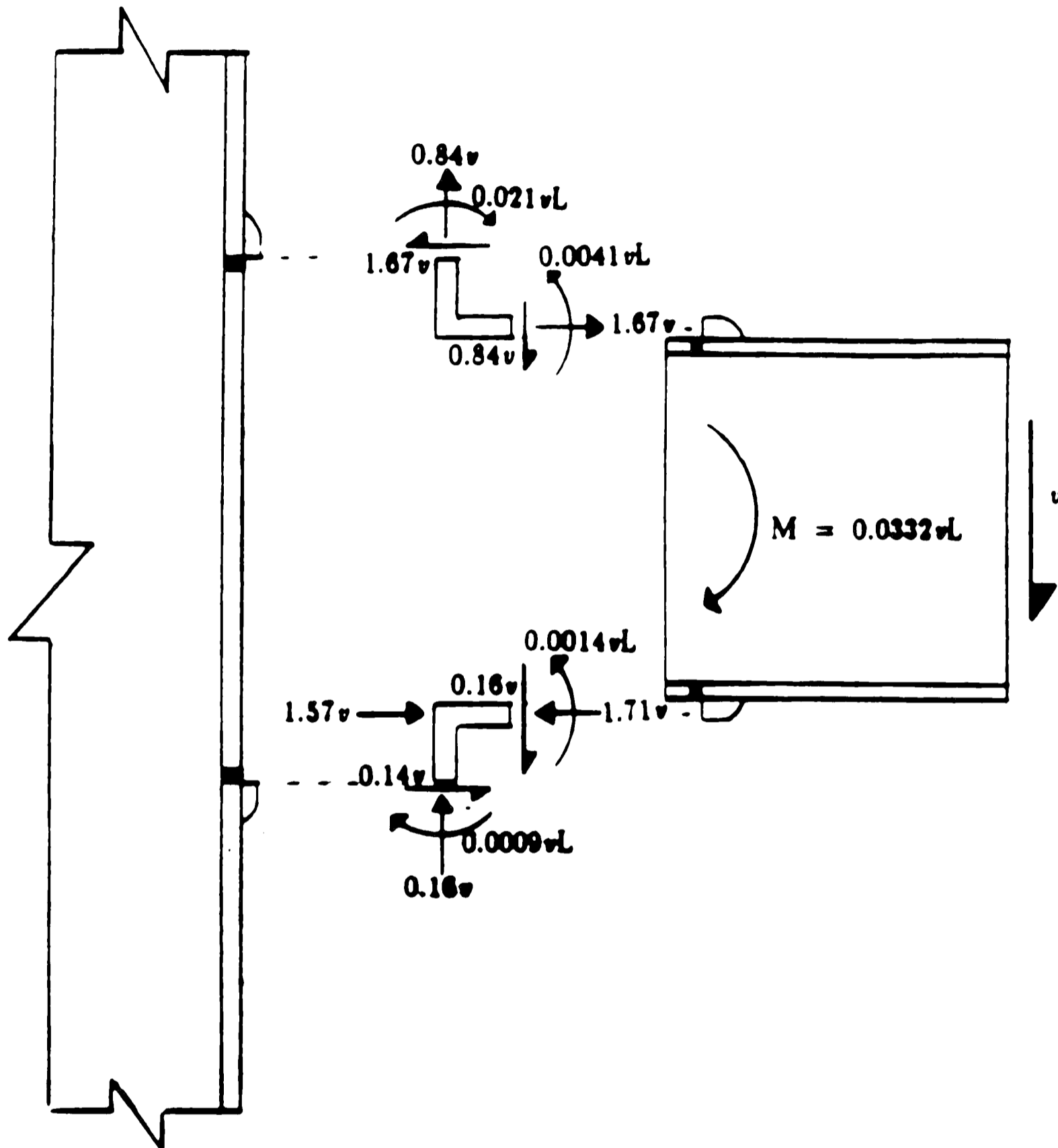


Figure 15: Initial Force Path from Original STRUCTR Model.

$L =$ distance from centerline column to midspan beam

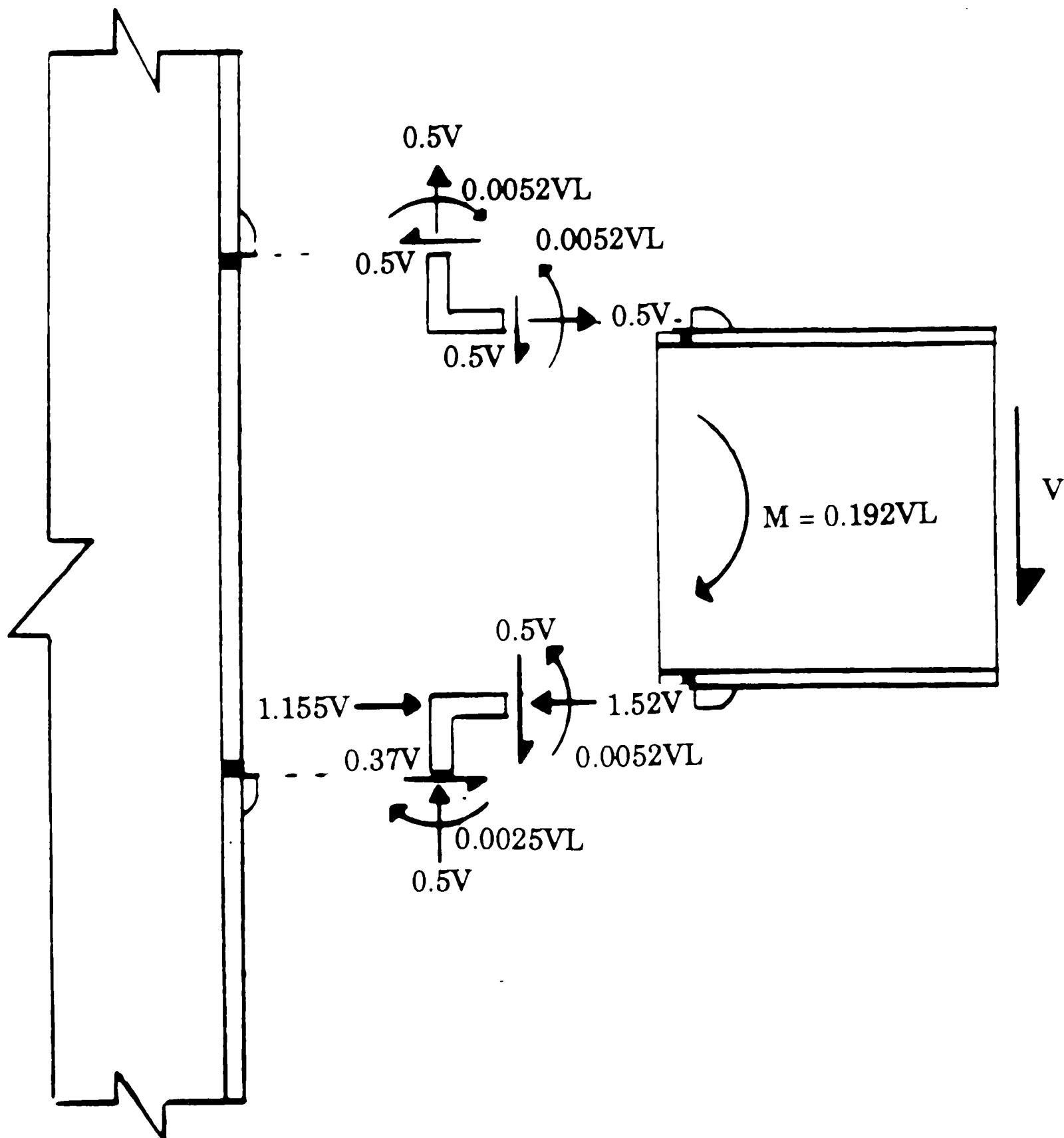


Figure 16: Ultimate Force Path from Original STRUCTR Model.

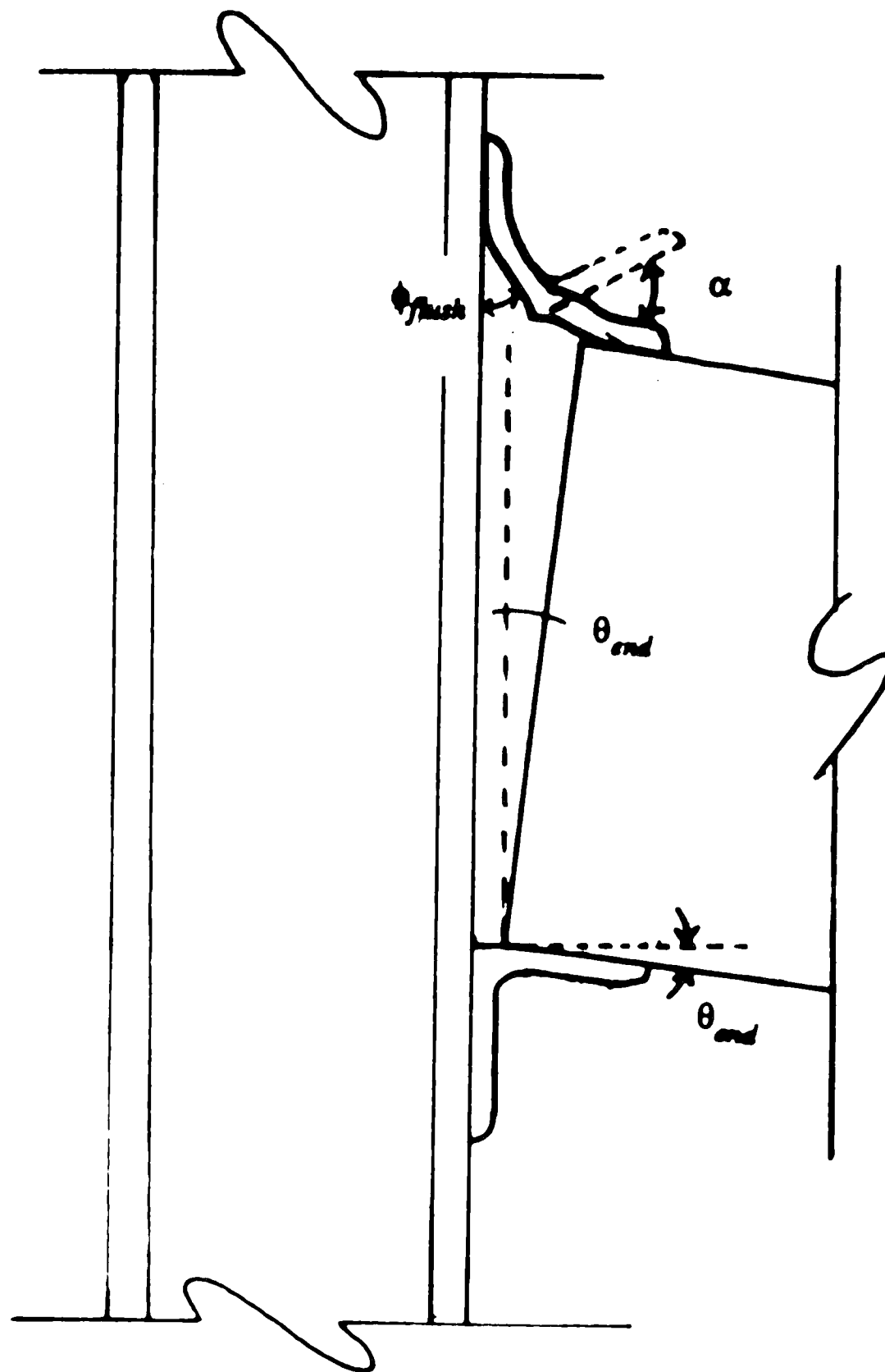


Figure 17: Relative Rotational Displacement of Outstanding Leg:
Top-Angle vs Seat-Angle.

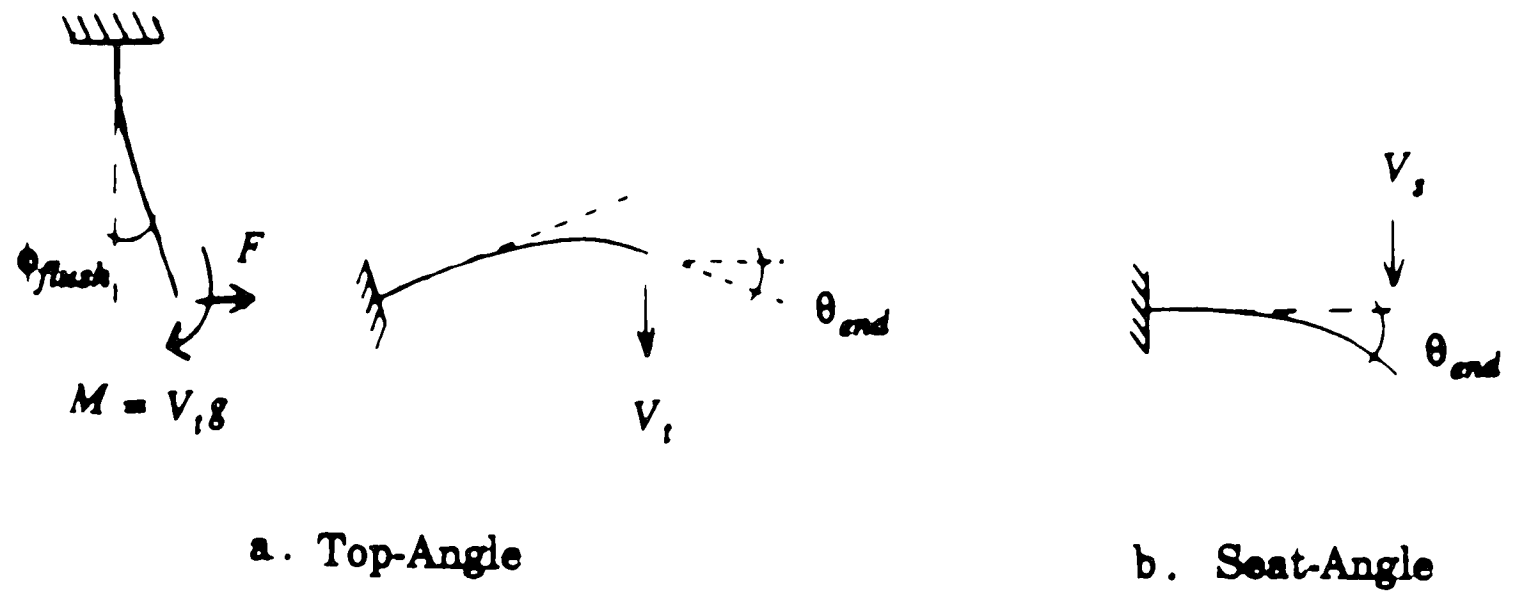


Figure 18: Cantilever Elements for Top-Angle and Seat-Angle Rotation.

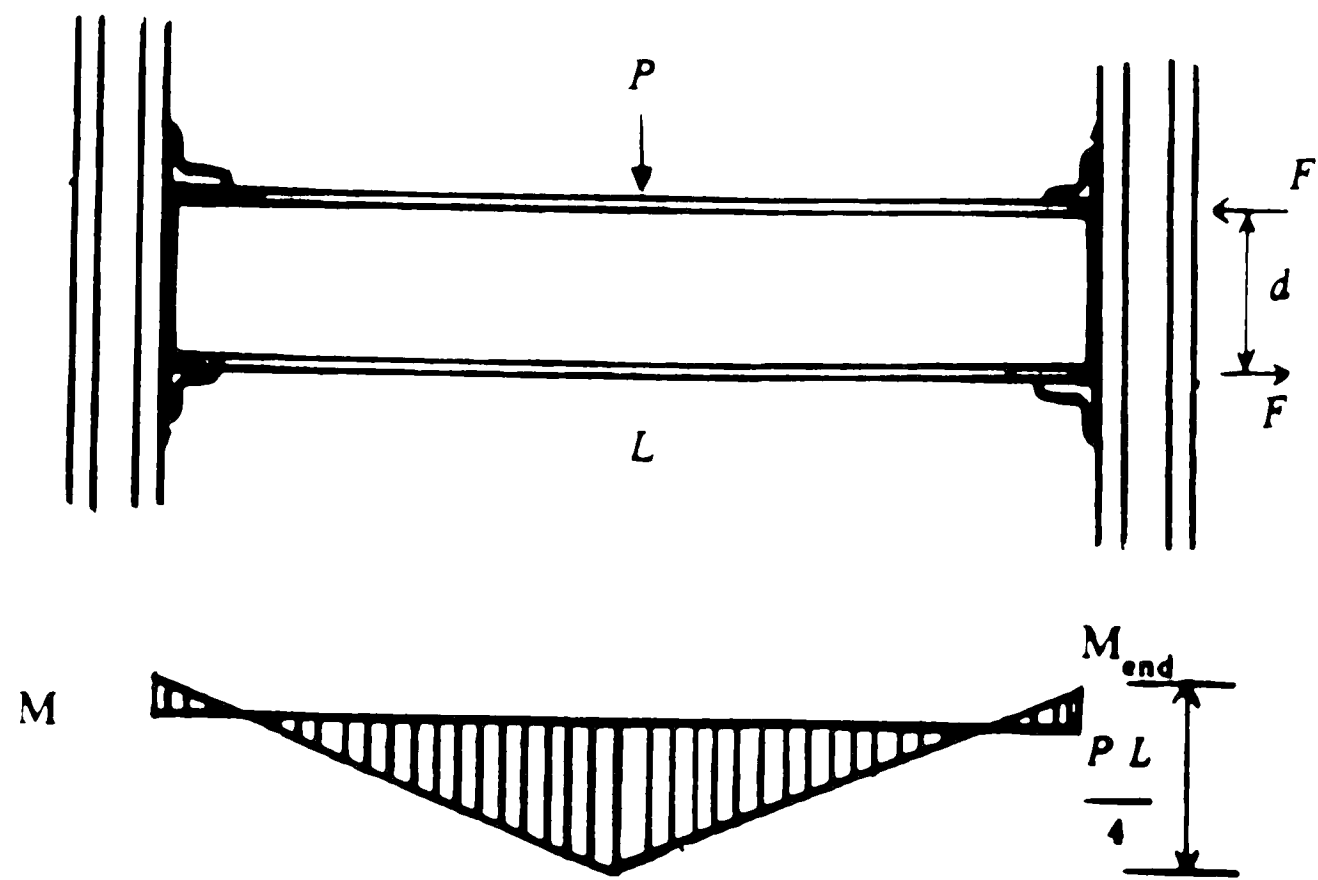


Figure 19: Beam Moment Diagram: TP2A.

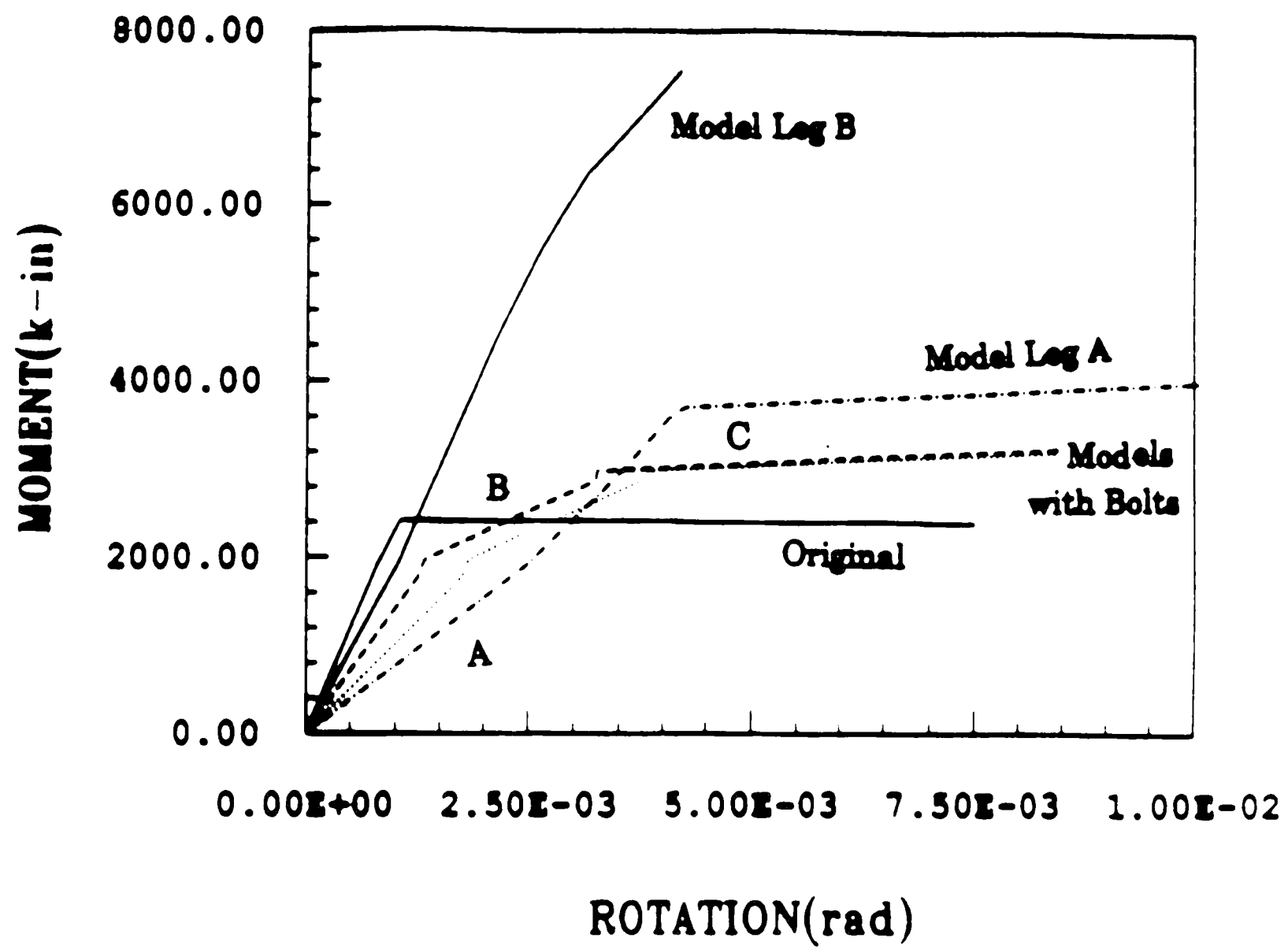
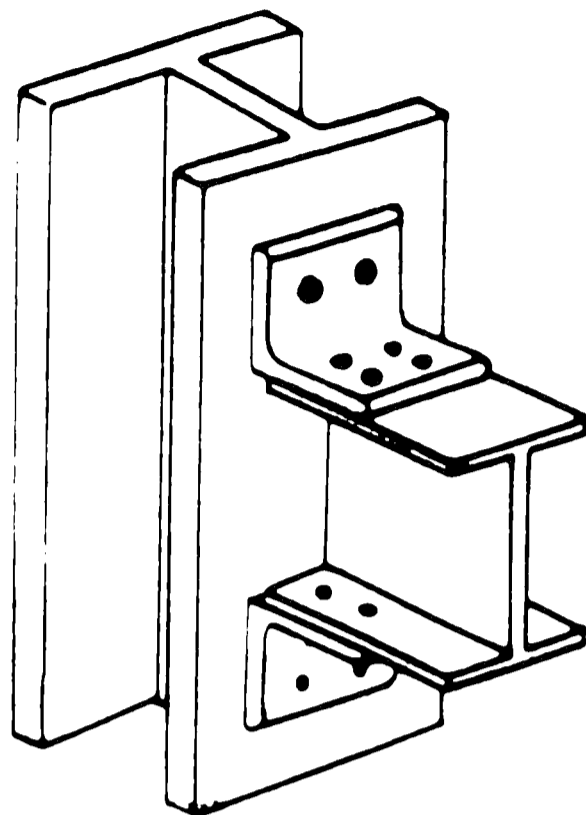
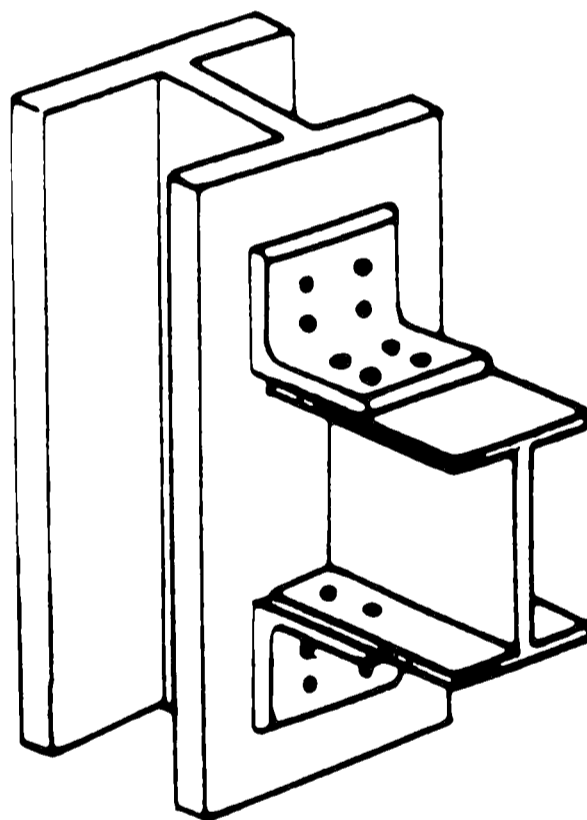


Figure 20: Comparison of STRUCTR Models.



B



A

Figure 21: Top-and-Seat-Angle Connection.

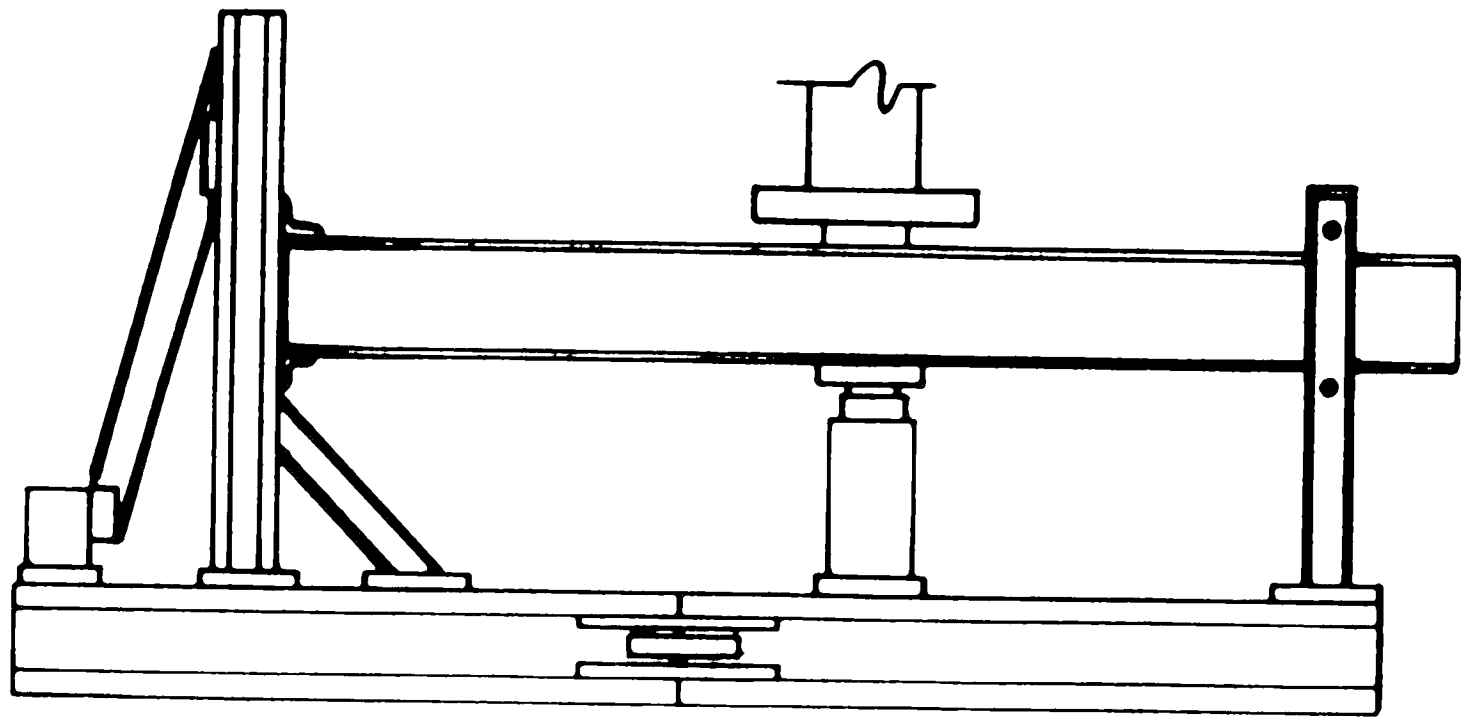


Figure 22: Propped Cantilever Test Frame for Beam-to-Column Connection.

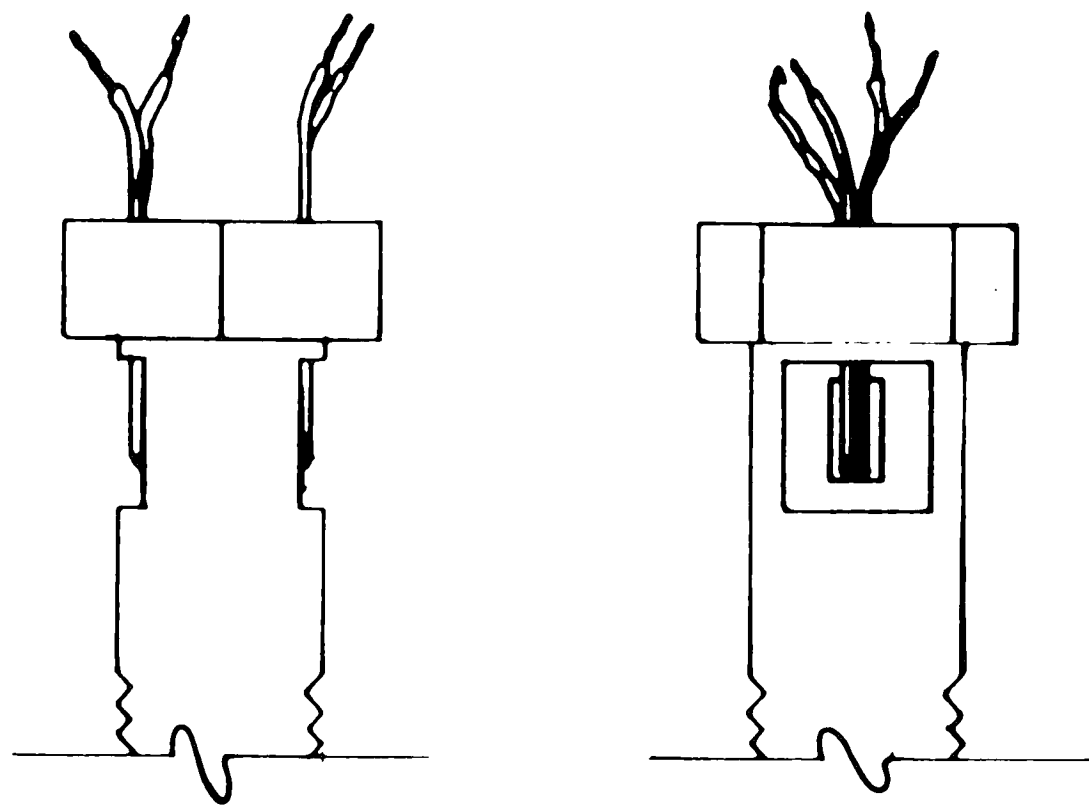


Figure 23: Strain Gage Locations on Bolts.

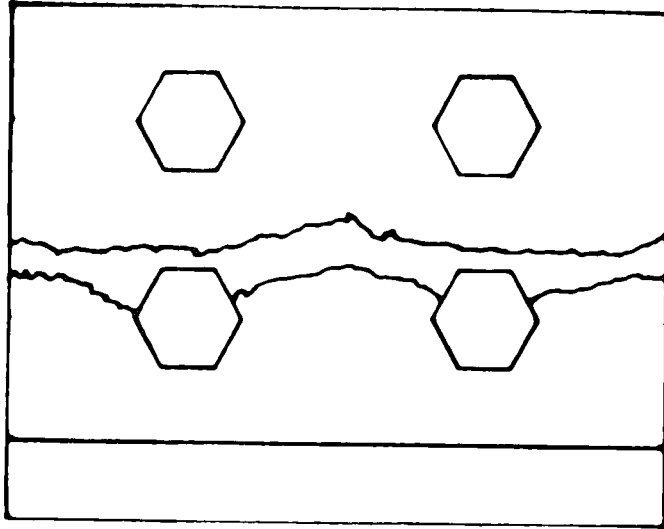


Figure 24: Initial Yield Line.

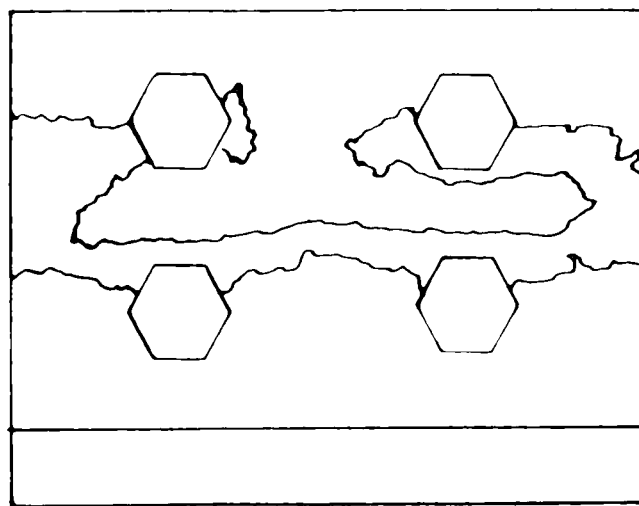


Figure 25: Progressive Yield Line: Test TP2A (Full Pre-tension Bolts).

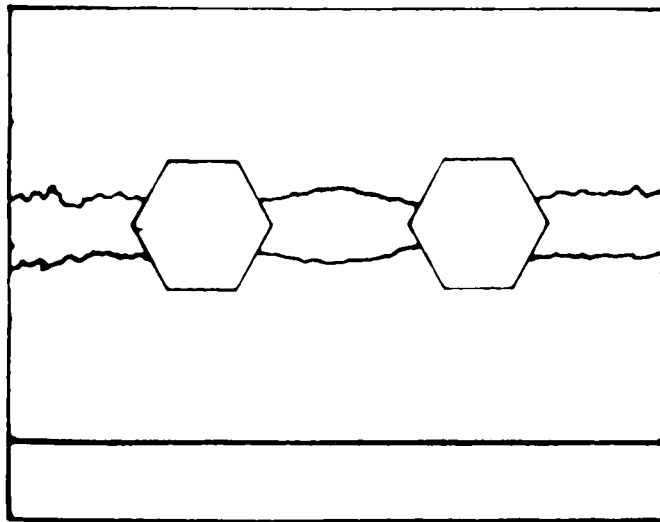


Figure 26: Yield Line: Single Bolt Row.

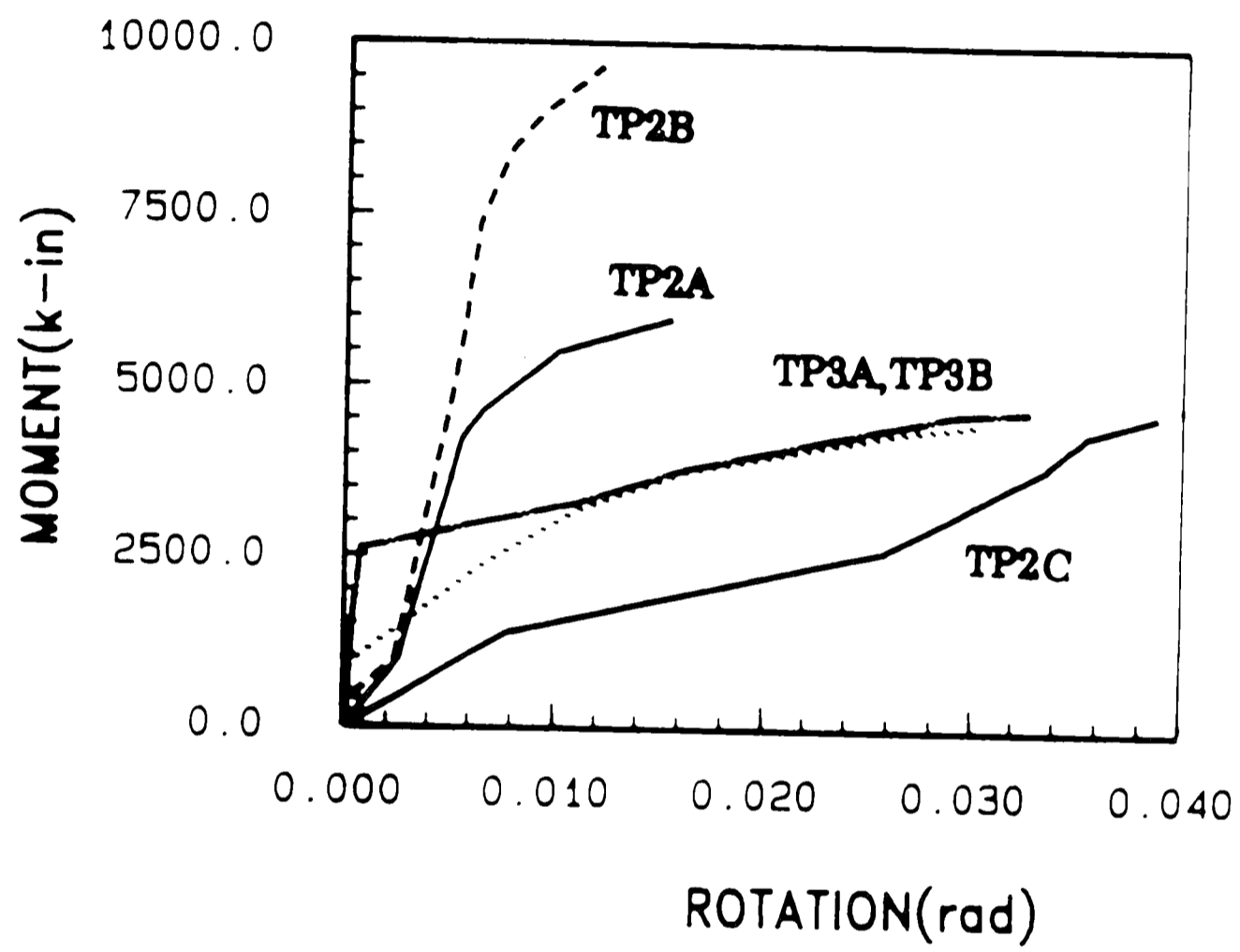


Figure 27: Moment-Rotation Relationships for Experiments.

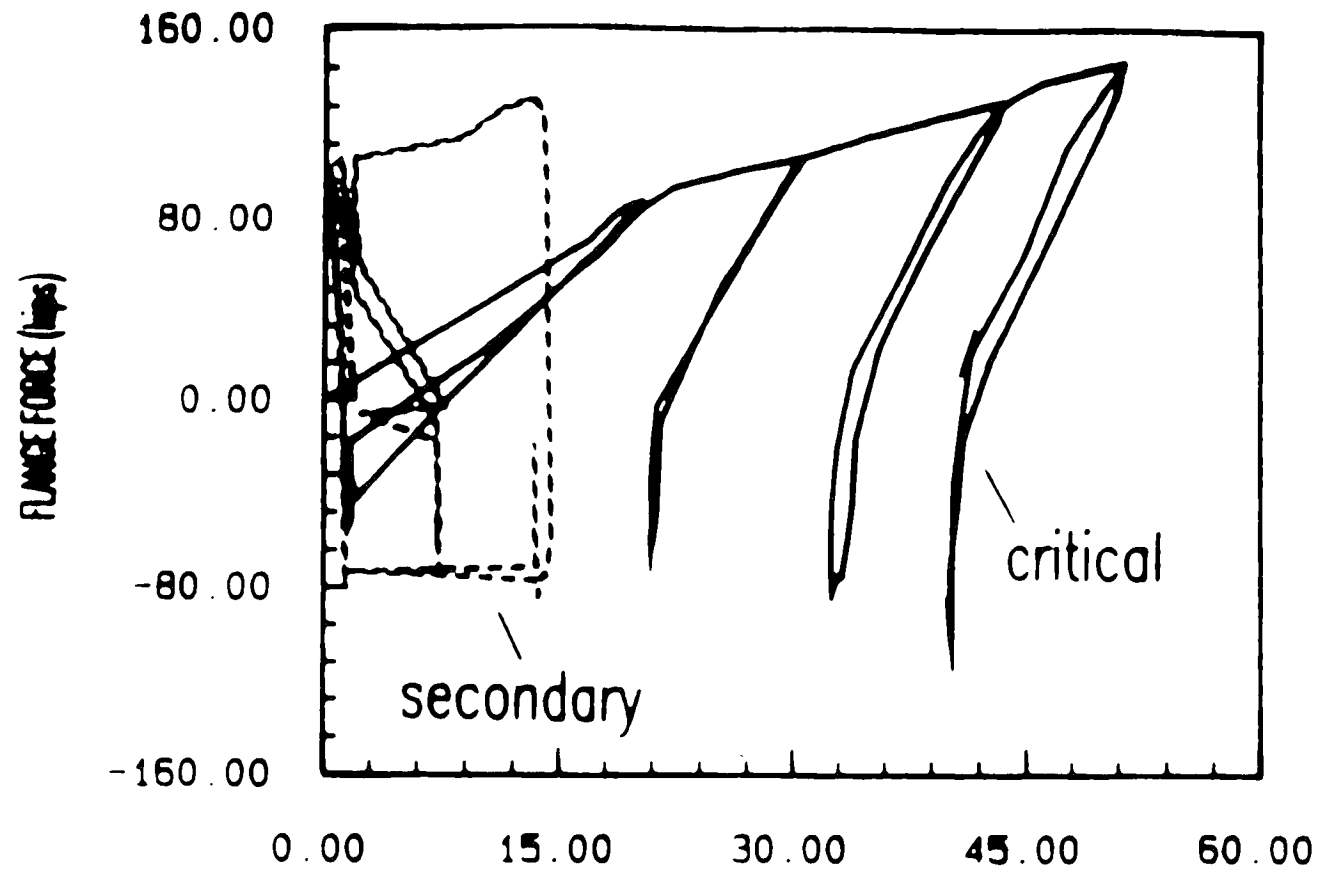


Figure 28: TP2A : Bolt Load Increment.

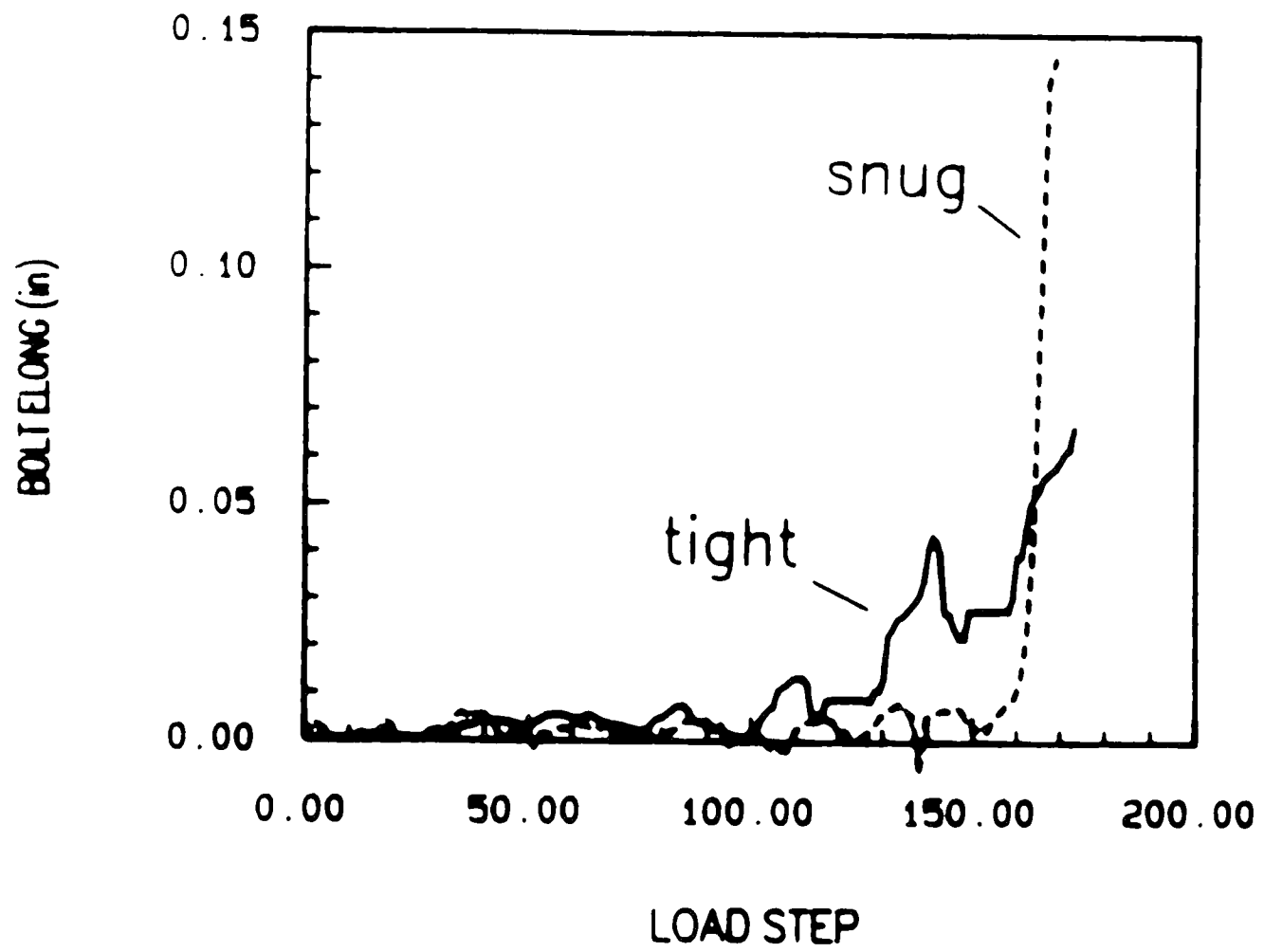


Figure 29: TP2A, TP2B : Bolt Line Elongation.

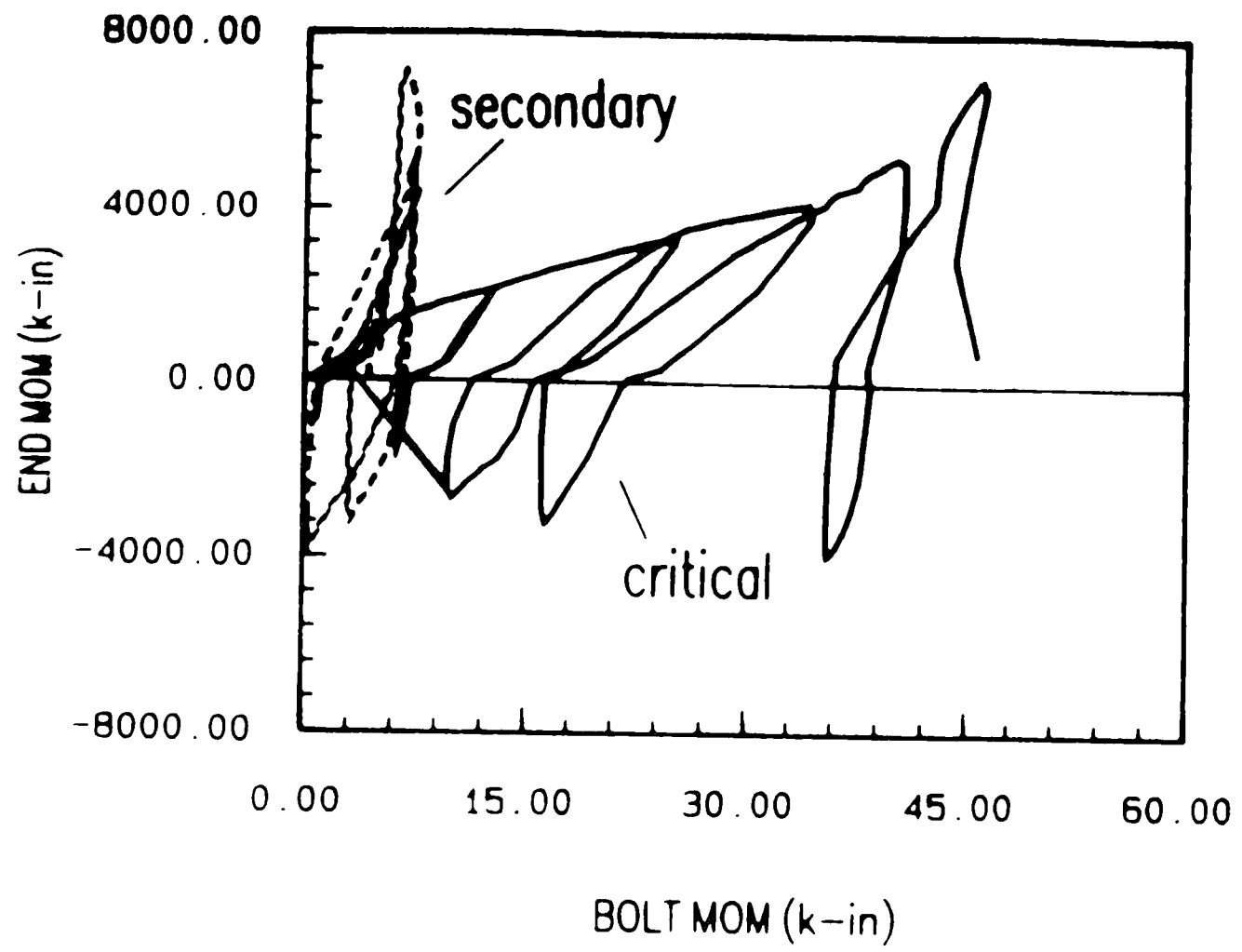


Figure 30: TP2A : Bolt Bending.

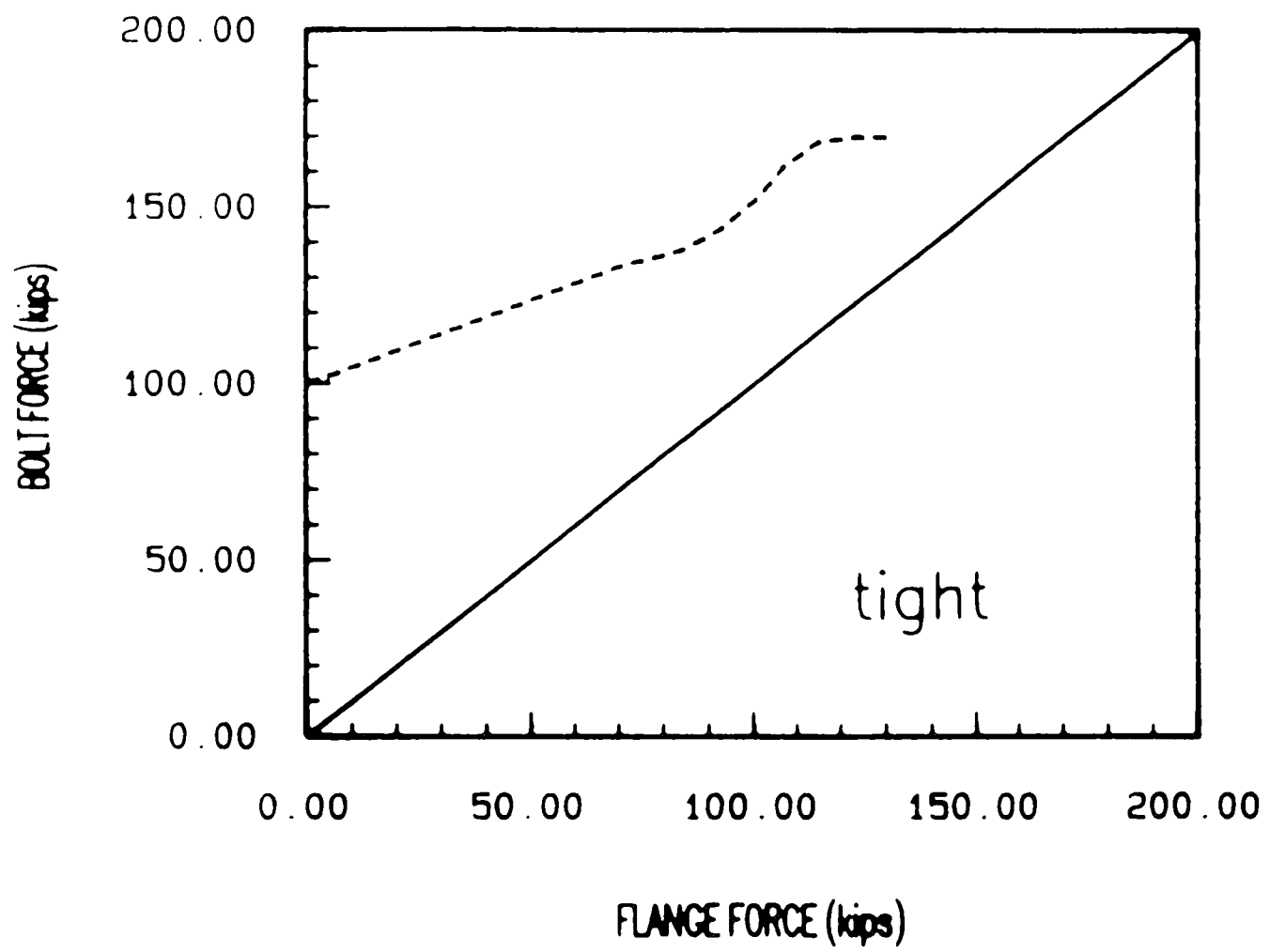


Figure 31: TP2A : Bolt Prying.

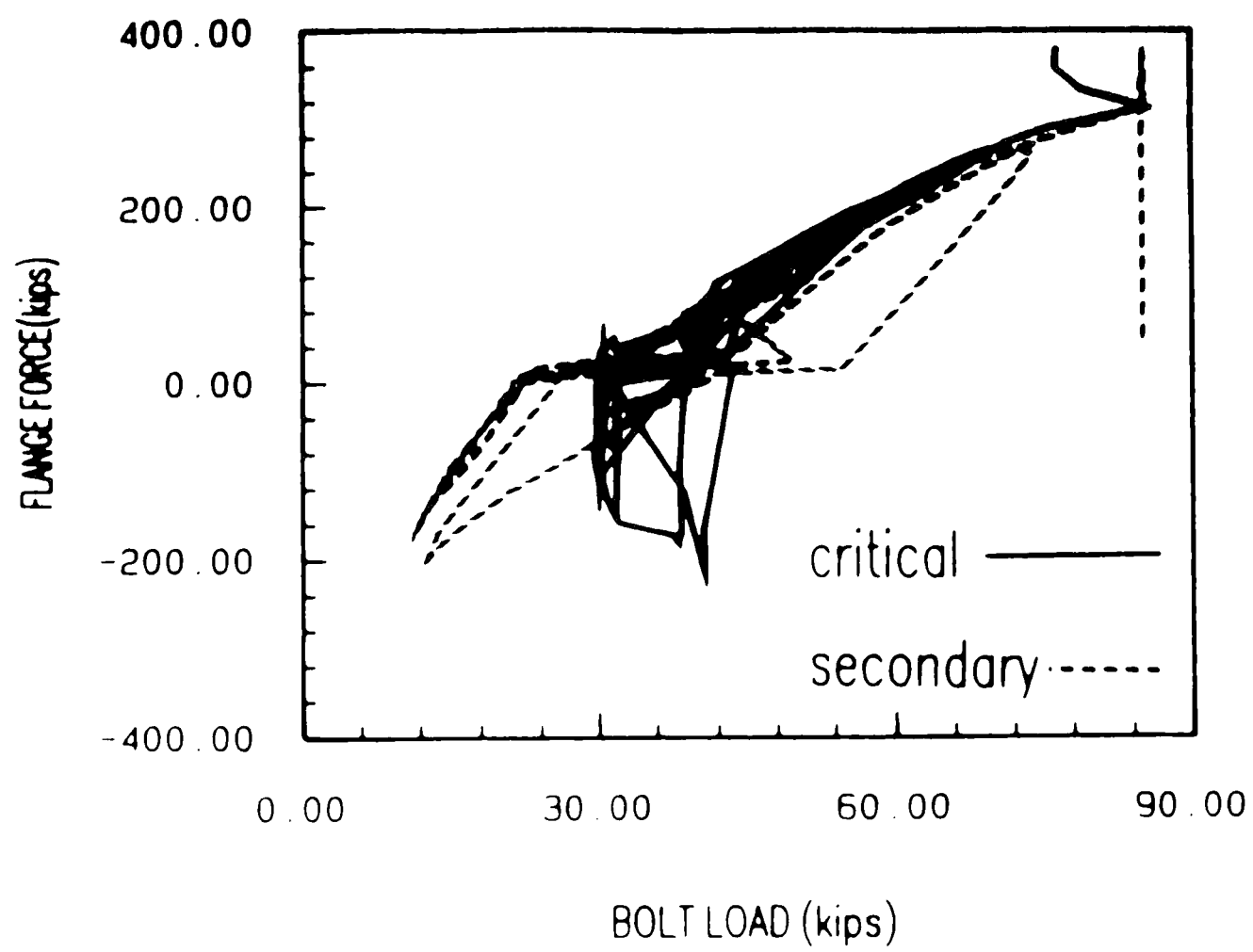


Figure 32: TP2B : Bolt Load Increment.

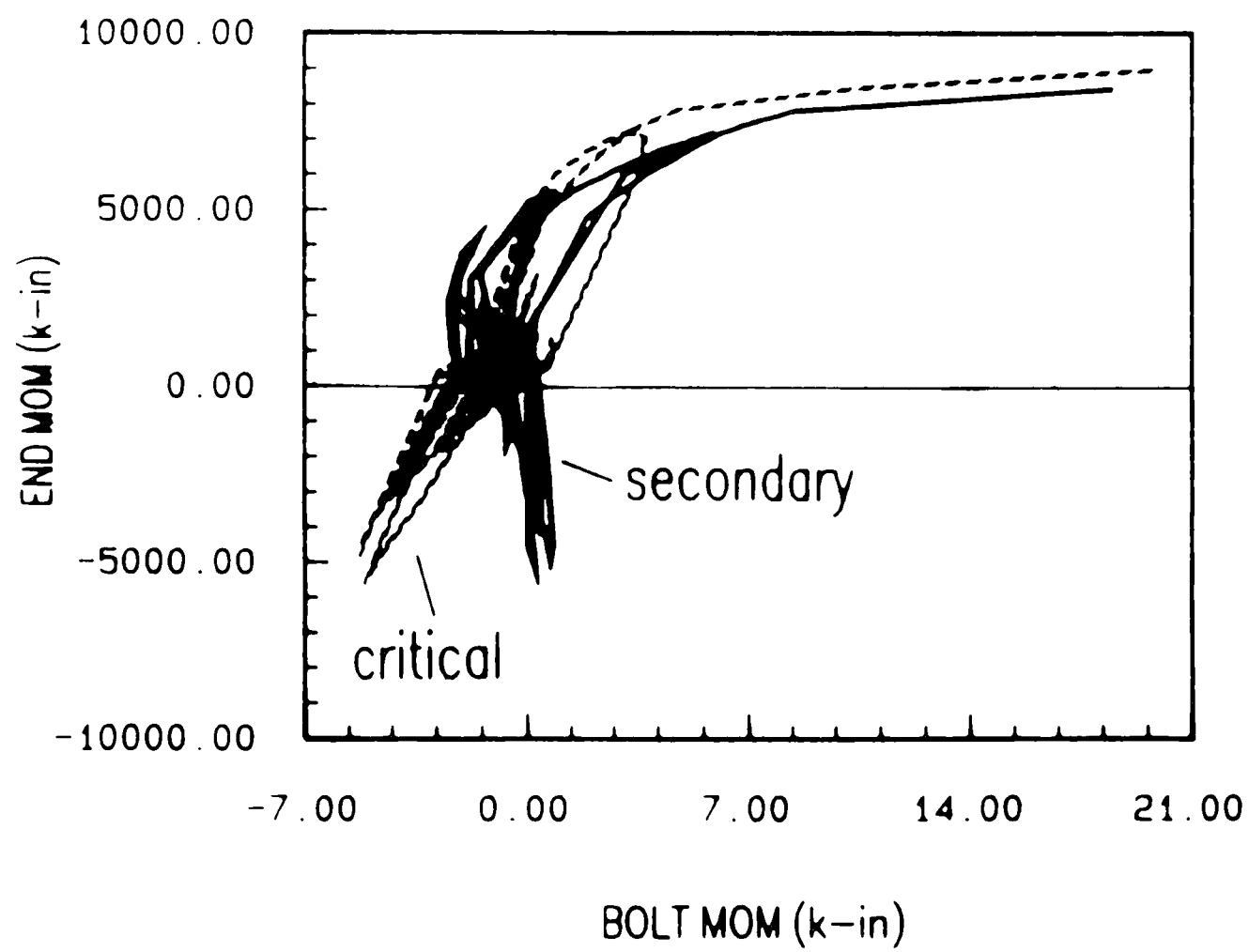


Figure 33: TP2B : Bolt Bending.

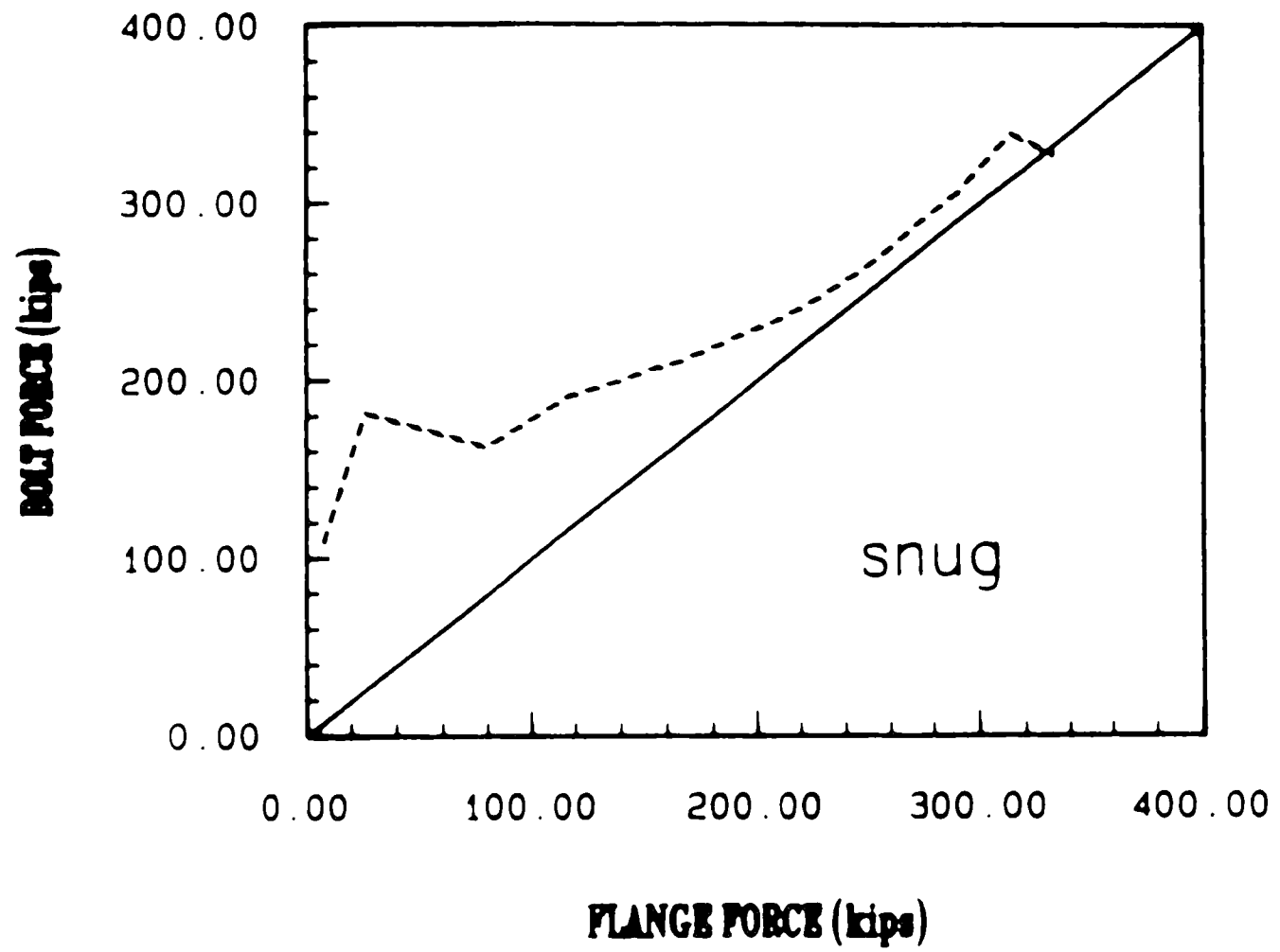


Figure 34: TP2B : Bolt Prying.

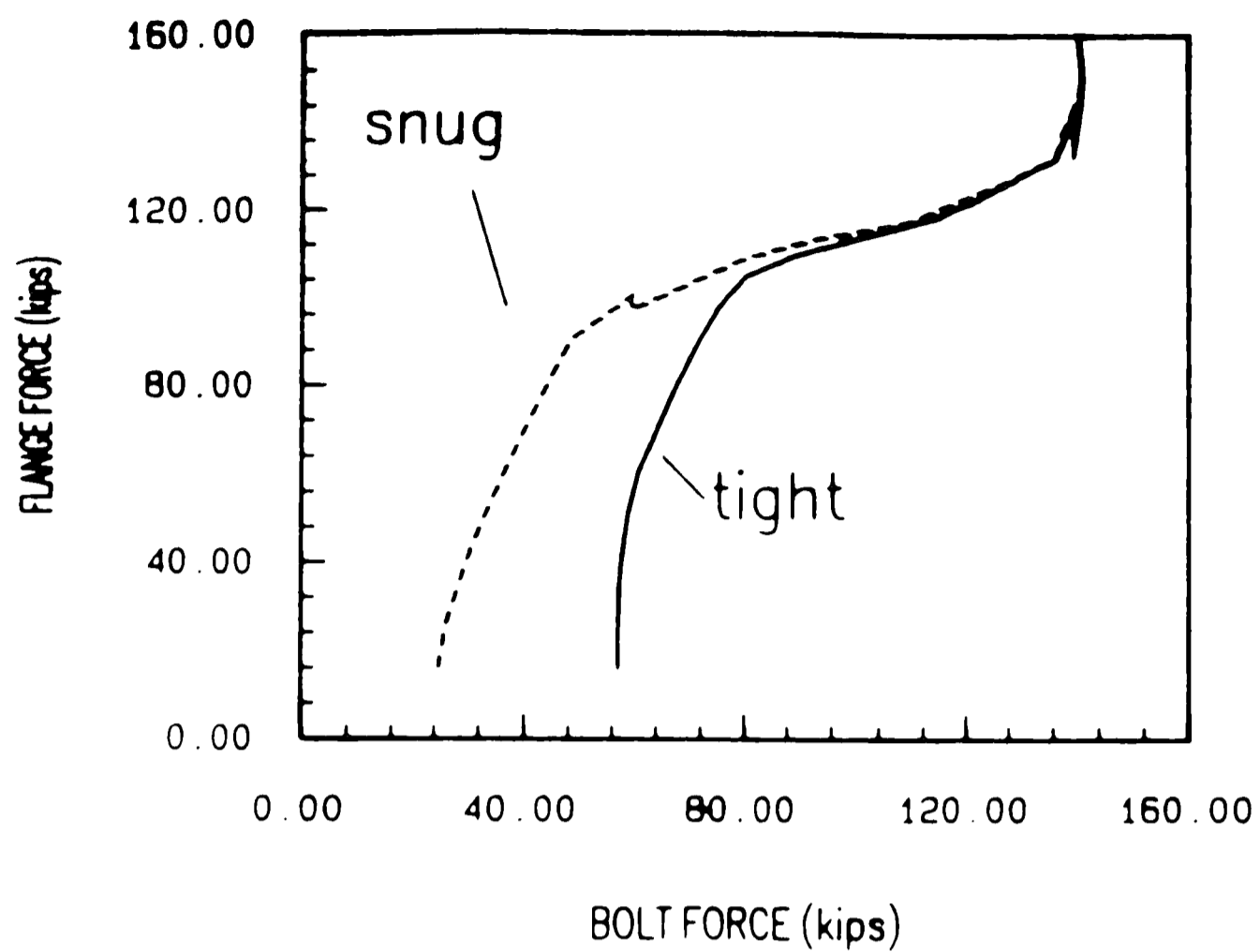


Figure 35: TP3A,TP3B : Bolt Load Increment.

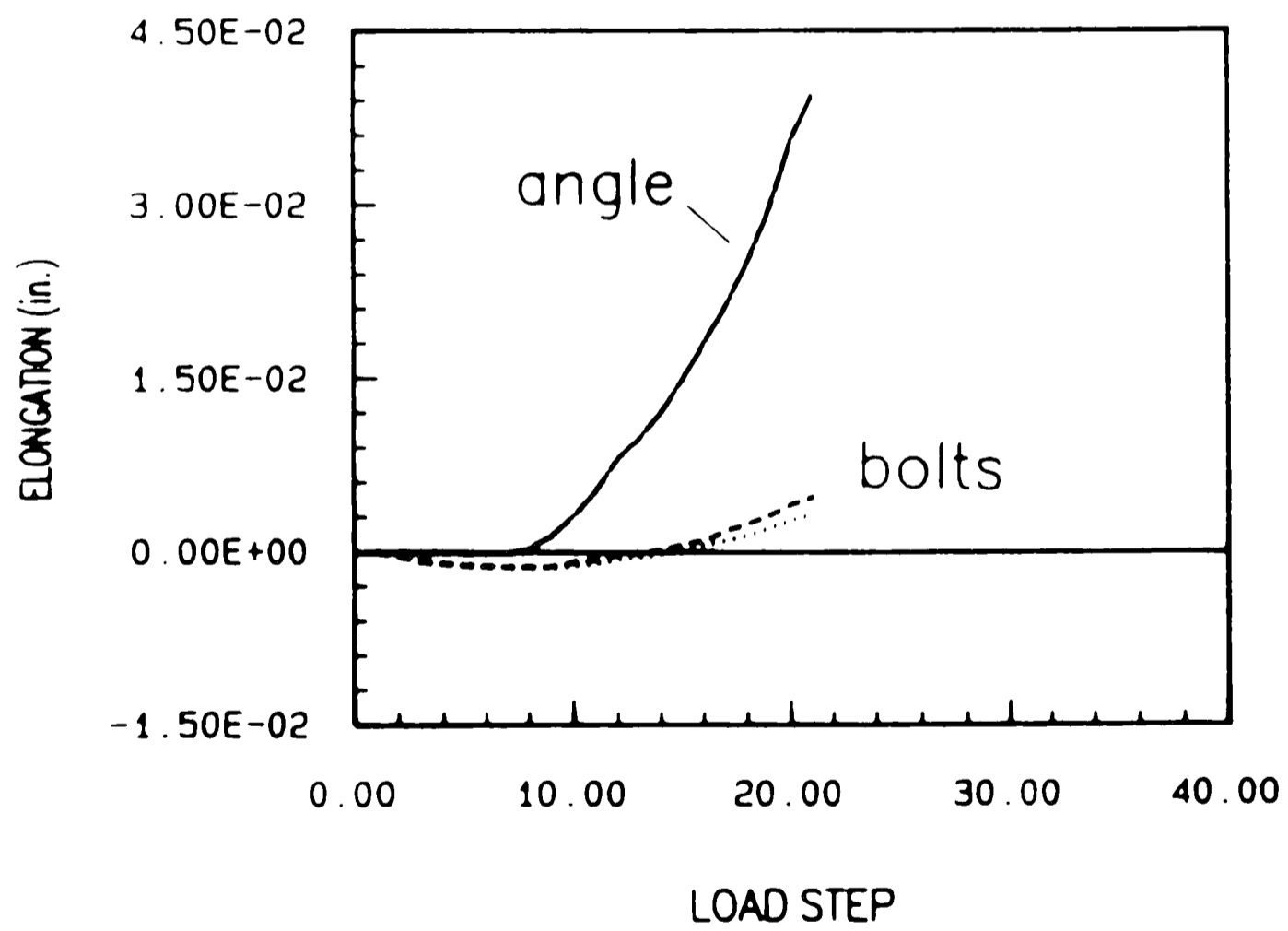


Figure 36: TP3A,TP3B : Bolt Line Elongation.

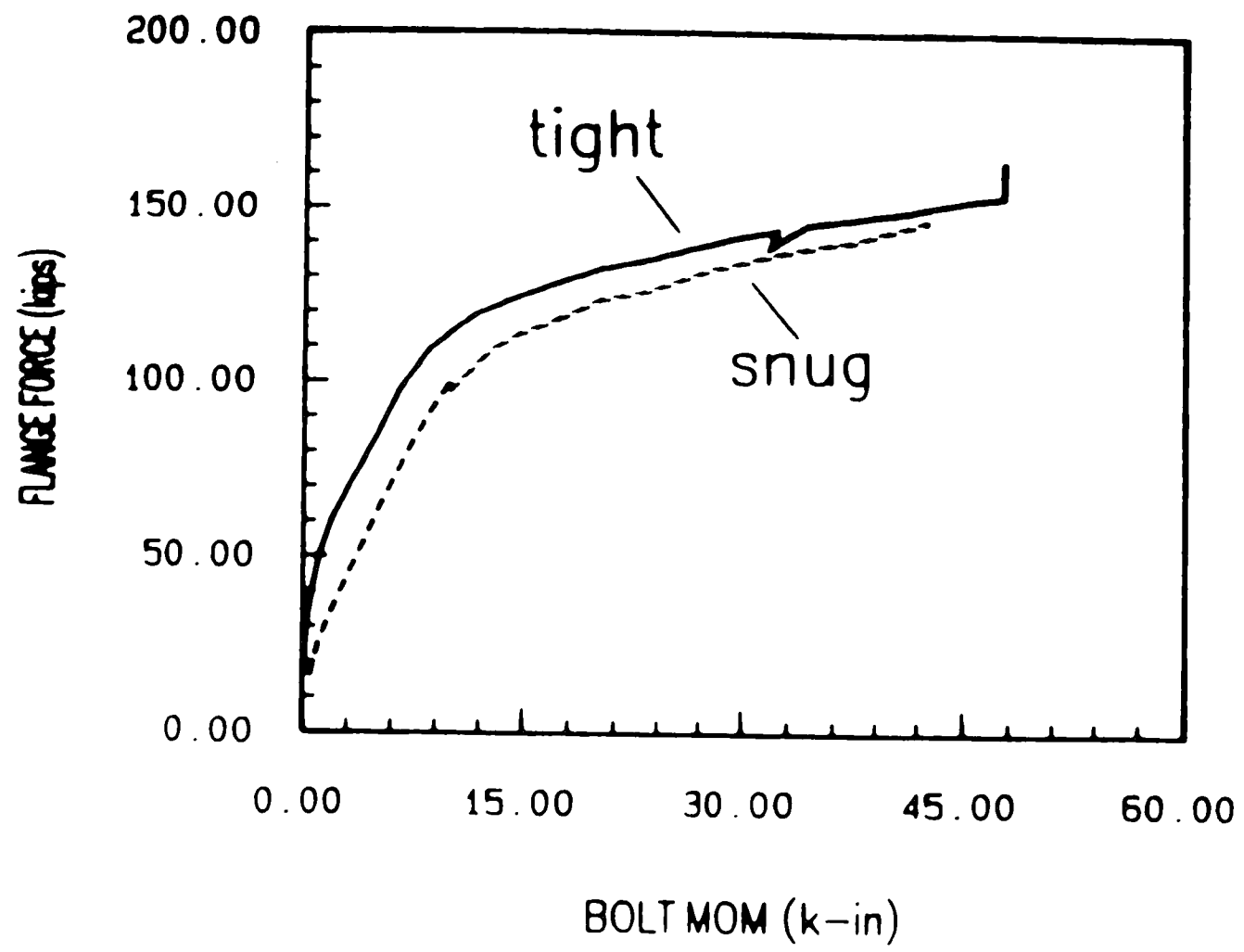


Figure 37: TP3A,TP3B : Bolt Bending.

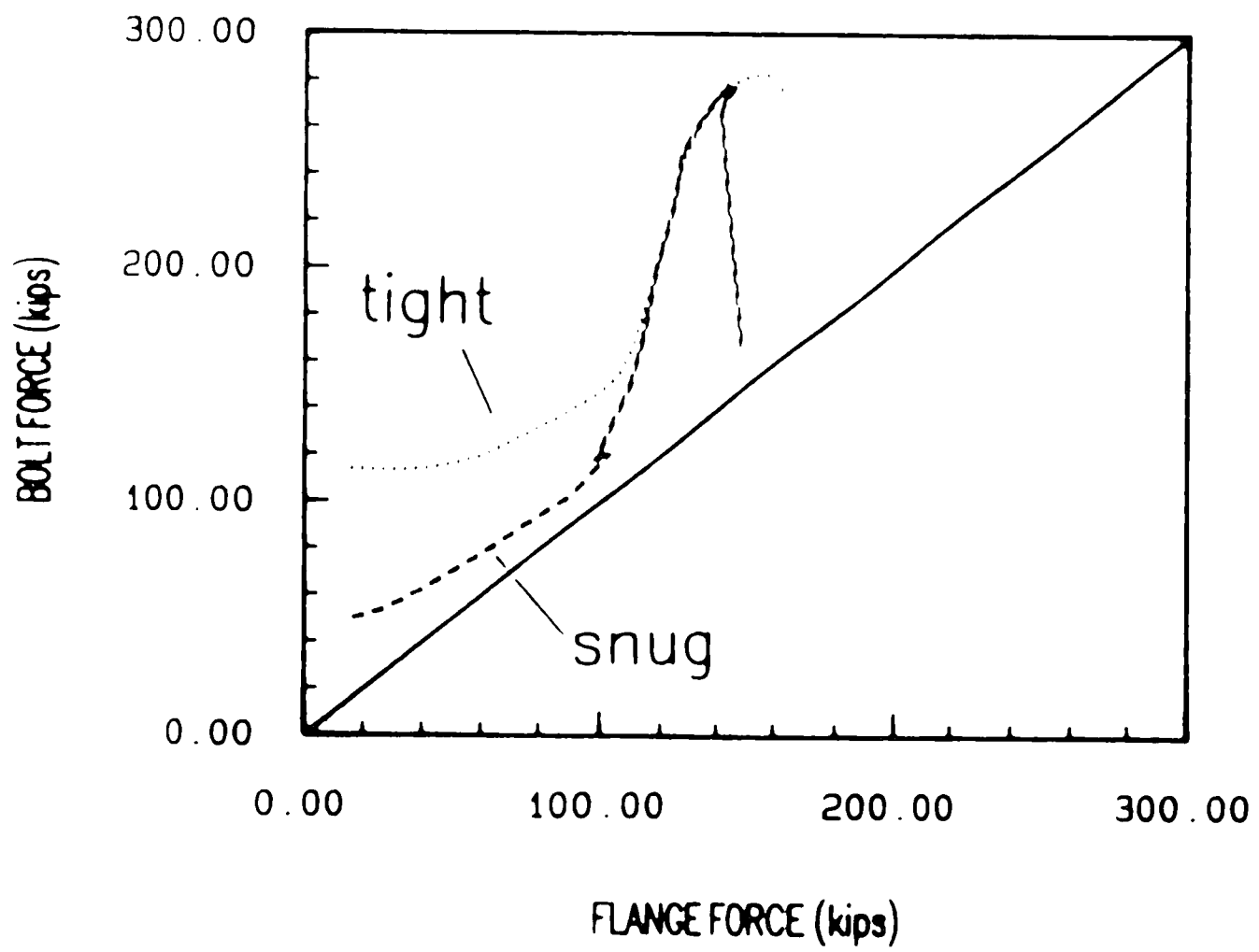


Figure 38: TP3A,TP3B : Bolt Prying.

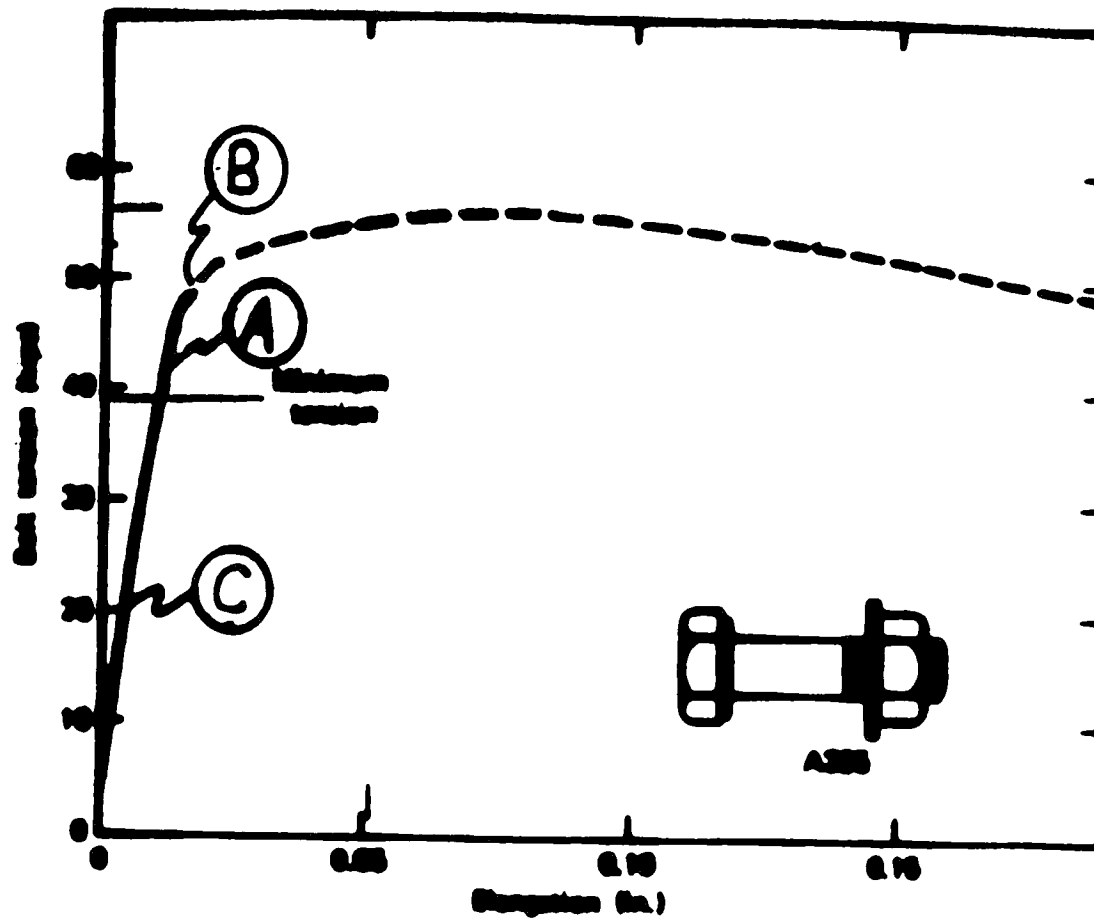


Figure 39: A325 Bolt Load-Deformation Curve.

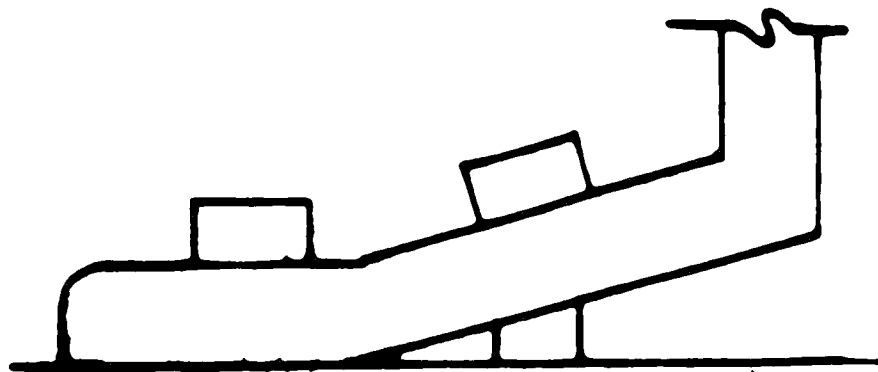


Figure 40: Full Pre-tension Mode.

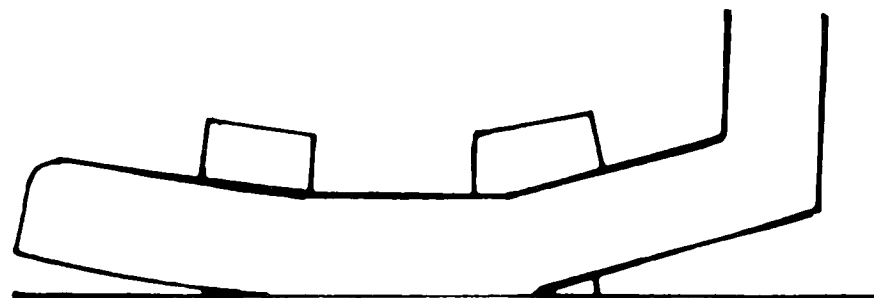


Figure 41: Snug Tight Mode.

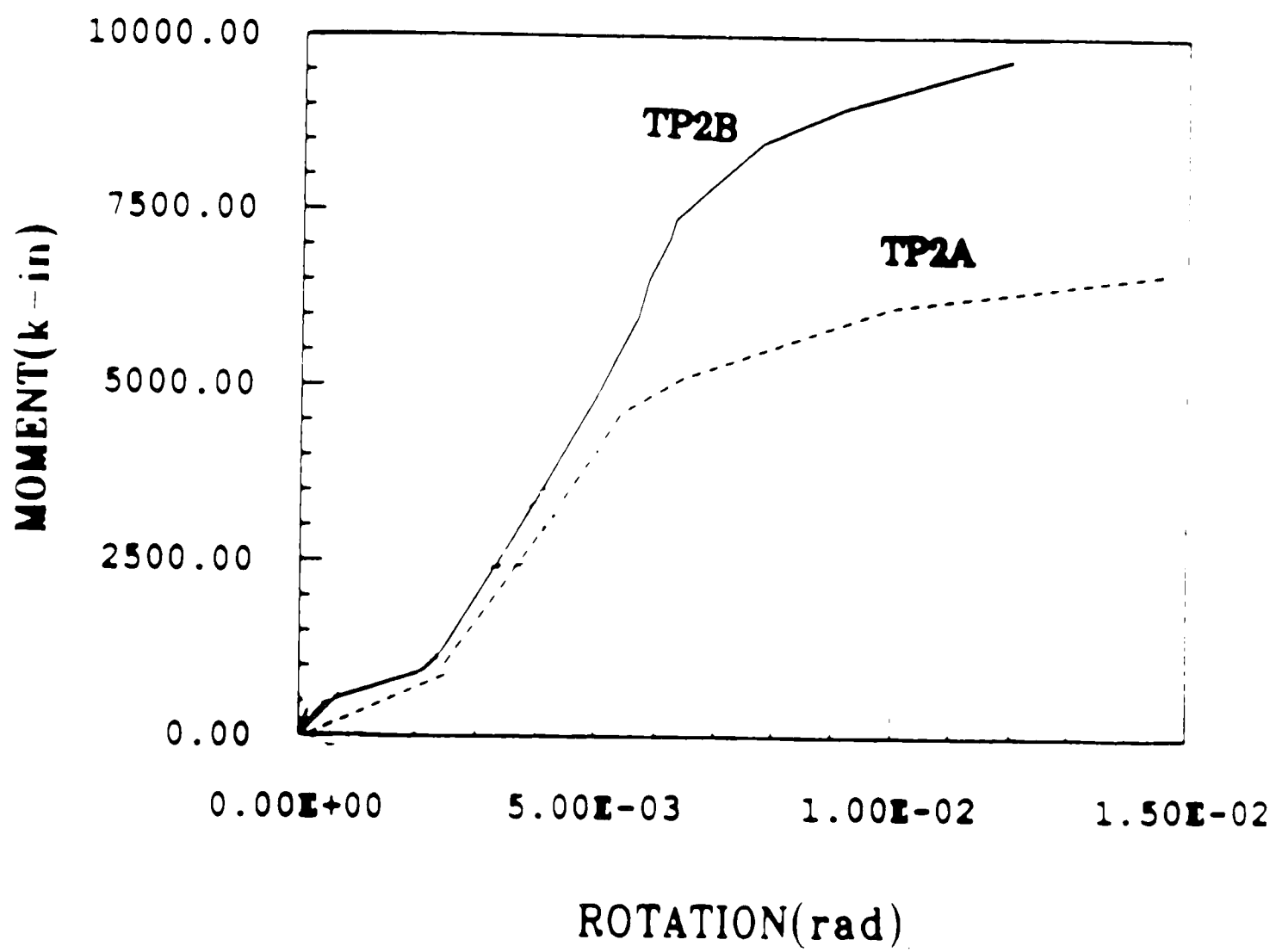
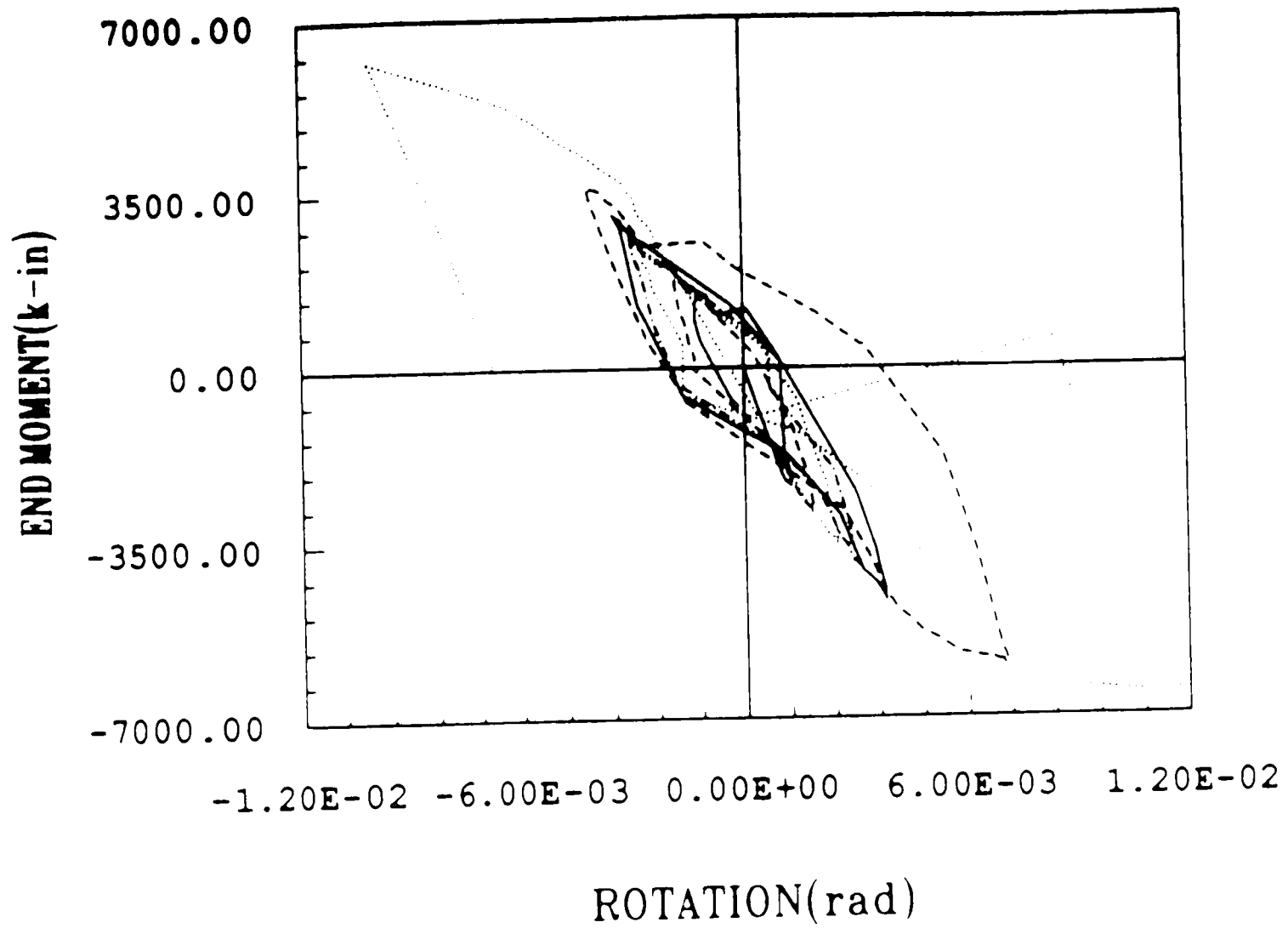
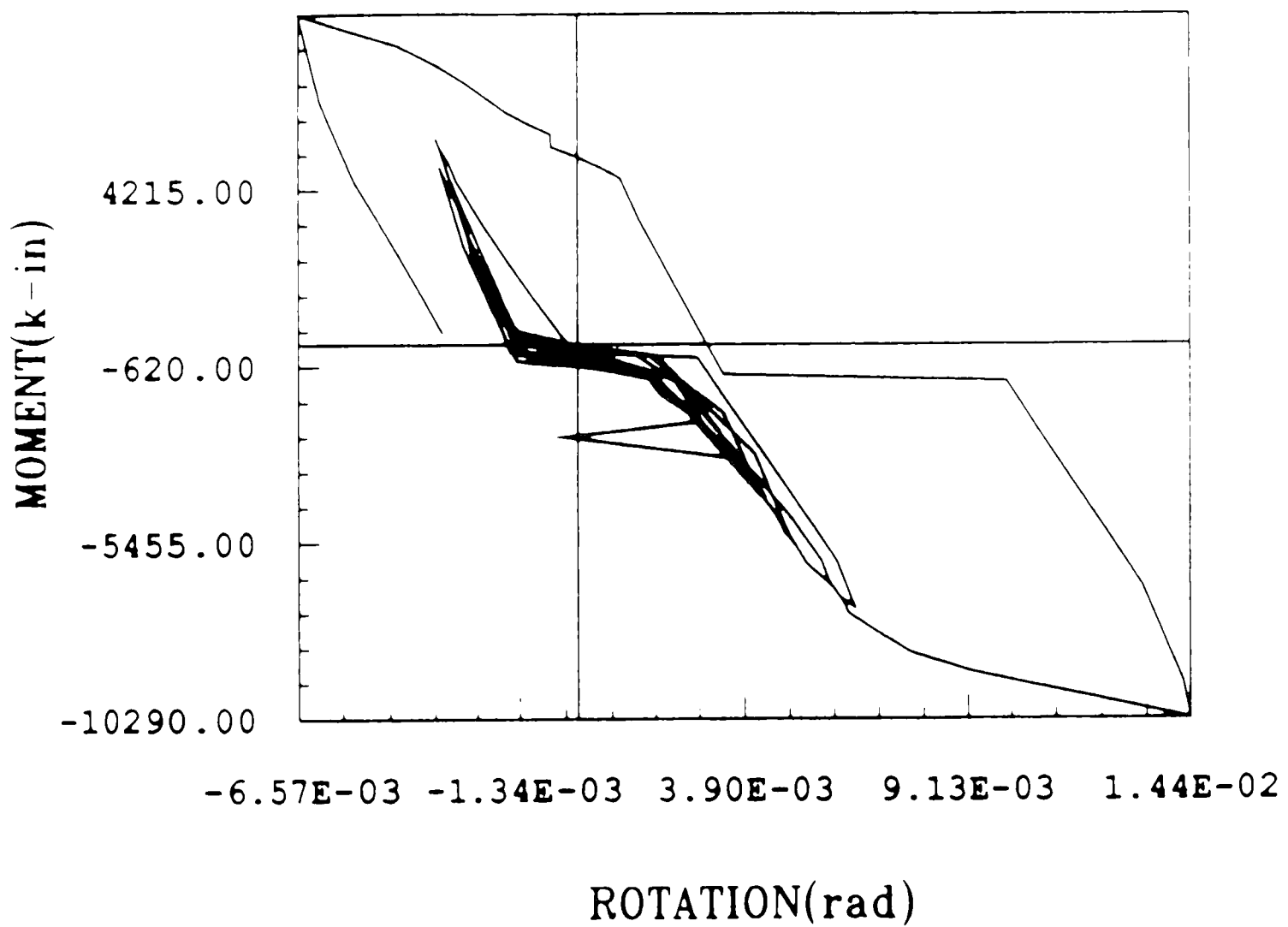


Figure 42: Final Moment-Rotation Curve: TP2A vs. TP2B



**Figure 43: Moment-Rotation Hysteresis Curve:
Test TP2A (Friction Tight Bolts).**



**Figure 44: Moment-Rotation Hysteresis Curve:
Test TP2B (Snug Bolts).**

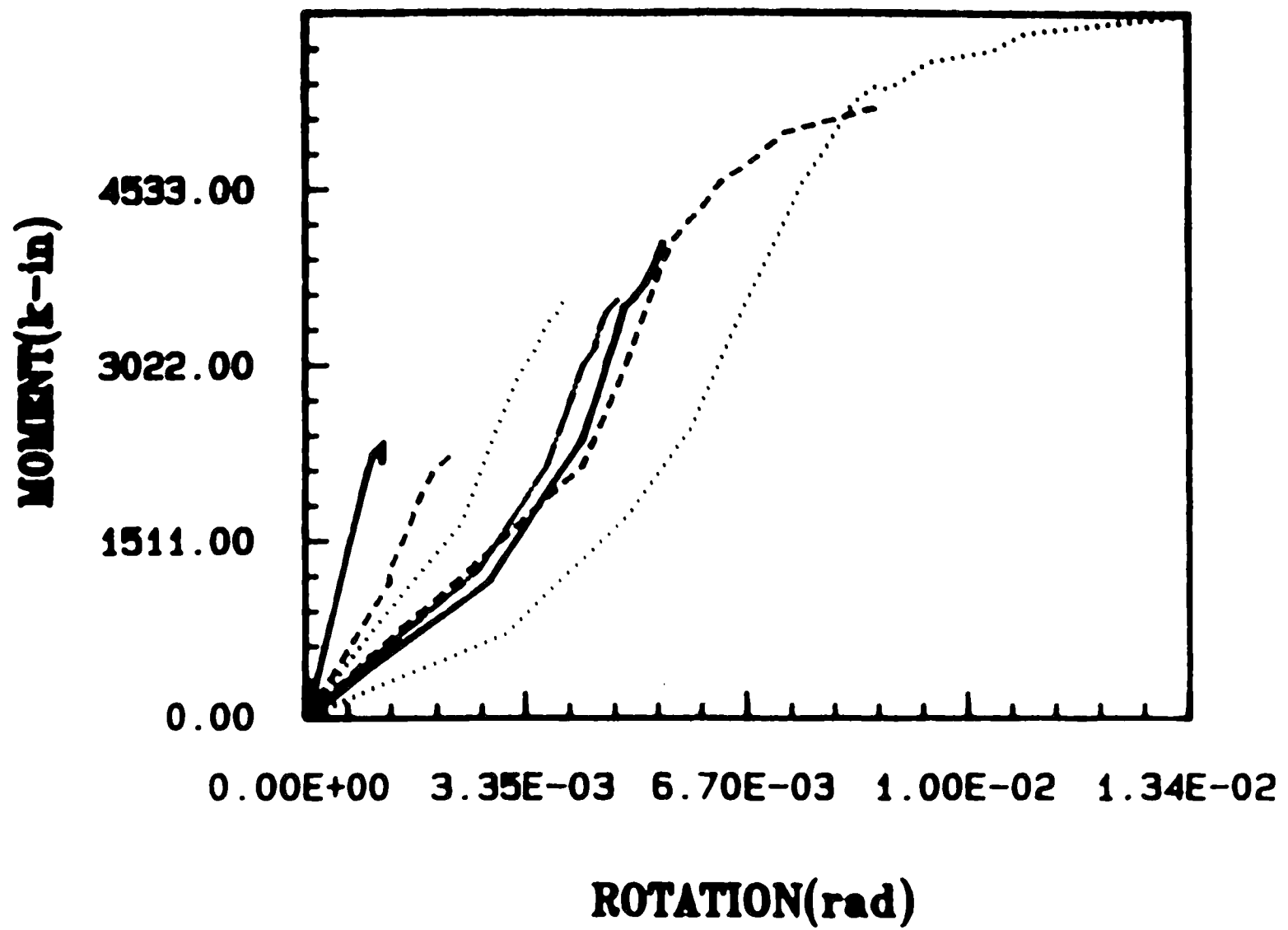


Figure 45: Progressive Softening of Fully Tight Connection.

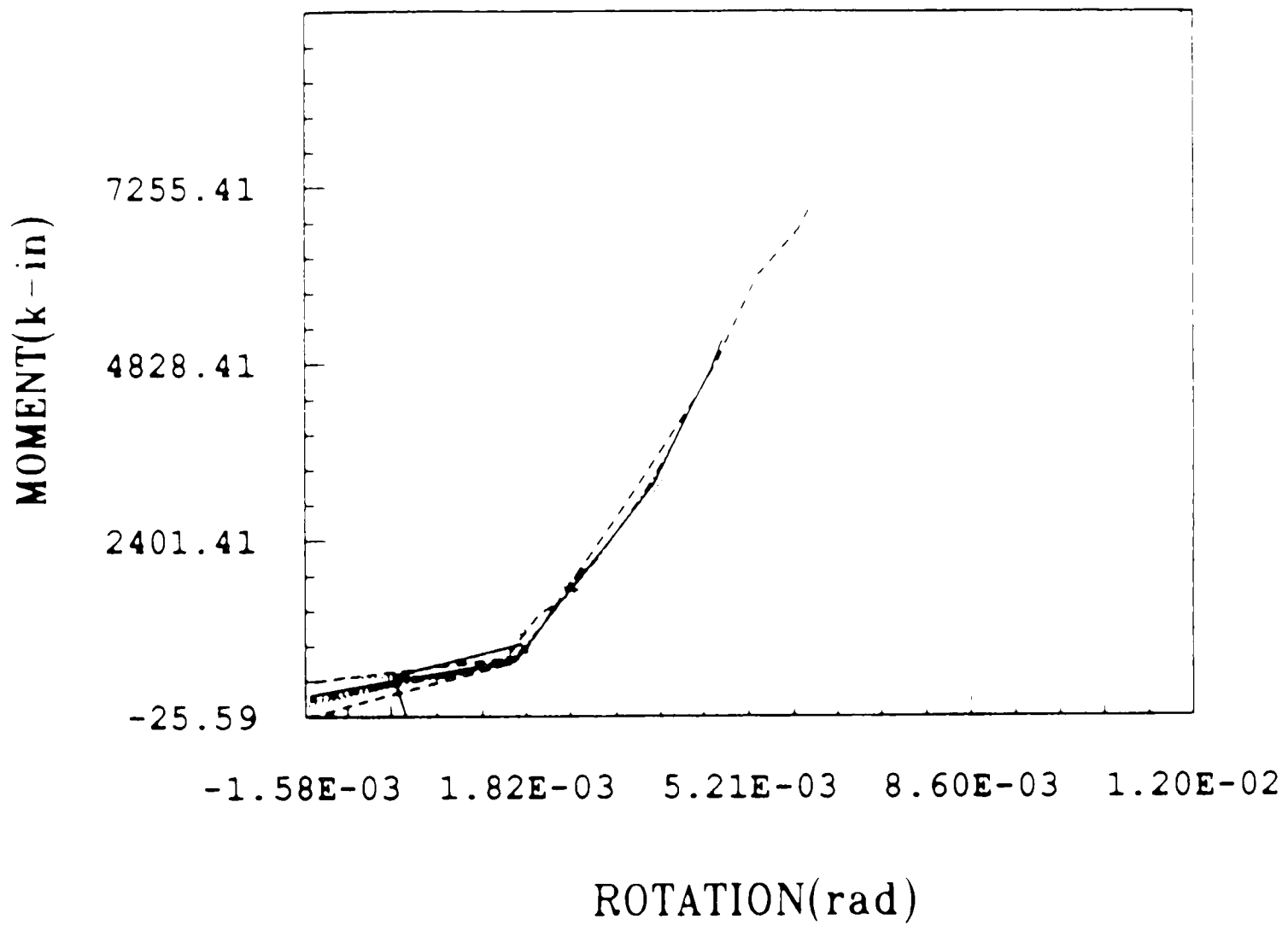


Figure 46: Stable Stiffness of Snug Tight Connection.

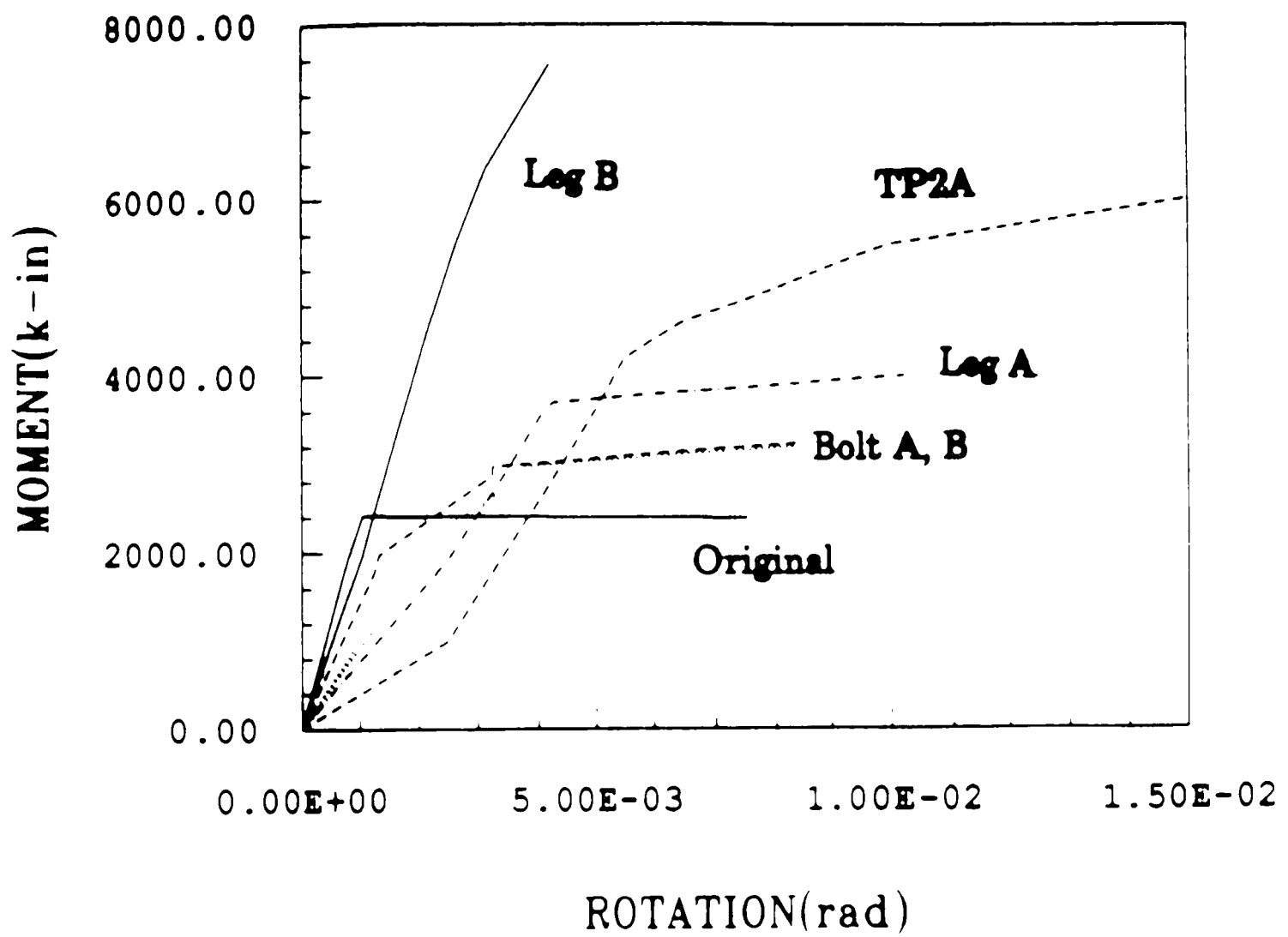


Figure 47: Comparison of Friction-Tight-Bolts STRUCTR Models with Experiment TP2A.

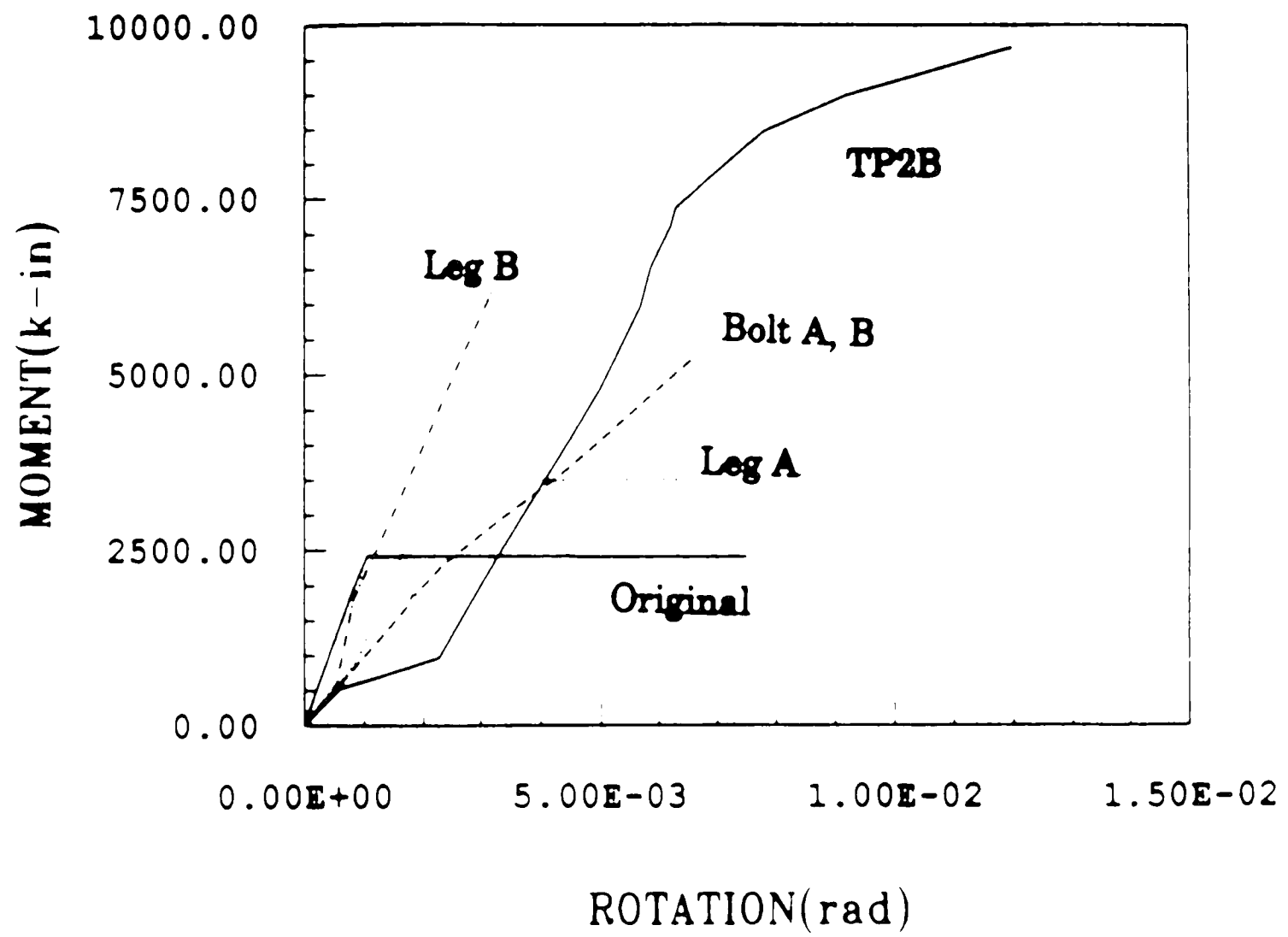


Figure 48: Comparison of Snug-Tight-Bolts STRUCTR Models with Experiment TP2B.

Vita

The author was born in Newark, New Jersey on April 11, 1963 to the parents Phyllis M. and William M. Fleischman. He graduated from Northern Lebanon High School in 1981, and received a Bachelor of Science degree in Civil Engineering in May, 1985 from Carnegie Mellon University located in Pittsburgh, PA. While at Carnegie Mellon, the author was a member of Chi Epsilon and ASCE.

The author was employed by Turner Construction Company in 1985 and 1986. He worked as an assistant superintendent and engineer on the construction project, 53rd at Third, a Manhattan high-rise. Since 1986, he has been a research scholar on Project A3.1 of the Engineering Research Center for Advanced Technology for Large Structural Systems (ATLSS).

REFERENCES

- AISC, 1980
MANUAL OF STEEL CONSTRUCTION, Eighth Edition, American Institute of Steel Construction, Chicago, Illinois.
- AISC, 1986
LOAD AND RESISTANCE FACTOR DESIGN MANUAL OF STEEL CONSTRUCTION, 1st Edition, American Institute of Steel Construction, Chicago, Illinois.
- Azizinamini, A., Bradburn, J. H., Radzinski, J. B., 1982
MOMENT-ROTATION CHARACTERISTICS OF SEMI-RIGID STEEL BEAM-COLUMN CONNECTIONS. Structural Research Studies 82-1, University of South Carolina.
- Chasten, C. P., Fleischman, R. B., Lu, L. W., and Driscoll, G. C. 1987
SEMI-RIGID STEEL CONNECTIONS AND THEIR EFFECTS ON STRUCTURAL STEEL FRAMES. ATLSS Report 87-02, Lehigh University.
Experimental and Theoretical Proposal.
- Chen, W. F., 1985
COLUMN WITH END RESTRAINT AND BENDING IN LOAD AND RESISTANCE DESIGN FACTOR. Engineering Journal, AISC 22(3):105-132.
- Chen, W.F., Kishi, N., 1987
MOMENT-ROTATION RELATION OF TOP-AND-SEAT-ANGLE CONNECTIONS. School of Civil Engineering Report 87-4, Purdue University.
- Douty, R. T., McGuire, W., 1965
HIGH STRENGTH BOLTED MOMENT CONNECTIONS. Journal of Structural Engineering, ASCE (ST2):101-117.
T's tested in tension and compression, then results combined to predict Moment.
- Driscoll, George C. 1987
ELASTIC-PLASTIC ANALYSIS OF TOP-AND-SEAT-ANGLE CONNECTIONS.
Constructional Steel Research Special Issue.
Fritz Engineering Laboratory Report No. 505.1.
- Fisher, J. W., Struik, J., 1974
GUIDE TO DESIGN CRITERIA FOR BOLTED AND RIVETED JOINTS. John Wiley & Sons, New York.
- Hechtman, R. A., Johnston, B. G., 1947
RIVETED SEMI-RIGID BEAM-TO-COLUMN BUILDING CONNECTIONS. Journal of Structural Engineering, ASCE (206).
- Hooper, I. 1987
ATLSS INDUSTRY ADVISORY PANEL DISCUSSION, Advancements in Connection Technology, July, 1987.

- Johnston, B. G., Mount, E. H., 1942**
ANALYSIS OF BUILDING FRAMES WITH SEMI-RIGID CONNECTIONS. Journal of Structural Engineering, ASCE (2152):993.
- Kishi, N., Chen, W. F., 1986**
DATA BASE OF STEEL BEAM TO COLUMN CONNECTIONS. Structural Engineering Report CE-STR-86-26, School of Civil Engineering, Purdue University.
- Radziminiski, J. B., Bradburn, J. H., 1984**
EXPERIMENTAL INVESTIGATION OF SEMI-RIGID STEEL BEAM-COLUMN CONNECTIONS. In . Eighth World Conference on Earthquake Engineering, San Fransisco, CA.
- Rathbun, J. C., 1936**
ELASTIC PROPERTIES OF RIVETTED CONNECTIONS. Transactions, ASCE 101:524-595.
- Salmon, C. G., Johnson, J. E., 1980**
STEEL STRUCTURES DESIGN AND BEHAVIOR. Harper and Row Publishers, New York.
- Sourochnikoff, B., 1950**
WIND STRESSES IN SEMI-RIGID CONNECTIONS OF STEEL FRAMEWORK. Transactions, ASCE 115:382-393.
- Yusof, Norzan Mohd. 1986**
SEMI RIGID CONNECTIONS ANALYSIS AND DESIGN. Master's thesis, Lehigh University.